On the Auxiliary Driving Mechanism for Blood Circulation

Zheng Li

A dissertation

submitted in partial fulfillment of the

requirements for the degree of

Doctor of Philosophy

University of Washington

2019

Reading Committee:

Gerald H. Pollack, Chair

Werner Kaminsky

Karl Böhringer

R. Jeffrey Wilkes

Program Authorized to Offer Degree:

Bioengineering

University of Washington

Abstract

On the Auxiliary Driving Mechanism for Blood Circulation

Zheng Li

Chair of the Supervisory Committee:
Professor Gerald H. Pollack
Bioengineering Department

This thesis discusses a driving mechanism for blood circulation over and above the pressure gradient.

Fluid commonly flows in response to an external pressure gradient. However, when a tunnel-containing hydrogel is immersed in water, spontaneous flow occurs through the tunnel without any pressure gradient. This flow was observed in a wide range of plant- and animal-derived hydrogels. The flow appears to be driven by axial concentration gradients originating from surface activities of the tunnel wall. Those activities include: (i) hydrogel-water interaction (ii) material exchange across the tunnel boundary. Unlike pressure-driven flow, this surface-induced flow (SIF) has two distinct features: incident infrared energy substantially increases flow velocity; and, narrower tunnels generate faster flow with faster velocity. Thus, surface activities

in hydrogel-lined tunnels may confer kinetic energy on the enclosed fluid, with infrared radiation as an energy source.

The existence of the surface-induced flow mechanism was tested in a blood circulation system.

In the three-day-old chick embryo vitelline-circulation model, it was found that blood flow continued for up to an hour after the heart stopped beating. Albeit at a slower velocity, postmortem blood flow was directional, following the same course as the original blood flow, i.e., from artery to vein. Infrared radiation appears to supply energy for driving this flow: when infrared energy was applied to the postmortem blood-flow model, velocity increased by 300%. Alternative explanations such as gravitationally driven flow, vascular contraction or convection flow could be ruled out. This finding implies that a mechanism beyond the pressure gradient, potentially SIF mechanism, helps drive the blood circulation, using infrared energy as a fuel.

TABLE OF CONTENTS

List of Figures

ACKNOWLEDGEMENTS

I would like to thank my advisor, Gerald Pollack, a great advisor and a wonderful friend. What he taught me can be summarized by a quote by Nobel laureate Albert Szent-Györgyi: "Discovery consists of seeing what everybody has seen and thinking what nobody has thought." This PhD project will not exist without his insight and courage. I am honored to be his student.

I would like to thank my parents, Fengxia Zhao and Hongen Li, a pair of traditional Chinese parents. They never said they love me, but they just practiced their love without conservation. Being the first teachers in my life, they bought me books on various scientific topics hen I was a kid, and I was intrigued since then. The seed they planted in my heart finally grown into a tree!

I would like to thank my wife Rui Hua, the most important people in my life. Her support, emotionally and financially — she pays the bill while her husband being a forever graduate student — made it possible for me to finish the PhD. Besides the support and love; she plays another important role: for countless nights she accompanied with me in the lab. Whenever I observed something new, I ask her to confirm my observation. I couldn't believe myself until she told me so. She was the first witness of the discoveries described in this thesis!

At last, I would like to thank everybody who had helped me along the way: my committee members, colleagues and friends. The help could be a lengthy discussion on the project or detailed suggestions on the manuscripts; the help could also be some nice words or an encouraging smile. Thank you for being with me during the journey.

DEDICATION

To Mother Nature:

I am amazed by your design.

Chapter 1. Introduction

As of today, it is clearly stated in any physiology textbook that a pressure gradient, from various sources and mainly from the heart, is the *only* driving force for blood circulation. This is a long-accepted dogma that leaves seemingly little room for doubt.

This thesis challenges this dogma.

First, let us see why blood circulation is important.

1.1 Blood circulation

Overview

For organisms of different sort, big or small, simple or complex, the most fundamental need is metabolism, a set of necessary chemical reactions to maintain life. To get the needed reactants and unwanted wastes in and out of a cell — the smallest structural and functional unit of an organism — material exchange between a cell and its surrounding environment is necessary.

Material exchange has two critical requirements. They are:

1) Water. The reactants and wastes are always dissolved in the universal solvent, water. Essentially, the "material" in "material exchange" is a water-based solution.

2) Surface. Material exchange happens between the organism and its environment. Thus, the exchange must go through the surface of a cell.

The importance of blood circulation lies in the fact that organisms need material exchange.

A single-cell organism has a high surface to volume ratio, comparing to multi-cellular organisms. Via diffusion, the requirements of the whole cell can be quickly fulfilled. If a single

cell with 7 μm in diameter is placed in pure oxygen of 1 atm, it will be fully saturated with oxygen in 0.0054 seconds (*1*).

For more complex multi-cellular organisms, most of the cells are not in contact with the surrounding environment, and the surface to volume ratio of the organism dramatically decreases. If the materials are only allowed to exchange through the outer boundary of the whole tissue, then the process of material exchange will be slow. For a cylindrical tissue with a diameter of 1 cm placed in pure oxygen of 1 atm, 90% saturation will be reached after three hours (*1*).

Thus, for multi-cellular organisms, the circulatory system is essential for adequate oxygenation and material exchange. The circulatory system has two roles: transport and material exchange. The tubular blood vessels transport blood, a complicated water-based suspension which dissolves the chemicals to be exchanged. Material exchange happens in the capillaries, blood vessels that are large in quantity and small in diameter. From thicker arteries to narrower capillaries, the surface area of the blood vessels per unit tissue volume is greatly increased. With the increased surface to volume ratio, each cell can easily exchange the materials with the blood. This is why blood circulation is one of the most fundamental physiological activities (*2*).

Transport water-based solution and **material exchange**. These two fundamental roles of blood vessels will be critical for **explaining why blood can flow without a pressure gradient**, which is the goal of this thesis. The later chapters will analyze this in depth.

Before that, I would like to give a review on the history of blood circulation, to see how we obtained the current understanding on blood circulation.

A brief history of blood circulation

It took several thousand years for human beings to achieve the current understanding of the blood circulation (*3-10*). To figure out how blood circulates is no easy task: When a dead body is dissected, it is not obvious which vessel is an artery or a vein, since these blood vessels are not nicely marked with blue and red color, as in modern textbooks. With a diameter that is less than 1/10 the diameter of human hair, the capillaries are not visible to the naked eye. Before the microscope was invented, it was not even evident that the blood circulates. The current understanding of the circulation has taken effort, wisdom, and sometimes great sacrifice, of many brilliant minds.

The earliest written records on the circulatory system are found in the Ebers papyrus, an Egyptian medical papyrus written in about 1500 BC. Air was considered to come into the body through the mouth, and then travelled into the lungs and heart. From the heart, it was speculated that air travelled to other parts of the body through arteries (*6*, *10*).

In *Huangdi Neijing*, a Chinese medical text considered to be written between 475 BC and 220 CE, it is written that (*5*): "The blood resides inside the vessels; it is tied to the heart."; "The flow in the conduit vessels does not stop. It circulates without break. When cold qi enters the conduits, stoppage and retardation result."

Blood circulation is well documented by ancient Greek physicians and scholars (400 BC). It was acknowledged that animals as well as humans needed to be nourished to survive. Aristotle (384 BC) believed that heart played a central role in physiological function; it communicated with the rest of the body. Praxagoras (340 BC) was able to differentiate arteries and veins. Erasistratus (304 BC) considered heart to be the source for both arteries and veins, drove blood in the veins and air in arteries (*4*).

In second century AD, a Greek physician, Galen of Pergamon, built his work based upon the ideas of the ancient Greeks. He stated that the arteries contained not only air but blood. He also stated that the venous blood and arterial blood were connected through invisible pores in the interventricular septum in the heart. Galen's model of the cardiovascular system well stood for over a thousand years (*3*).

A thousand years later, new discoveries started to emerge. In the Islam world, Ibn al-Nafis, an Arab scholar (1213-1288), stated that the interventricular septum was not porous and proposed the existence of the pulmonary circulation (*4*, *7*). In Europe, Leonardo da Vinci (1452-1518) experimentally proved that air did not enter the heart from the lungs; he also proved that valves allowed blood to flow in only one direction. Michael Servetus (1511-1553) described the pulmonary circulation. Realdus Columbus (1515-1559) independently discovered the pulmonary circulation. Andreas Caesalpinus (1524-1603) first used the term "circulation". Hieronymus Fabricius (1537-1619) noticed that blood could not move from the heart to periphery through the veins, and also discovered the valves in the veins (*4*).

In 1628, William Harvey (1578-1657) published his monumental work, the 72-page *Exercitatio Anatomica de Motu Cordis et Sanguinis in Animalibus (On the Motion of the Heart and Blood in Animals),* also as known as *De Motu Cordis (9).* In this book, the systemic circulation was completely described, and the heart was considered to drive blood circulation. Harvey could not predict the existence of capillaries; thus, he wrote: the blood "permeates the pores" in the flesh and "absorbed and imbibed from every part" by the veins.

Galen's theory of circulation was prevalent in Harvey's time. Harvey's theory contrasted sharply with this existing dogma and was considered controversial. Harvey anticipated the opposition to his revolutionary theory and wrote: "…not only do I fear danger to myself from the

malice of a few, but I dread lest I have all men as enemies (*3*).” By the time of Harvey’s death, his view of circulation became widely accepted.

In 1661, Marcello Malpighi discovered the capillaries when observing a frog’s lung through a microscope. The current blood circulation theory was established with the discovery of that last piece of the puzzle (*8*).

Pressure gradient as a driving force

In today’s blood circulation theory, the pressure gradient from the heart is considered as the major driving force. Pressure gradients of other kinds, like musculovenous pumps, respiratory pumps, vena cava compression, gravity, etc. (*11*), arguably provide auxiliary driving forces. The blood vessel is seen within current theory as a tube with an external force that is either pushing or pulling the blood.

Mathematically the pressure-gradient driven flow is described by Hagen—Poiseuille equation:

$$Q = \frac{\pi R^4 \Delta P}{8 \mu L}$$

Where ΔP is the pressure difference between the two ends of the blood vessel, L is the length of the blood vessel, μ is the dynamic viscosity of the blood, Q is the volumetric flow rate, R is the radius of the blood vessel.

Although the blood flow does not follow this equation exactly since assumptions are made for this model (long, straight tube, Newtonian fluid, and laminar flow) (*11*), this equation shows the significances of several important parameters in blood circulation. The narrower the blood vessel, the slower the flow rate. The lower the pressure gradient, the slower the flow rate. The higher the viscosity, the slower the flow rate. To understand the regulation of blood flow, one can just

investigate what factors may affect the blood vessel diameter or increase the power output from the heart.

The Poiseuillian view of human circulation is important. This principle has good explanatory power on many physiological activities. It is a principle that points out directions for further scientific research and designing medical applications. Compared to previous understanding of blood circulation, the current understanding is more advanced, and countless lives have been saved because of the advancement----it is not hard to imagine that any medical devices designed based on the understanding that air flows in arteries would be less effective. This Poiseuillian principle also prevails in the classroom, hospital, and beyond: for the general public, it is one of the most well-known scientific facts: the heart drives the blood.

As much as we benefit from this circulation model, science does evolve. It is fair to ask: is this model adequate? Does it explain everything? Are there are phenomena that contradict this model? In the next section, I will review observations that this model fails to explain.

1.2 Evidence beyond the current model's explanatory power

Surviving without a heart?

Is it possible to survive without a heart?

Some early studies on embryos showed that embryos can continue to develop after their hearts had been intentionally arrested or removed. The earliest work starts from the beginning of 20th century (*12*). In 1907, Knower demonstrated that frog embryos can live up to 2 weeks after the removal of their heart. In this study, the hearts of the larvae were excised even before the initiation of the circulation.

In 1954, Kemp showed that frog larvae could still develop for 4-5 days after the heart had been removed surgically. In this study, the heart was removed two days after the initiation of the circulation. Kemp stated that after the heart was removed, "although no continuous flow of blood was possible, some ebb and flow of fluid did occur in the blood vessels near the heart (*13*)". In a subsequent study (*14*), Kemp removed hearts from the larvae of axolotl, or Mexican walking fish. 80% of the larvae survived up to 7 days. A few survived even up to 15 days.

Blood flow without a heart

Blood flow is essential for life. Is it possible that the blood can flow after the heart has stopped beating?

Logically, Blood flow should stop after the heart stops beating. Let us look back into the Poiseuillian equation:

$$Q = \frac{\pi R^4 \Delta P}{8\mu L}$$

If $\Delta P = 0$, it is not hard to conclude that Q should be 0. In the narrower capillaries, since the radius is very small, the resistance is quite high. The red blood cells have a diameter larger than the smallest blood vessels; they have to bend themselves to travel through these capillaries (*15*). It is a tight fit! As the blood travels in the capillaries, its kinetic energy dissipates in the form of frictional heat (*16*). If the heart stops beating, a logical expectation is that blood flow should quickly cease.

However, experiments suggested otherwise. In a 2007 study conducted by Kalchenko et al. (*17*), the major arteries within the mouse ear were occluded by local mechanical pressure. Then, with occluded blood vessels, the mouse ear was imaged via a dynamic light scattering imaging technique. It was observed that mechanical occlusion of major blood vessels in the mouse ear

could never lead to a complete blood flow cessation in the capillaries. Even after maximal occlusion, the red blood cells in downstream capillaries continued to flow. What's more, red blood cells were moving for up to 1 h after animals were euthanatized. This phenomenon was observed in all experimental animals (N=10).

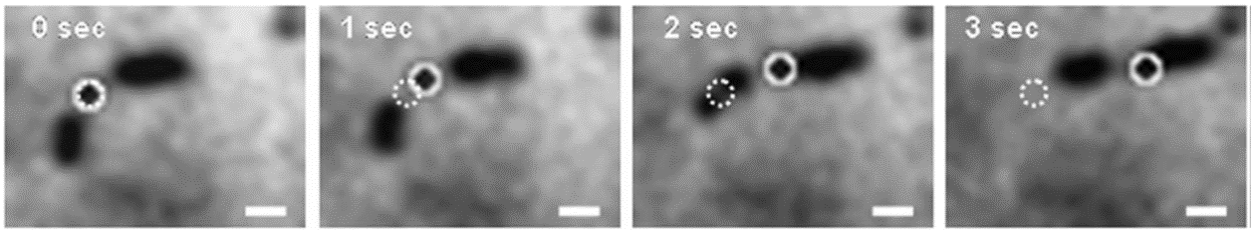

Fig. 1.1. Sequential microscopic images of RBC motion inside a single capillary with Major blood vessels occluded 5 min prior to imaging. Single RBC is outlined (starting point is outlined by the dashed line). Scale bar =5 μm. The image was taken using transmitted light illumination. Image contrast was enhanced (*17*).

In a 2013 study, Meglinski et al. (*18*) measured blood flow of euthanized mice and rats. The goal of this research was to determine the 'biological zero' signal, i.e., imaging signals of the blood vessels after the blood stopped flowing. The stoppage of the heart was expected lead to a stopped blood flow; and the red blood cells were expected to exhibit only Brownian motions. The blood flow was measured via diffusion wave spectroscopy (DWS). To the surprise of the researchers, the blood flow continued to flow after the heart stopped beating, albeit at reduced velocity. With microscopic observation, the researchers further confirmed postmortem blood on various body regions of mice and rats that may last up to two hours (Fig. 1.2). Lacking a clear explanation, the investigators attributed this flow to "partially retained basal tonus of the vessels and leveling of the static pressure along the vascular bed" — essentially, a pressure gradient caused by vascular contraction and gravity force.

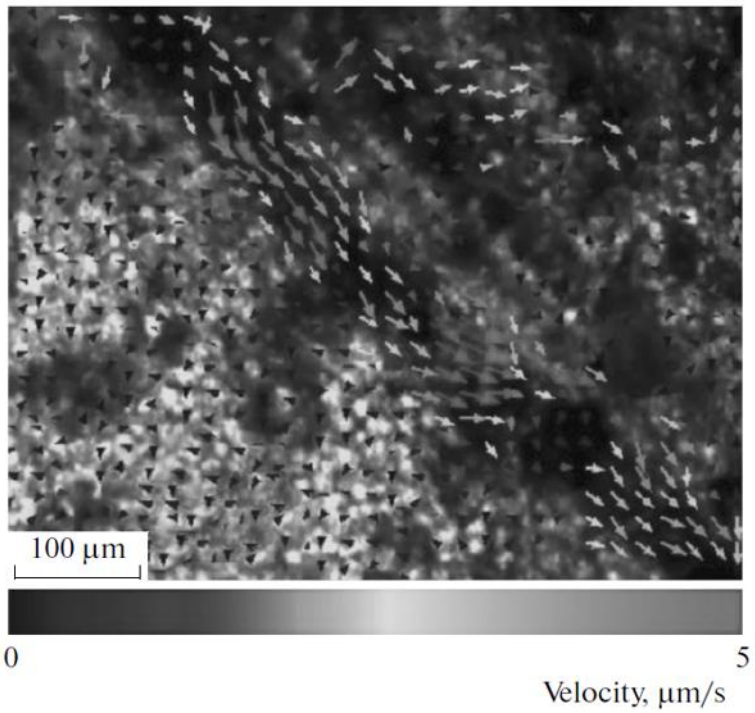

Fig. 1.2. Monochrome image of the blood flow obtained an hour after euthanasia. The arrows show the motion direction of the blood corpuscles and their average velocity (*18*).

Inspired by the 2013 study (*18*), in 2016 Stiukhina et al. (*19*) studied the postmortem blood flow using a chick embryo chorioallantoic membrane (CAM) model. Fertilized chicken eggs were incubated for 10 to 15 days, and the heart was arrested by injection of potassium chloride. The blood flow was measured afterwards (Fig. 1.3). It was reported that the blood flow lasted up to 30 minutes, a surprisingly long time for a small-size object as chick embryo. In this work, the author tried to describe the postmortem blood flow with a modified Windkessel model, a model that is based on pressure gradient driven flow. The model failed to explain the flow: according to the simulation, the cessation of blood flow should occur within 10 seconds instead of 30 minutes. In their conclusion section, the authors noted: "Our main finding is that this happens not as may be 'naively' expected thinking in terms of basic physical laws. At least, the experimentally observed behavior is not consistent with simple model of two connected chambers."

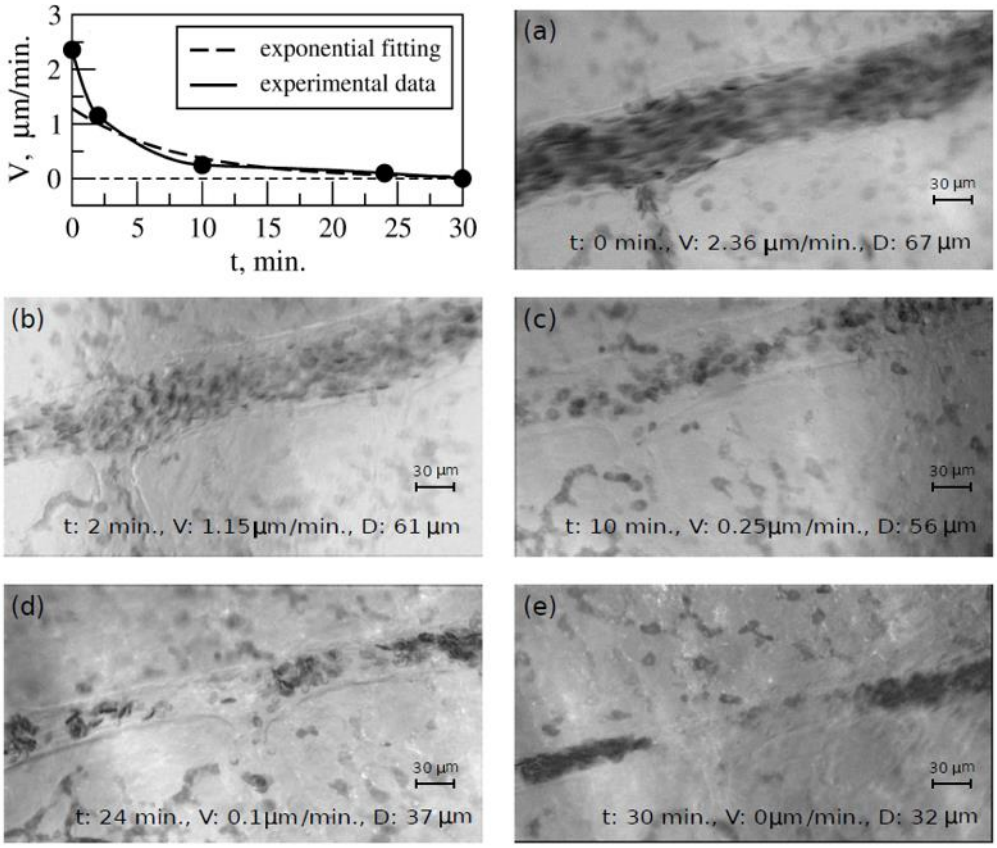

Fig. 1.3. Postmortem blood flow dynamic in chick embryo chorioallantoic membrane CAM. Panels (a) - (e) indicate the observed changes in blood velocity and vessel diameter. The top left plot summarizes the data on drop of blood velocity with time. Note that the single-timescale exponential approximation (dashed line) is not suitable (*19*).

During my PhD project, I actively sought evidence of postmortem blood flow. However, the above three studies are the only ones I could find in the modern literature, i.e., during most recent 20 years.

On the other hand, older studies go back to the 1960s. Manteuffel-Szoege studied postmortem blood flow in dogs. He found that blood flow in canine omental vessels persisted for up to 2 hours after asphyxiation (*20*). The author further studied postmortem blood flow in other models, and reported that following surgical removal of the heart in four-day old chick embryos, flow persisted

for up to 15 minutes (*21*). He also did hypothermia studies on the chick embryo, and found that at lowered temperature (20-25 °C), even though the heart was still beating, the blood was not flowing. Blood accumulated the capillaries. He concluded that: "I believe that the observations I have put forward favor the conception that there exists, besides the work of the heart, another, additional, source of circulatory energy. The additional energy of the circulation manifests itself most distinctly in the venous system and is strictly connected, as is the whole circulatory action, with the temperature in various organs (*21*)."

In 1964, Manteuffel-Szoege also documented "vestigial movement" of blood in excised organs of dogs (hearts, kidneys and livers) (*22*). In the excised heart, the coronary sinus opening bled, but the coronary arteries remained empty. In the excised kidney, only the veins bled, while the artery was empty (Fig. 1.4). In the excised liver, the hepatic veins bled but the portal vein was empty.

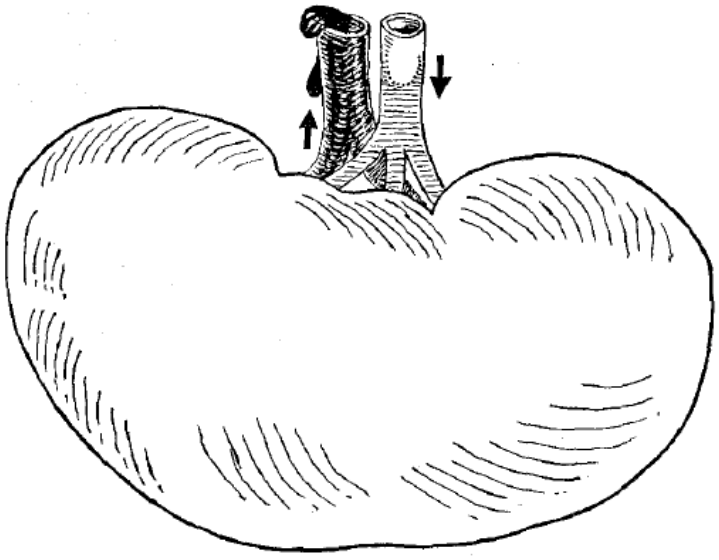

Fig. 1.4. Semi-diagrammatic drawing of kidney, showing the "vestigial movement" of blood in the vessels immediately after separating the organ from the body. The blood flows out, drop

after drop, from the vein. The artery is not bleeding. Its lumen is dry. Deep in the artery, a concave meniscus of blood could be observed, retreating slowly towards inside (*22*) .

In Manteuffel-Szoege's 1966 publication (*20*) , he used the phrase "blood having its own motive energy". He did not comment on how the blood gained its own motive energy.

It is worth noting that all the publications by Manteuffel-Szoege received little attention. His work has been cited very few times over the past 50 years.

Even earlier evidence on postmortem blood flow goes back to thousands of years, and was documented in a unique way. The word "artery" itself is the evidence. The ancient Greeks found the arteries of the deceased devoid of blood; thus, the artery was initially considered as an "air duct" (in Greek, "*ἀρτηρία", in Latin characters, "arteria")*. This finding not only led to the coining of the word "artery", but also to the (mis)understanding that air circulates in arteries, a concept that initially hindered the development of circulation theory (*23*). Today, we all know that the arteries are filled with blood when the animal is alive. Empty arteries indicate that the blood moved away from the arteries after the heart stopped beating.

Other counter-intuitive evidence

The postmortem blood flow is only the tip of the iceberg. Evidence that shows the inadequacy of the current model is hardly sparse---on the contrary, I have found too much to reasonably include in this thesis.

Here I will just pick out several examples, which raise question as to the adequacy of the current model:

-The embryonic vertebrate heart is usually considered as a peristaltic pump. A peristaltic pump pushes the blood through the heart tube by progressively reducing the tube volume (*24*). However,

Forouhar el al. (*25*) found that in embryonic zebrafish heart, blood cell trajectories do not follow local endocardial wave trajectories and exhibit velocities *greater* than those of the traveling wave. How is that possible?

-When atropine, a medication that make the heart pump more strongly, is injected into a patient, the cardiac output starts to increase considerably. But after about two minutes the venous pressure goes down; and the cardiac output is reduced to its original level (*26*). With increased pressure gradient from the heart, the cardiac output could not continue to increase. A similar result was reported by Henderson et al (*27*). When adrenalin was injected into a cat, only the arterial blood pressure increased; the venous pressure increased briefly, quickly decreasing to its previous level (*27*). If the blood pressure is the only driving force in the whole vascular system, then, when the heart pumps harder, the venous pressure should increase accordingly. But it does not.

-For patients with coarctation of the aorta, the arterial blood pressure in the upper body is high, while the arterial blood pressure in lower body is low. However, the venous pressure of the femoral veins in the leg, is higher than then cubital veins in the arm (*26*). If the arterial pressure determines venous pressure, then a lower arterial pressure gradient should result a lower venous pressure, but it does not.

I would like to list a few references here for the interested readers. My major reference is B. Furst's 2014 book (*28*), *The Heart and Circulation - An Integrative Model.* This book cites over 800 supporting references regarding the inadequacy of the current blood circulation model (*29*). A capsuled version by Furst (*30*) and an even more capsuled version by Alexander (*29*) can provide a quick read. I also found other literature that questions the current circulation model (*21, 23, 26, 27, 31-33*).

All the evidence listed here suggests that a mechanism can drive flow without a pressure gradient should exist — especially the evidence that blood can continue to flow even when the heart is not pumping. What mechanism could possibly do that?

In the next section, I will review a phenomenon that allows fluid to flow without a pressure gradient — the "self-driven flow."

1.3 Exclusion Zone and self-driven flow

Self-driven flow is a flow that occurs spontaneously in a tube/tunnel made with hydrophilic material or hydrogel.

The self-driven flow was a side finding, observed during studies on the Exclusion Zone (EZ) — the latter being an aqueous region formed next to various solid-water interfaces, that exclude suspended particles and many solutes.

In most previous experiments, EZ was studied by immersing a tube made of hydrophilic material into an aqueous microsphere suspension. The microspheres are tiny polystyrene spheres, with a diameter of 1-2 μm. The role of the microspheres is to enable visualization of the EZ. The microspheres move away from the tube wall, leaving a microsphere-free zone, which we label the "EZ." Inside the tube, we found flow that was essentially incessant. The term "self-driven flow" was coined as a descriptive name for this intriguing flow.

Subsequent studies showed that EZ was critical to the formation of the self-driven flow. To understand the mechanism of self-driven flow, it is important to understand EZ. Thus, in this section, EZ will be introduced before self-driven flow.

Exclusion Zone

Interfacial water

Water is the essence of life. Water makes metabolism possible: nutrients and wastes can be easily dissolved in liquid water, conveniently transported, and exchanged between cells and the environment. Albert Szent-Gyorgyi, the father of modern biochemistry, suggested: "Life is water, dancing to the tune of solids."

The omnipresent existence of water makes it a seemingly usual substance. The real situation, however, is that water is one of the most unusual substances (*34*, *35*). For starters, it is extremely rare to find a non-carbon-containing compound in nature to be a liquid at standard temperature and pressure; but water is liquid at standard temperature and pressure. Most substances in nature are denser when the temperature is lowered; but the solid form of water, ice, has a density that is lower than liquid water. Further, the surface tension of water is surprisingly high, among all liquids lower only than mercury.

At the interface where water meets a solid material, the properties of water differ. Many earlier studies suggest that the water adjacent to hydrophilic surfaces has different characteristics than bulk water, both physically and chemically (*36*, *37*). Interfacial water became the major topic of our laboratory (Pollack Lab, Bioengineering department, University of Washington) since 2003.

One of the most interesting phenomena that happens at the interface is the presence of an Exclusion Zone (EZ) — a region formed at multiple solid-water interfaces that excludes particles and most solute. Fig. 1.5 shows an example of an EZ.

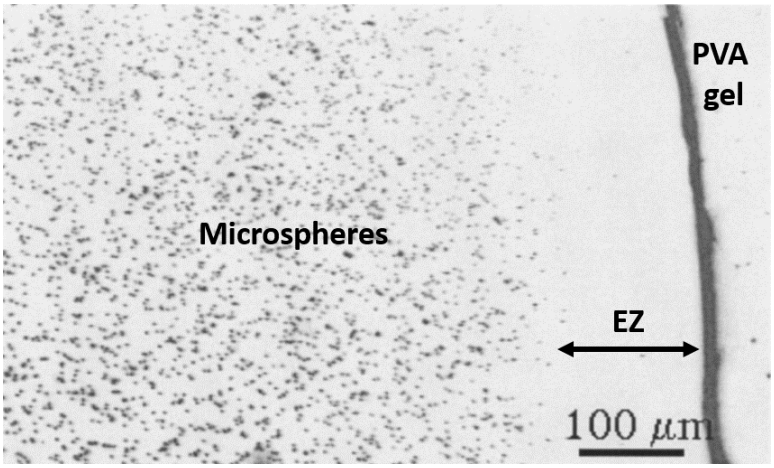

Fig. 1.5. EZ next to a piece of PVA (polyvinyl alcohol) gel. The black dots are microspheres (polystyrene microspheres with carboxylate functional groups), which are excluded from the exclusion zone (*38*).

Such exclusion zones were observed in the vicinity of many types of surfaces, including artificial and natural hydrogels, biological tissues, hydrophilic polymers, monolayers, ion-exchange beads (*39*) and metals (*40*).

Profound solute exclusion is only one distinguishing feature. Several other physicochemical features differentiate EZ water compared to ordinary bulk water: (1) EZ absorbs light at 270 nm. (2) EZ emits less infrared radiation than bulk water. (3) EZ shows more molecular restriction under magnetic resonance imaging (MRI). (4) EZ has a higher viscosity than bulk water. (5) Charge separation happens across the EZ boundary. These differences have been reported in multiple journal publications (*38-44*), and summarized in a recent book (*45*).

For the self-driven flow, the **charge separation** at the far EZ boundary is the most important feature, and also the topic of next section.

Charge separation

EZ is charged. For most cases, the EZ is negatively charged and the bulk water beyond the EZ is positively charged.

The electrical potential distribution can be measured by using microelectrodes (*44*). Fig. 1.6 shows the experimental configuration to measure the potential distribution in the EZ. A piece of hydrophilic material that generates EZ — in this study, PAA (polyacrylic acid) or Nafion — was placed at the bottom of the chamber. The measurement microelectrode was controlled by a stepwise motor, which allowed the electrode to move along the vertical axis. The reference electrode was placed in the bulk water. By gradually advancing the position of the measurement electrode, the electrical potential between the two electrodes could be measured. Zero potential difference was set as the probe electrode just pierced the solution surface, after which the probe was driven downward.

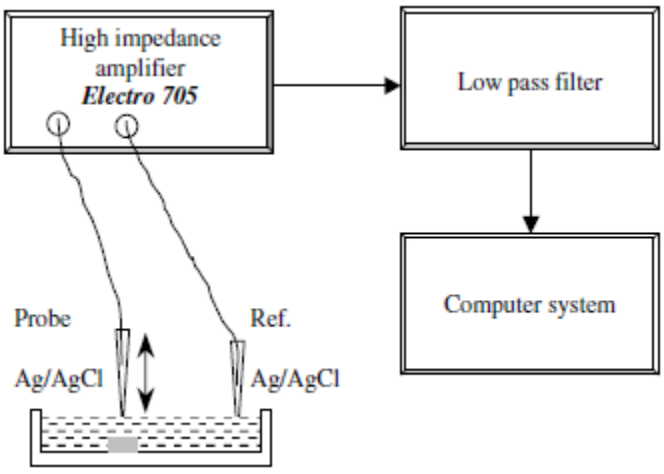

Fig. 1.6. Schematic of instrumentation used for measuring electrical potential of EZ (*44*). The result is shown in Fig. 1.7. Negative potentials were observed in both cases. The magnitude of the negative potential increased as the probe approached the specimen surface (right to left in the

figure). It increased gradually at first, and then more steeply within several hundred micrometers of the surface. This result indicated that the EZ was negatively charged.

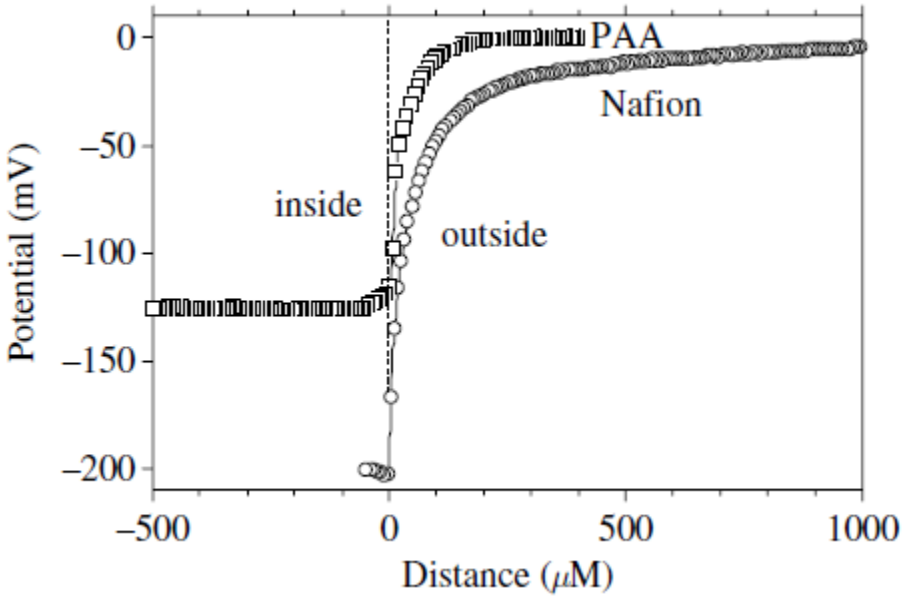

Fig. 1.7. Electrical potentials measured in the vicinity of Nafion and PAA gel surfaces (*44*). "Inside" refers to inside the gel. "Outside" refers to the aqueous zone.

The positively charged region that was found to exist beyond EZ was confirmed by pH dye experiments (*43*). A thin Nafion film was first cut and glued at the base of a chamber, which was made from standard microscope slides. Standard pH dye was then diluted and poured slowly into the chamber. The local pH change was recorded using a camera.

The result is shown in Fig. 1.8. At the Nafion-water interface, the dye was excluded; i.e., it was excluded from the EZ. In the region beyond the EZ, the red color indicated a region of low pH. The result shows that the region beyond EZ contains positively charged protons.

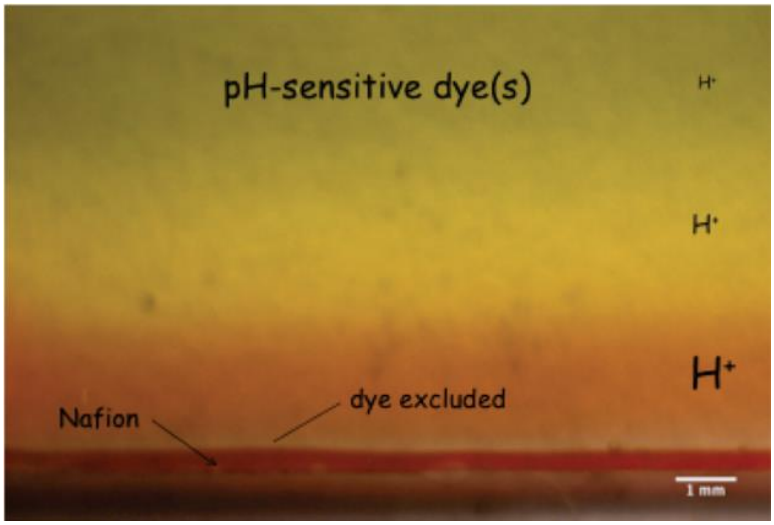

Fig. 1.8. Chamber containing Nafion tube (bottom), and filled with water containing pH-sensitive dye. The view is normal to the wide face of a narrow chamber. The image was obtained 5 min after the dye-containing solution was added to the chamber. The red color indicates pH < 3; the colors above the red indicate progressively higher pH levels, with near neutrality at the top (*43*).

In less common cases, EZ is positively charged, while the bulk water beyond is negatively charged (*40*, *45*). Positively charged EZ has been observed next to various metals as well as cationic ion-exchanged gel beads. Fig. 1.9shows the electrical potential distribution in EZ next to zinc and aluminum. The positive electrical potential distribution indicates that EZ is positively charged. The negatively charged region in bulk water was confirmed with pH sensitive dye. The region beyond had a higher pH, indicating the existence of negatively charged hydroxyl groups, as shown in Fig. 1.10.

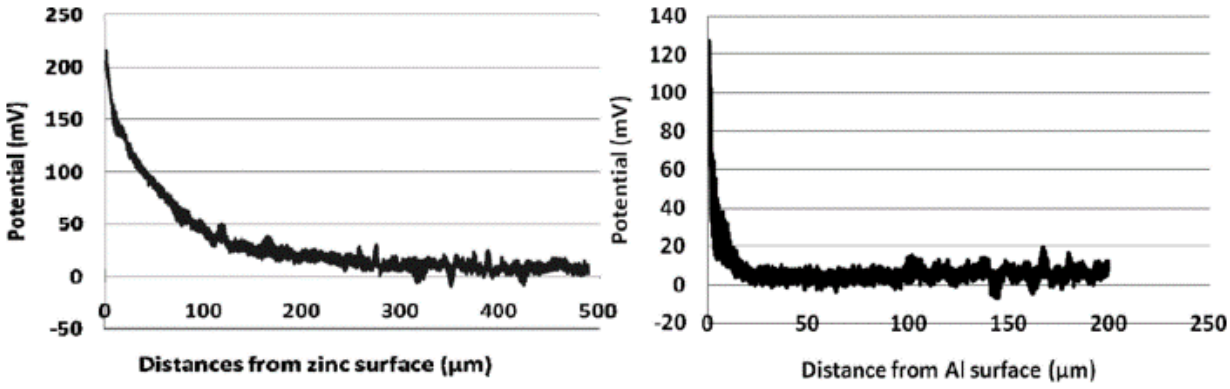

Fig. 1.9. Potential distribution near surfaces of zinc and aluminum. In both panels the results are averages of three measurements (*40*).

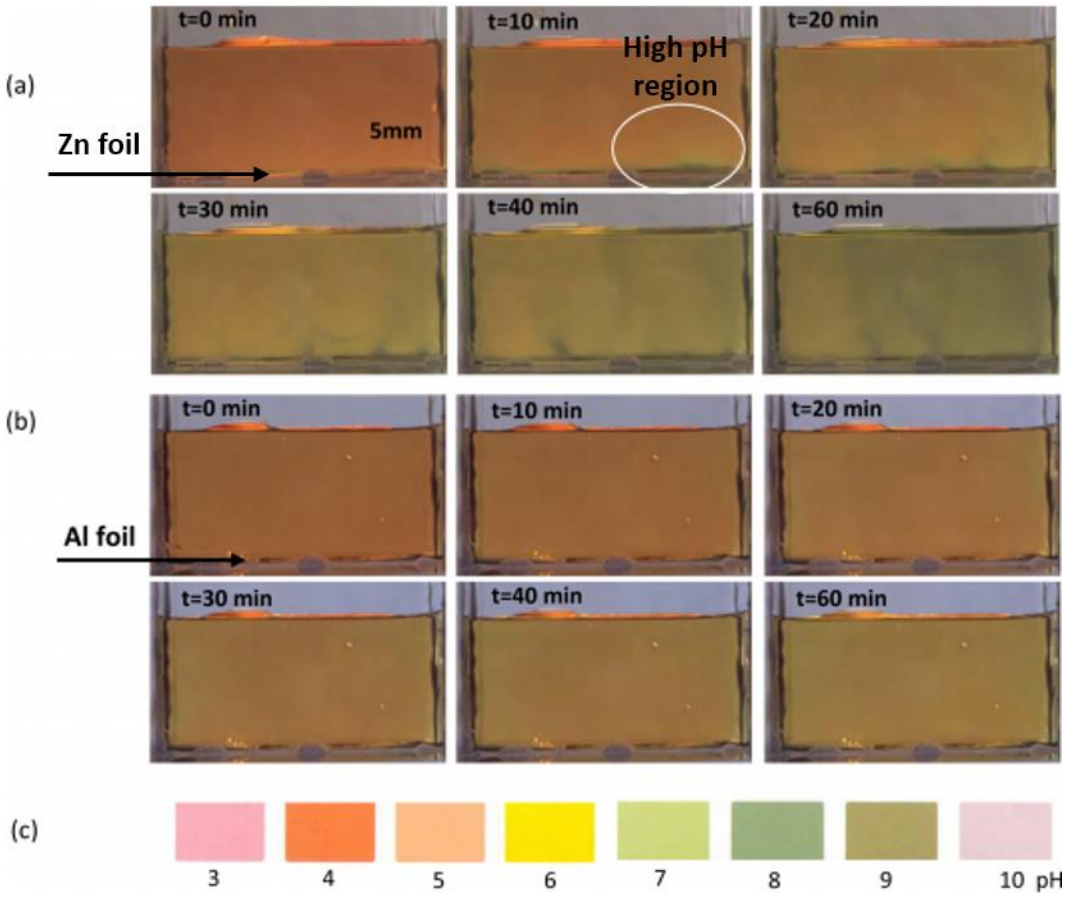

Fig. 1.10. Time course of pH changes when a zinc (a) or aluminum (b) sheet covered the bottom of the glass chamber containing pH indicator. In (a), notice the green region, which indicated a high pH region. In (b), notice the color turned green gradually, which indicated increasing pH. (c) pH color scale for universal pH indicator (*40*).

In sum, to form the EZ, positive charges and negative charges separate. In most cases, the negative charges coalesce to form the EZ, while the positive charges are released beyond.

To separate charges, energy is needed. In this process, light can be utilized as a source of energy.

Light as energy source to grow/expand the EZ

An accidental discovery showed that light can expand EZ (*46*). Thus, the effect of light on the EZ was systematically studied.

Light with different wavelengths was shone through a pinhole into an experimental chamber that contained Nafion and a polystyrene carboxylate microsphere suspension. Each of various LEDs were used as the light source, covering the UV-Vis-IR range. The goal was to see how effectively each of those wavelengths could expand the exclusion zone.

The results are shown in Fig. 1.11. Light effectively expanded EZ, with infrared (IR) radiation being the most effective wavelength range.

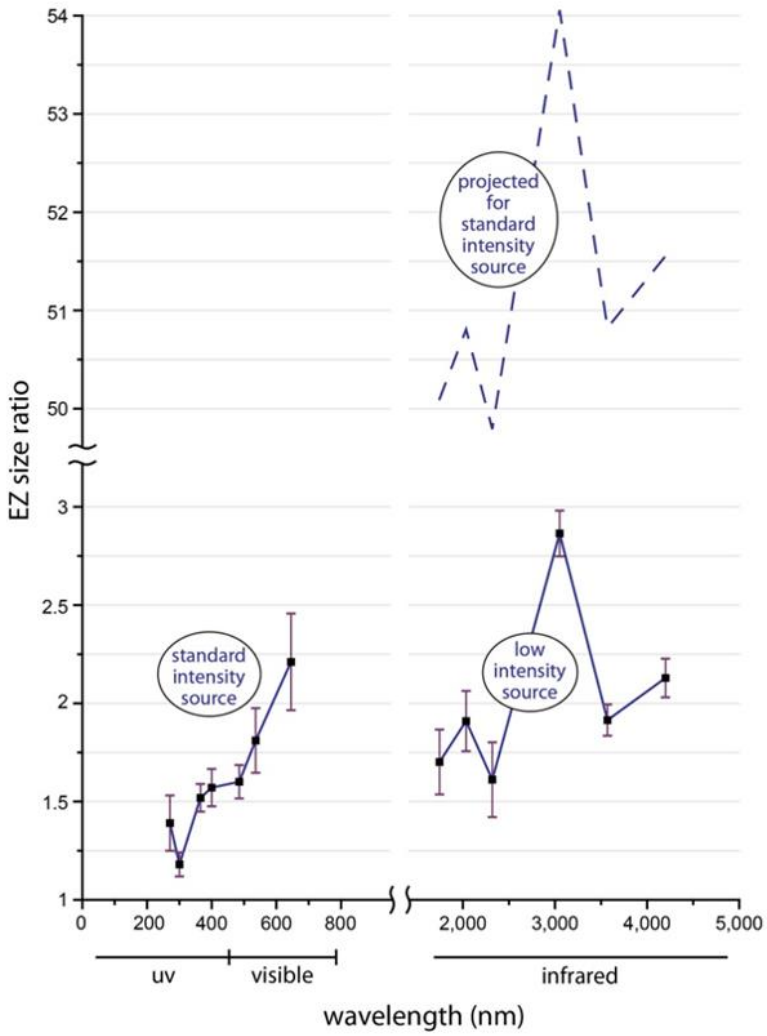

Fig. 1.11. Effect of incident light wavelength on EZ growth. EZ size ratio (ordinate) refers to EZ size at the end of a five-minute exposure to light, relative to its size before adding light. For technical reasons, the data on the right side were obtained with low-intensity light sources. Intensities similar to those used for obtaining the data on the left would have elevated the graph, as estimated by the dashed curve above (*47*).

Also tested was the intensity of light vs. the EZ expansion ratio. An LED that emitted IR at 2100 nm was shone into Nafion-microsphere suspension contained in a chamber. Different power

outputs were tested. The result is shown in Fig. 1.12. Increasing the intensity of the IR effectively expanded the size of EZ.

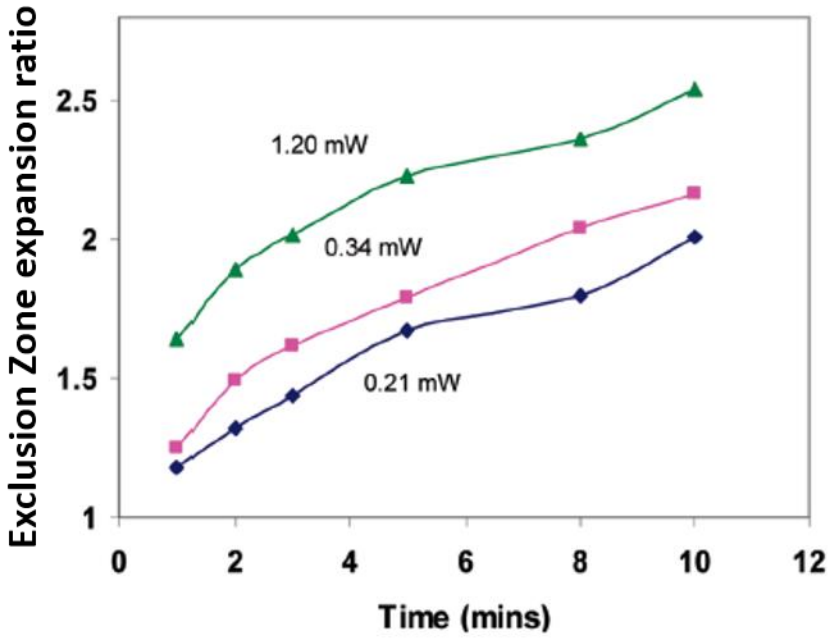

Fig. 1.12. EZ expansion ratios as a function of time during 10 min exposure at different intensities using an LED that emits IR at a wavelength of 2100 nm (*43*).

Light expands EZ, and the expansion of EZ is associated with charge separation. Thus, light facilitates charge separation at the interface.

Current hypothesis

EZ is currently hypothesized to arise from a water-surface interaction. Water molecules at the interface split into two parts after absorbing radiant energy. The negatively charged parts, the hydroxyl groups, form the negatively charged, ordered EZ region (Fig. 1.13). On the other hand, the positively charged parts are released into the region of bulk water beyond.

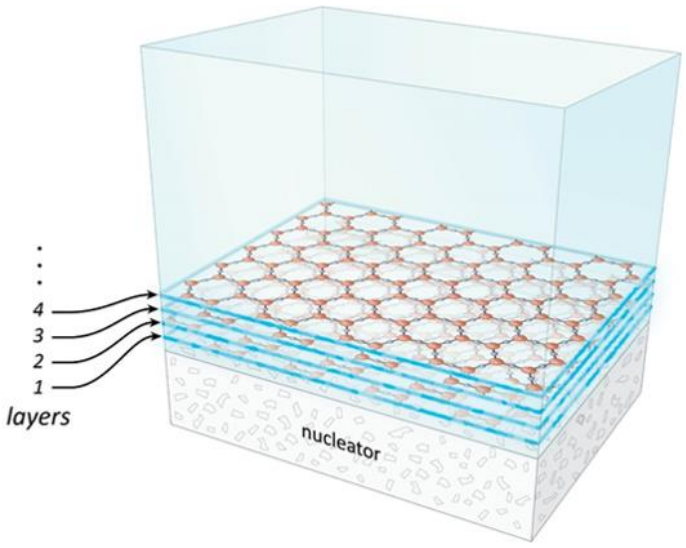

Fig. 1.13. Current hypothesis on the formation of EZ. After absorbing radiant energy (light), water molecules split into two parts. The negative parts (hydroxyl groups) form sheets of honeycomb structure building from the nucleator surface, stacking layer by layer. The positive parts, protons (not shown in this figure), are released into the region beyond (*48*).

A detailed model has been proposed in the 2013 book *The Fourth Phase of Water (48),* written by my advisor, Dr. Gerald Pollack.

Now, with all the background knowledge, we can move to the issue of self-driven flow.

Self-driven flow

Prior to my PhD project, two studies were published on the topic of self-driven flow. One named: *Unexpected axial flow through hydrophilic tubes: Implications for energetics of water,* by Yu et al. (*49*); Another one: *Flow through Horizontal Tubes Submerged in Water in the Absence of a Pressure Gradient: Mechanistic Considerations*, by Rohani et al. (*50*). These two papers will be referred as Yu study and Rohani study. This section will review the main findings of these two studies.

Features of Self-driven flow

It is quite straightforward to observe self-driven flow. A typical experiment starts by cutting a section of Nafion tube. This piece of Nafion tube is first hydrated in de-ionized water for 10 minutes. Then the tube is immersed horizontally at the bottom of a chamber filled with a microsphere suspension, ready for observation with a microscope.

During the first several minutes, the microspheres within the Nafion tube exhibit jittery back-and-forth motions, which can be attributed to Brownian motion and drift. Towards the end of this transition period, an axial flow develops gradually in a single direction.

In some experiments the direction of flow might change during this transition period of approximately 5 min, but after this time it finally becomes unidirectional.

In the Yu study, 'significant fluid flow was defined as particle movement in an axial direction whose velocity was higher than 0.5 μm/second. The axial velocities of the particles were on the order of ~10^1-10^2 μm/s. The flow could last hours. This is a slow and stable flow. The calculated Reynolds number is many orders of magnitude below that required to produce turbulence.

Besides the flow in Nafion tubes, self-driven flow and EZ (Fig. 1.14) have also been reported in tunnels made of various hydrophilic materials, including poly(acrylic acid) (PAA) (*49*), poly(ethylene glycol) (PEG), and poly(vinyl alcohol) (PVA) (*50*).

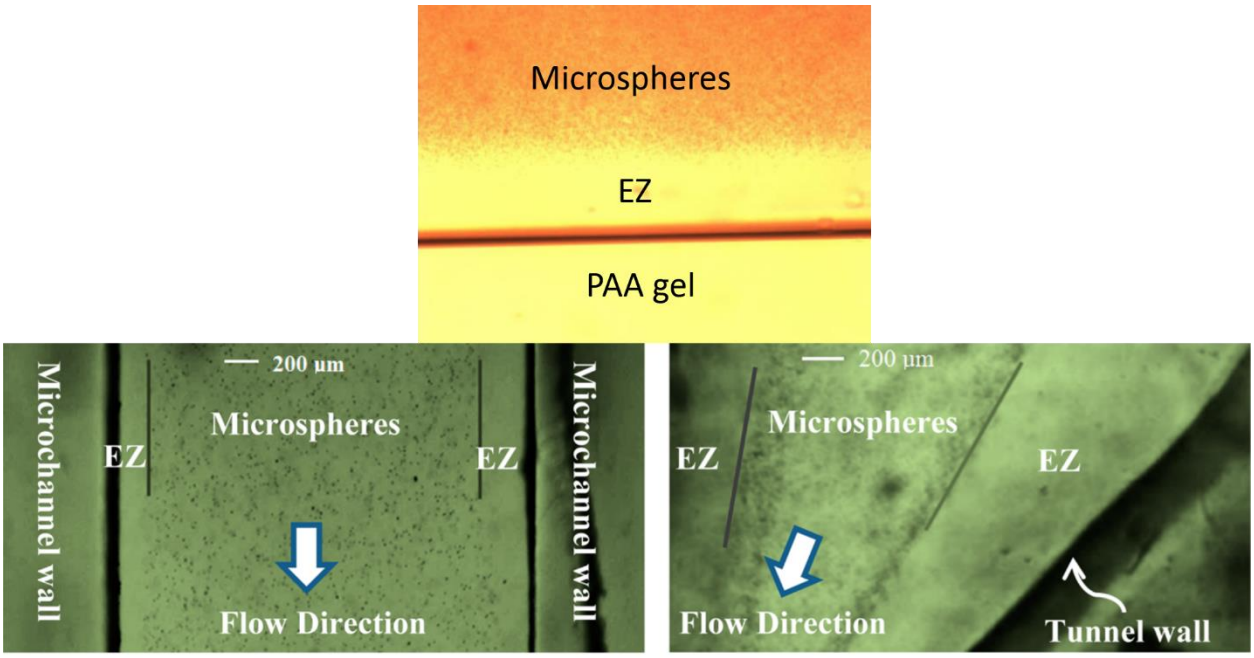

Fig. 1.14. EZs observed next to PVA, PEG, and PVA. Top: EZ next to PAA gel, reconstructed from Yu study (*49*); Bottom: EZ next to the inner wall of PEG and PVA tunnels, from Rohani study (*50*). The tunnels are made by either molding or boring.

The flow velocity varied among the different materials. In the Rohani study(*50*), the flow velocity in PVA could sometimes reach 100 μm/s, although that flow did not persist as long as that in Nafion tube (typical velocity of 10 μm/s). PEG tunnels showed slower flow velocity (5 μm/s) but could persist for several hours. In Yu study (*49*), the mean velocity of the flow in PAA tunnel was ~20 μm/s.

Teflon tubes were employed in Yu study (*49*) as a negative control, i.e. no flow was expected. The axial velocities of the particles in Teflon tubes were never higher than 0.5 μm/s; instead, minor drifts and Brownian motions were observed.

What is the direction of the self-driven flow? This is usually the first question raised by audiences. Based on these two studies, however, the answer was not quite straightforward.

In the most studied experimental model, the Nafion tube, the direction of self-driven flows was unpredictable — sometimes in one direction, other times in the opposite direction.

In both Rohani study and Yu study, the flow direction was hypothesized to be determined by the asymmetry feature of the tube/tunnel. This hypothesis was tested in both studies. The commercially available Nafion tube are symmetric; thus, follow-up studies were done using tapered tunnels made with other materials.

The results were conflicting. In tapered polyacrylic-acid tunnels, Yu et al. reported flow pointed from the smaller end to the larger end (*49*); but in polyvinyl alcohol tunnels, Rohani et al. reported flow pointed from the larger end to the smaller end (*50*). In the Rohani study, a comment was made on the flow direction: "Serious efforts in the future may settle this interesting but challenging question."

The diameter of the tube should affect the self-driven flow. The effect of tunnel diameter was studied, and the results were conflicting as well. In the Yu study, it was briefly mentioned that decreasing the diameter of the PAA tunnel increased the flow velocity by a factor of almost 300% (*49*). However, in the Rohani study, flow velocities decreased with decreasing the diameter of the Nafion tube (*50*).

Proton concentration gradient as the driving mechanism

What drives the self-driven flow in the absence of any pressure gradient? The flow is hypothesized to be driven by a proton concentration gradient[1] (*49-51*). In a piece of Nafion tube filled with water (Fig. 1.15), an annular EZ builds at the inner wall of the tube (Fig. 1.15a) in the presence of radiant energy. As the EZ builds, positively charged protons are released into the core of the tube (Fig. 1.15b). As the concentration of the protons rises, the accumulated protons will exit the tube because of self-repulsion, thereby forming a flow (Fig. 1.15c).

[1] To be precise, the concentration gradient should be hydronium concentration gradient, since protons will combine with a water molecule and form hydronium ions. For the sake of simplicity, the hydronium ions are referred as protons.

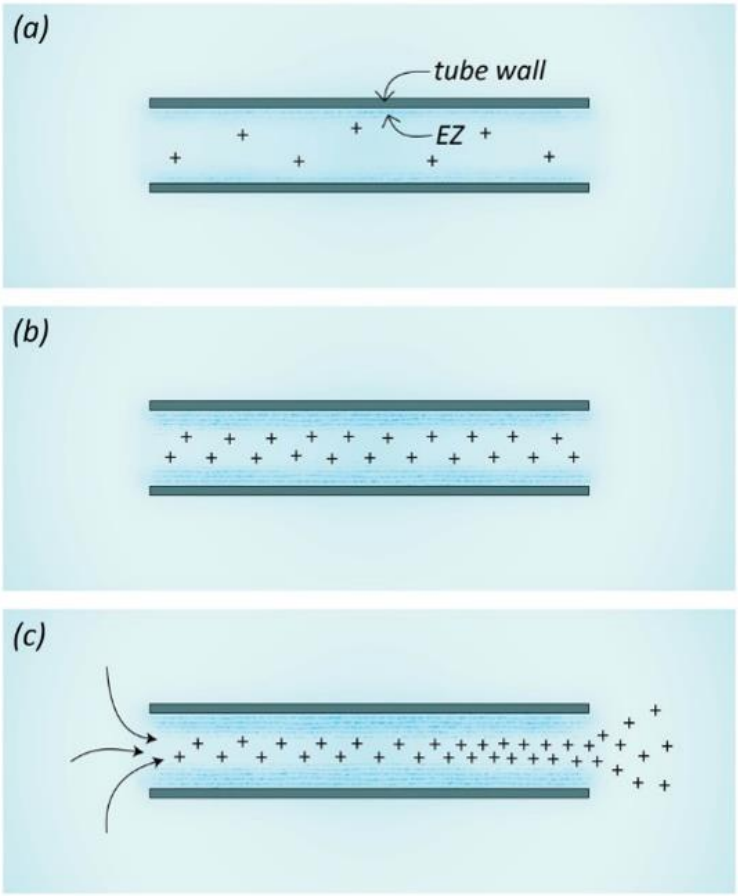

Fig. 1.15. Mechanism of self-driven flow (*51*).

An expectation of this proton concentration gradient hypothesis is that the protons will accumulate in the chamber and decrease the pH of the chamber water. This expectation was tested and confirmed in the Rohani study. For self-driven flow in Nafion tubes, the pH in the chamber decreased from 7.48 to 2.77 over 2.5 hours. The pH decline stopped when the flow stopped (*50*).

Another piece of evidence supporting the proton concentration gradient hypothesis is that the chamber size had a positive correlation with the duration of the self-driven flow (Fig. 1.16) (*50*). Nafion tubes were used in this study. In the largest chamber with a volume of 6,000 µl, self-driven flow was also the longest-lasting, usually persisting for more than 1.5 days. In smaller chambers,

with a volume of 350 µl, flow duration did not exceed 3 to 4 hours. The finding that the duration of the flow is proportional to the chamber size is in line with the proton gradient hypothesis.

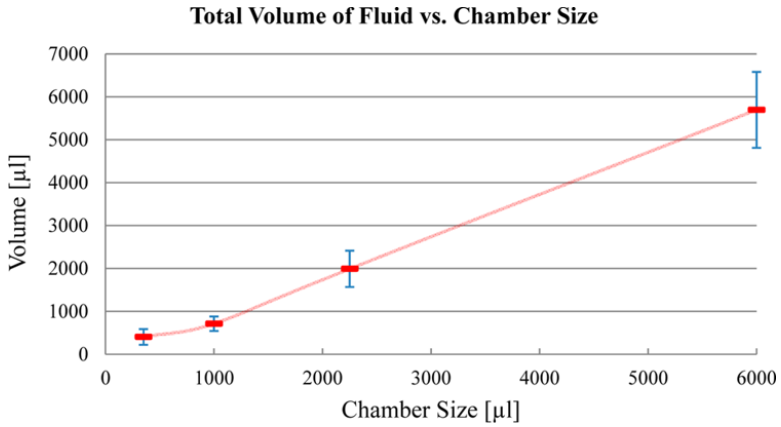

Fig. 1.16. Total volume of fluid passing through the tube before flow ceased, for various chamber sizes.Averaged data in red; standard deviations in blue (*50*).

From the studies described above, a natural conclusion is that a proton concentration gradient is the driving mechanism. Charge separation happens at hydrophilic surfaces, as protons are released into the region beyond EZ. If the hydrophilic surface in question is the inner surface of a wall/tube, the protons that are constantly accumulating in the core of the tube must repel one another. Repulsion will cause the protons to exit at one end of the tube or the other.

Similarly, in situations in which the EZ is positive and the charges released beyond the EZ are negative, the negative charges should generate a flow in a similar way. Thus, a more generic hypothesis is that a "charge concentration gradient" drives the flow. The concentration gradient could arise from protons (positive) or OH groups (negative).

Ultimately, the cause of the self-driven flow is the charge separation that occurs at the inner surface of the tube.

Light as an energy source

If light can facilitate the charge separation (*43*), then light should enhance the self-driven flow.

Rohani et al. tested the effect of light on self-driven flow in Nafion tubes. The halogen lamp from the microscope, with adjustable intensity, was used as the first type of light source. The lamp produces white light (wavelength range 400-1000 nm, peaking at ~600 nm), and the effect of white light intensity on self-driven flow velocity was studied. The result is shown in Fig. 1.17: the self-driven flow velocity increased with increased light intensity.

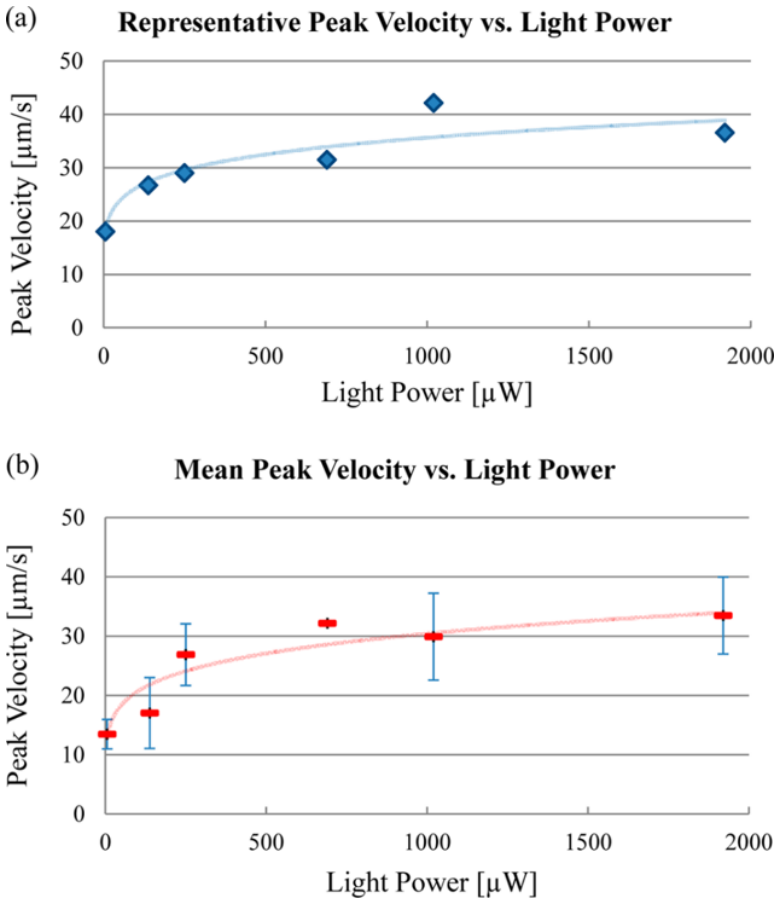

Fig. 1.17. Effect of white light power on peak velocity. (a) representative test; and (b) mean peak velocity (n = 4). The means are shown in red, and the standard deviation is shown in blue (*50*).

The second type of light tested was a combination of white light and a custom-made UV-Vis lamp (wavelength range 332-392 nm, peak at 365 nm). The effect of UV light is shown in Fig. 1.18. When UV light was turned on, the flow velocity could be boosted by up to five times. The boost was not long-lasting. The boost lasted for ~ 20 minutes, after which the flow velocity quickly decreased, and flow stopped. This could be explained by proton concentration gradient: after receiving UV illumination, more protons released, more quickly filling the chamber and therefore more quickly stopping the flow.

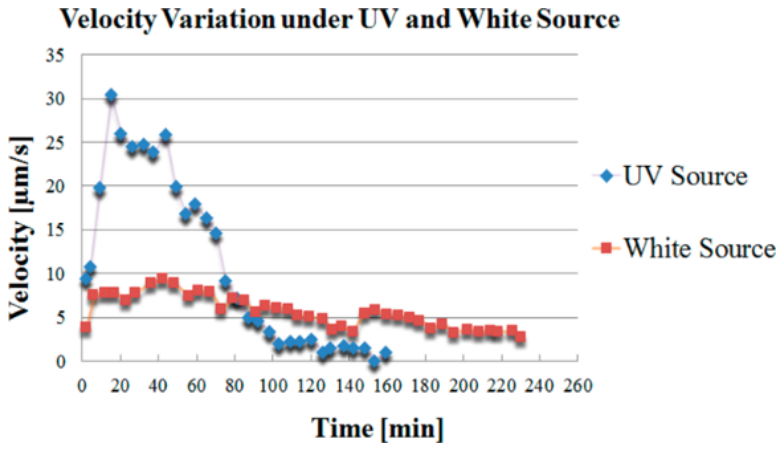

Fig. 1.18. Velocity variation over time with the white light source and UV source at the same optical power levels.Representative runs are shown (*50*).

A protocol of alternating white light source and UV light source was adapted as well. The flow was enhanced while UV was on; and decreased when UV was turned off. Fig. 1.19 shows a representative example.

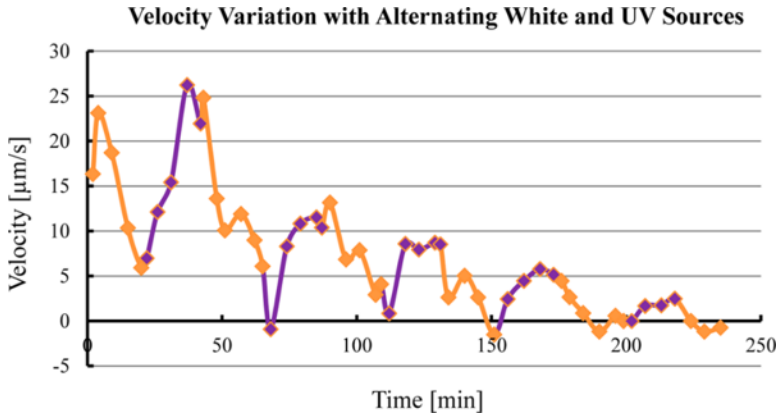

Fig. 1.19 Effects of alternating white and UV sources on the measured velocity.Purple corresponds to the period of UV illumination, and gold corresponds to the period of white light illumination. White and UV illumination were alternatively applied to the sample every 20 minutes (*50*).

In sum, the self-driven flow mechanism allows fluid to flow in the absence of a pressure gradient. Flow was observed with several kinds of materials that can generate EZ, including Nafion, PVA, PAA and PEG. It was not observed with (hydrophobic) materials that cannot generate EZ, such as Teflon. The driving force was hypothesized to arise from the repulsion force among protons, and the protons are originated from water-surface interaction. High proton concentration within the tube forms a gradient with the low proton concentration outside the tube, driving the flow. The mechanism underlying the direction of the flow has remained unclear.

An important feature of self-driven flow is the utilization of electromagnetic radiation energy —i.e., light. Light enhances the self-driven flow, confirmed with both full spectrum white light and UV.

If the self-driven flow were utilized in the cardiovascular circulatory system, then, a logical (though seemingly radical) prediction can be made: incident light could make the blood flow faster; and, light could perpetuate flow even after the heart had stopped beating.

Testing those hypotheses constitutes the ultimate goal of this PhD thesis.

1.4 Aims

The goal of this PhD project was to explore whether light could be an auxiliary source of energy for driving blood circulation, through the self-driven flow mechanism.

In this context several questions arise:

1) How general is the self-driven flow? Does it generally exist in nature, or are they merely a specific feature of certain materials?

2) What caused the inconsistency in the direction of the self-driven flow? From the previous studies, it was clear that the geometry of the tunnel determined the direction, but the results contradicted one another. According to the proton concentration gradient hypothesis, a flow should flow to the narrower part to the wider part in a tapered tunnel, since the protons are originated from the inner surface of the tunnel, and a narrower tunnel has a higher surface to volume ratio. Yet, the results are conflicting with each other. The inconsistency indicates that mechanisms other than proton concentration gradients induced by water-surface interaction might be at play. What are they?

3) What is the most effective wavelength to drive self-driven flow?

4) What would be a good *in vivo* model to explore the existence of self-driven flow in circulatory system?

5) Will that effective light for drive self-driven flow drive the blood flow? Even after the heart has stopped beating?

We will attempt to answer these questions in the following chapters.

Before that, I will review what has been found on the effect of light on the circulation, to see what is already known about this topic.

Chapter 2. Effect of light on the circulation: a mini review

This chapter reviews the effect of light on circulation.

If a self-driven flow mechanism exists in the circulatory system, then the effect should exist in blood vessels, drive the blood *directly and locally*, instead of driving the blood flow by imposing a pressure gradient at some remote locale. A proper experiment for distinguishing between these hypotheses should be testing the effect of light on a postmortem blood flow model, to see whether light have any effects after the source of the pressure gradient, heart, is excluded. Yet, this kind of experiment has not been reported to the best of my knowledge.

Nevertheless, I reviewed previous studies regarding the effect of light on the circulation, to learn how light can affect the blood circulation system. The studies are categorized according to the wavelength range: UV, visible, and infrared.

In general, light affects the circulation system in two ways: ocular or extraocular (through the eye, or not) (*52*). The review focused on the extraocular effects — effect of light on circulation that is irrelevant to the visual perception.

2.1 UV light

Studies of the effects of light date back more than a century. In 1907, Hasselbach and Jacobäus (*53*) reported that repeated exposure of patients with angina pectoris to radiation from a carbon-arc lamp caused a fall in the blood pressure in medium sized arteries; the drop was about 10%. In a 1925 study, Harris (*54*) explored the effect of UV from a mercury-vapor lamp applied to the arms of healthy volunteers. After a latency of 1.5 minutes, he noted a plethysmographically determined increase of blood volume.

In more modern studies, Drouard et al. (1984) (*55*) studied the circulatory effects of light of different UV wavelength ranges (UVA, 290-320 nm; UVB, 290-320 nm, and UVC, 100-280 nm). UV light was applied to the backs of human volunteers. Quantification involved use of laser-Doppler flowmetry, capillary-perfusion monitoring, and a subjective grading of skin erythema. UVA brought no detectable perfusion changes, while UVB and UVC caused tanning, erythema, and increased flow. The percent increases in flow were not given, only the incremental increases.

More recently, Oplander et al. (2009) (*56*) applied whole-body UVA to healthy volunteers to investigate changes of blood pressure. 15 minutes of UVA irradiation caused a rapid, significant decrease of both systolic and diastolic pressure, lasting up to 60 minutes. Also, the author confirmed with electron paramagnetic resonance spectroscopy that UVA significantly increased the intradermal levels of free nitric oxide.

2.2 Visible light

The effect of visible light from an operating microscope was studied on a cat cortical microcirculation model (Bertalanffy et al., 1993) (*57*). The diameters of pial arterioles were measured. After switching the light intensity from 8400 lux to 61000 lux, the diameters dilated slightly, to 106.8 ± 2.6 % of their resting diameters.

Kobayashi et al., (2000) (*58*) used a needle-type laser-doppler blood flowmeter to explore changes in blood flow of the rat's tail skin due to visible-light irradiation. Monochromatic light was exposed to the central region of the tail. Blood flow showed a synchronized transient increase, with peaks at 410-420 nm, 540-550 nm, and 570-580 nm. The increase of blood flow occurred on a scale of 500 milliseconds. The blood flow increase vanished when the rats were first injected with an inhibitor of guanylate cyclase and NO synthase.

Schindl et al., (2002) (*61*) studied the effect of HeNe laser (30 mW, 632.8nm) on the forefoot region of patients with diabetic microangiopathy. The microcirculation was quantified by measuring surface temperature of the foot skin with infrared thermography. HeNe laser light was applied to a randomly chosen foot, while thermographic measurement was made on both feet. The microcirculation improved at both the irradiation site as well as the non-irradiation site.

In a more recent study (Sikka et al., 2014) (*59*), the effects of different optical wavelengths (red, 620-750 nm; green 495-570 nm; and blue 380-495 nm) on blood flow were tested on mouse tails, using laser-Doppler flowmetry. Blue light could increase flow to ~120% of control in 10 minutes (Fig. 2.1). This effect was absent when the Opn4 (melanopsin) gene was knocked out. The authors also studied vasorelaxation on mouse aorta. Force-tension myography showed no vessel response to red or green light, but displayed maximal vaso-relaxation at low-intensity blue light.

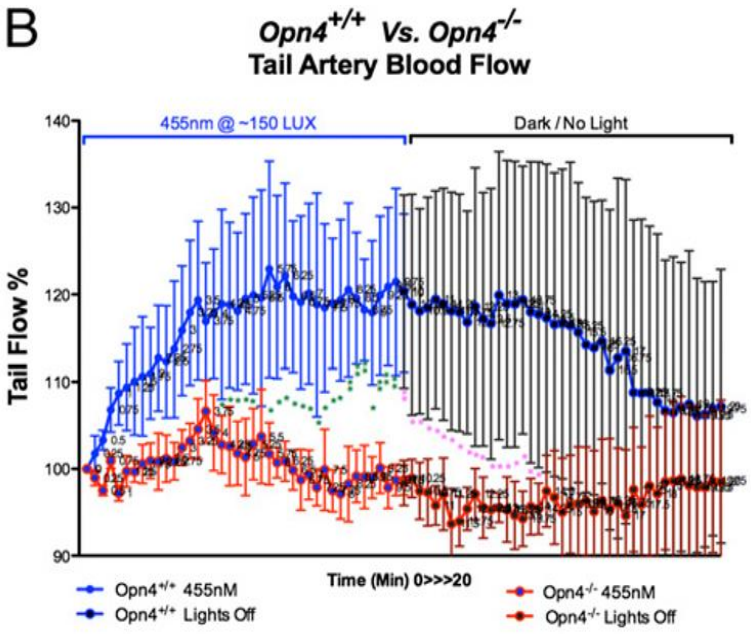

Fig. 2.1. In vivo laser-Doppler flowmetry of mouse tail demonstrates a significant increase in tail blood flow after 10 min of cumulative blue light (455 nm at 40 lux) exposure in $Opn4^{+/+}$ but not in $Opn4^{-/-}$ mice (*59*).

2.3 IR light

In a 2000 study, low-level laser infrared irradiation (LLLI, 830 nm) was applied to the rat mesenteric microcirculation (*60*) (Maegawa et al., 2000). Blood velocity was quantified using a combination of optical microscopy and a velocimeter. Vessel diameter was measured as well. IR light was applied to the mesenteric area for five minutes, and blood velocity and vessel diameter were measured before and afterward. After exposure, arteriolar diameter increased to ~120% of the pre-irradiation value (Fig. 2.2A). Red cell velocity was slightly reduced during light exposure, but reached ~130% of the pre-irradiation value by ~5 min after exposure (Fig. 2.2B). In order to rule out the effect of temperature, the authors increased the temperature by injecting warmed medium to the vessel; no significant arteriolar vasodilation was detected. They also tested the effect of LLLI on surgically denervated mesenteric arterioles, and the response was similar to the non-denervated group. The authors also applied an inhibitor of nitric oxide synthase activity (LLI+L-NAME). LLLI still enhanced the microcirculation although the enhancement was not as large as without the nitric oxide inhibitor. However, in the late stage of LLLI irradiation, enhancement was the same with or without the inhibitor.

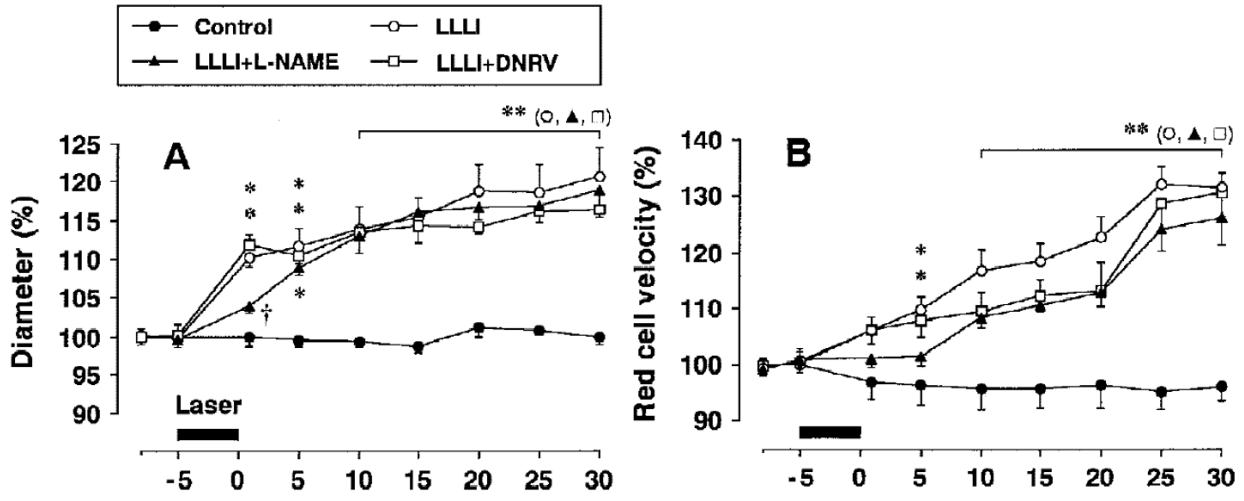

Fig. 2.2. Relative changes in (A) arteriolar diameter, (B) red cell velocity after low-level laser irradiation (*60*).

The effect of far-infrared light (>1,000 nm) on the rat skin was studied using a laser-Doppler flowmeter (Yu et al., 2006) (*62*). Far-infrared light was applied for 30, 45, or 60 minutes. In all experiments, skin blood flow increased significantly after the removal of the FIR emitter, although not during emission (Fig. 2.3). The stimulating effects of IR were suppressed when the animal was pretreated with the inhibitor of nitric oxide synthase activity L-NAME. Nitric oxide can relax smooth muscle, thus increasing microcirculatory flow.

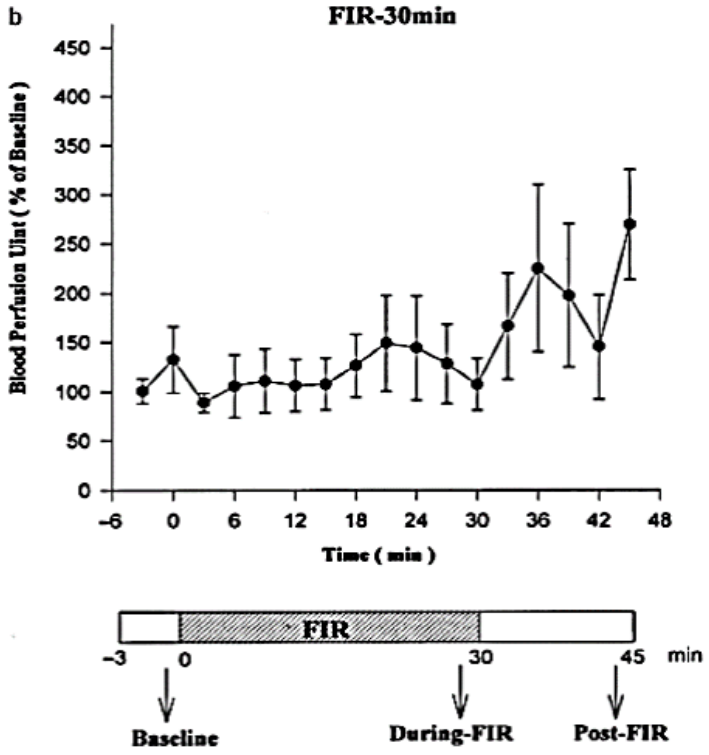

Fig. 2.3. Effect of far-infrared (FIR) therapy (30 min) and post-FIR effect on skin blood flow.There was no significant change of skin blood flow during FIR treatment. Skin blood flow increased significantly after the removal of the FIR emitter (*62*).

The effect of low-intensity laser light therapy, LLLT, (810 nm) was studied on the carotid arteries of cerebral palsy patients (Asagai et al., 2007) (*63*). Blood flow was quantified with Doppler ultrasound color flow imaging system. On the laser-irradiated side a significant increase in blood-vessel cross sectional area was seen after one minute, while a significant increase in blood volume was seen after 3 min, soon reaching a plateau extending over one hour even though the irradiation was removed. Even on the unirradiated side, a significant increase in the cross-sectional area and diameter of the blood vessel and blood flow volume were seen after 10 min, reaching a plateau at 15 minutes and persisting over one hour, even after the light was turned off.

In a study on rabbits, Komori (2008) (*64*) used low-power laser (830 nm) and polarized near-infrared light (600-1600 nm) applied to a rabbit ear chamber model. Microscopy was used to measure vessel diameter. Compared to the values before treatment (100%), the arteriolar diameter increased to 101.9% ± 5.9% in the control group, 130.1% ± 10.4% in the laser group, and 125.2% ± 16.9% in the near-infrared group. Blood-flow velocity increased as well (Fig. 2.4), from a baseline value of 100% to 101.3% ± 3.6% in the control group, 126.3% ± 14.8% in the laser group, and 129.1% ± 16.8% in the near-infrared group.

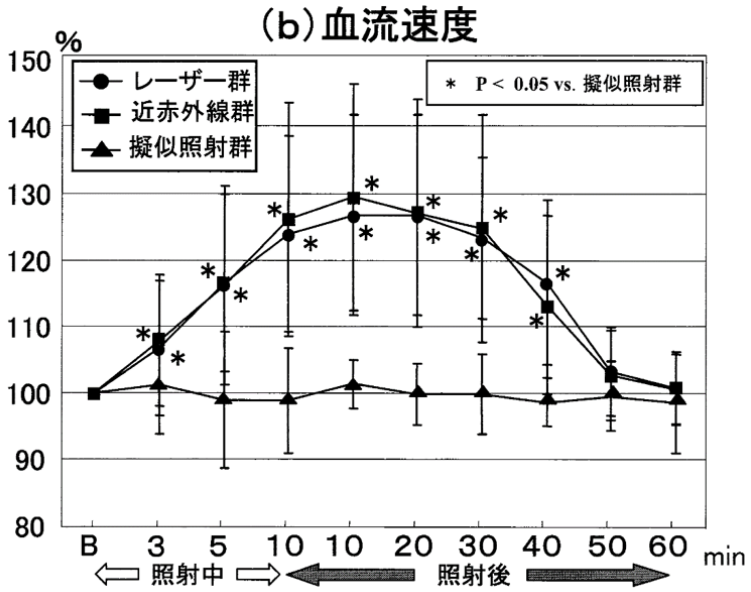

Fig. 2.4. Blood-flow velocity in arteriole before and after near-infrared light and low-power laser (*64*).

The effect of near IR (890 nm LED) was studied on the skin surface of the feet of healthy subjects (Mak et al., 2012) (*65*). Laser Doppler flowmetry was used to study the superficial skin blood flow. After a 30-minute session of IR illumination, the capillary blood velocity increased by an average of 20%. In the control group, warm packs similar in size to the near IR source were given to the volunteers to mimic the sensation of warmth of the IR source. Even though the warm

pack and IR source produced similar temperature increases, the blood flow increase in the IR group was 20% higher than in the control group (Fig. 2.5).

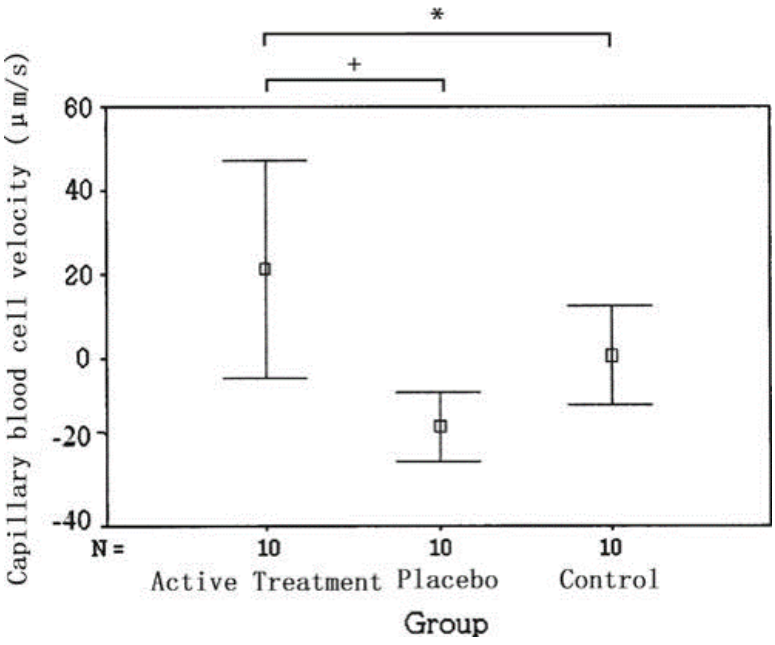

Fig. 2.5. Changes in the mean capillary blood cell velocity of the three groups: Active Treatment, Placebo, and Control.Error bars correspond to the standard deviations (*65*).

To sum, light of different wavelengths has effects on the blood circulation in various animal models. The effects are mostly positively. It is commonly explained as light stimulating the blood vessels in the skin or deeper tissues to release chemicals to change the diameter of the blood vessel. The explanations are based on our current understanding of circulation, based on the pressure-gradient driven model.

To explore the effect of light outside the pressure-gradient-driven framework, it is important to have a better understanding regarding why fluid can flow without a pressure gradient. Is the

self-driven flow general? Are there are other mechanism that can drive a flow without a pressure gradient? What is the most effective wavelength? The next chapter will focus on these questions.

Chapter 3. To generate a flow without a pressure gradient

The process of studying the self-driven flow is also the process of seeking the answers to the questions asked in Section 1.4 Aims. Some of these questions need to be answered through experiments, while others can be answered through logical thinking.

1) How general is the self-driven flow? Does it generally exist in nature, or are they merely a specific feature of certain materials?

Since the self-driven flow is close related to EZ, the question became: is EZ general?

Experimental verification is needed for answering this question.

If the surface-water hypothesis stands, then the self-driven flow as well as EZ should be general phenomena existing in nature. The protons released by EZ should be strictly due to water-surface interaction. Other potential origins of the protons should be excluded, such as a leakage of certain materials.

2) What caused the inconsistency in the direction of the self-driven flow? From the previous studies, it was clear that the geometry of the tunnel determined the direction, but the results contradicted one another. According to the proton concentration gradient hypothesis, a flow should flow to the narrower part to the wider part in a tapered tunnel, since the protons are originated from the inner surface of the tunnel, and a narrower tunnel has a higher surface to volume ratio. Yet, the results are conflicting with each other. The inconsistency indicates that mechanisms other than proton concentration gradients induced by water-surface interaction might be at play. What are they?

If a proton concentration gradient originating from the tube wall can generate a flow, an axial concentration gradient of other kind created along the tunnel could also generate a flow.

Material exchange across the wall is a common feature of naturally occurring vessels, such as capillaries. The rate of exchange may vary along the vessel, resulting in axial material gradients.

Material-exchange across the tunnel wall may generate a flow — this hypothesis needs to be tested experimentally.

3) What is the most effective wavelength to drive self-driven flow?

Among optical wavelengths, infrared radiation (IR) has shown the highest capability of expanding the EZ (*43*). Thus, IR should be the most effective wavelength to drive self-driven flow.

IR also have other advantages as a potential fuel for self-driven flow. IR is abundant. Over 50% of the solar energy received by the earth is IR. According to Plank's law, all the objects at all temperatures are emitting IR.

If IR is the fuel that utilized by the circulatory system, we also do not have to worry that animals live underground will die due to lack of IR, since their body can generate IR — the heat from the metabolic activities. Same applies for deep tissue blood vessels: metabolic IR can fuel flow in those vessels.

Now, the aims boil down to several points that can be tested experimentally. They are: (1) Is EZ as well as self-driven flow general? (2) Will IR enhance the self-driven flow? (3) Will material exchange induce a flow without a pressure gradient?

These questions will be answered in the following sections.

3.1 Self-driven flow

General existence of EZ

As previously stated, if EZ exists at the inner surface of a tunnel, then the self-driven flow should exist. The question of the generality of self-driven flow becomes the generality of EZ.

To explore the generality of EZ, I tested diverse hydrogels. They comprised plant-derived hydrogels including agarose, agar and starch, as well as animal-derived hydrogels including collagen and gelatin. These hydrogels, ranging from polysaccharides to proteins, were chosen based on their broad appearance in nature and wide application in science and technology (*66-69*).

The presence of EZs lining the exteriors of those gels was tested. A microsphere suspension was prepared by mixing de-ionized water and 1-μm non-functionalized polystyrene microspheres (volume ratio: 300:1). A piece of hydrogel material was fully immersed in this suspension, and the interfacial region was examined microscopically for the presence of microsphere-free regions (EZs).

EZ presence was confirmed with all materials tested (Fig. 3.1).

For generating the largest EZs, I found that low *ion concentration inside the gel* and *limited tendency to absorb water* were keys. This is consistent with a previous study about the effect of salt concentration on EZ size---higher salt concentration will lead to smaller EZ (*38*).

Standard preparations of collagen contain extraneous ions (*70*); and, gelatin has an appreciable tendency to absorb water. When those two gels were freshly made, EZs were not observed.

Dialyzing the gels against DI water removed ions and fully hydrated the gel. After dialysis, EZs clearly appeared. For starch, agar, and agarose, EZs were readily visible without dialysis, although dialyzing those hydrogels against DI water could increase EZ size.

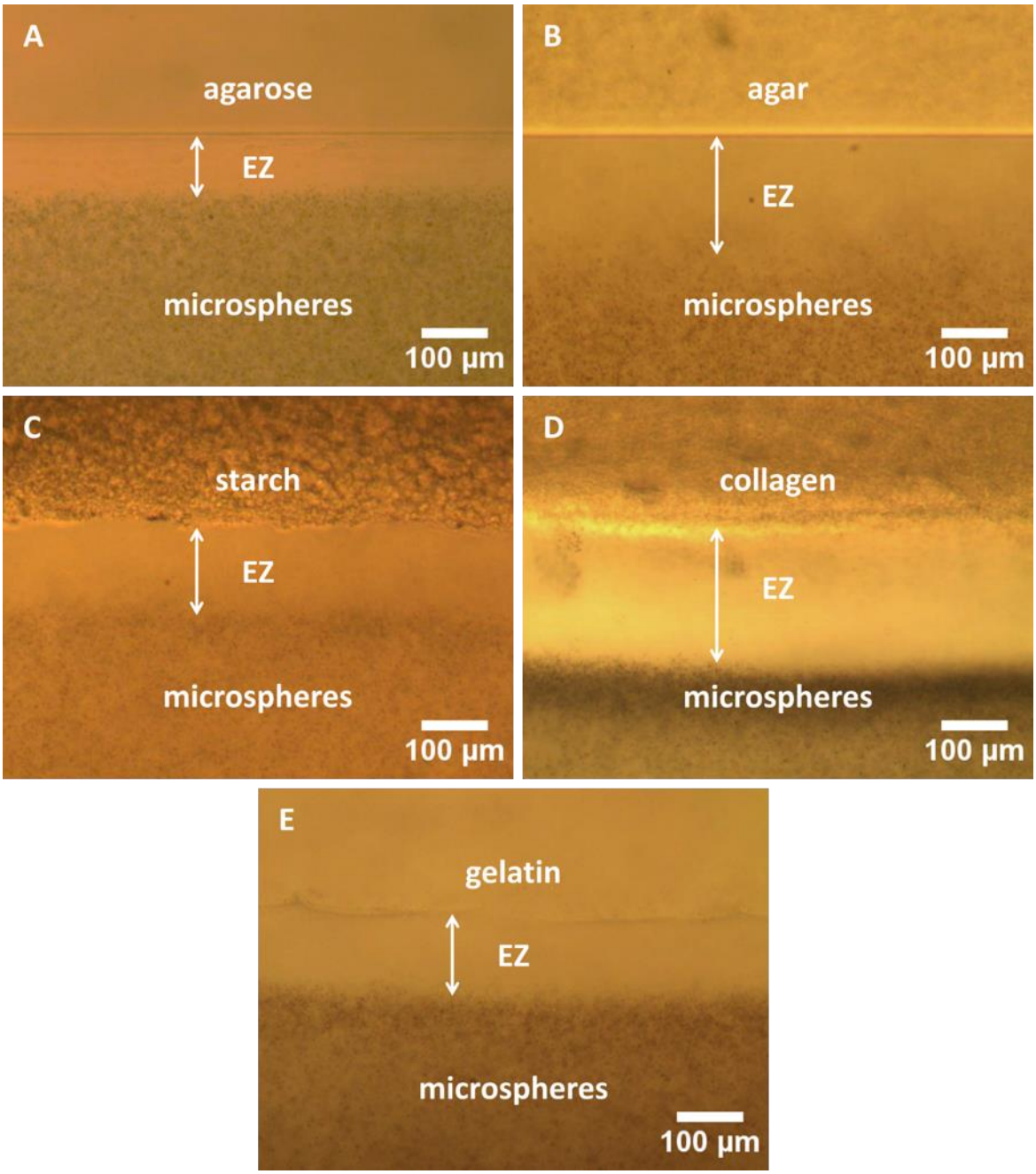

Fig. 3.1. Exclusion Zones formed next to various hydrogels. (A) agarose; (B) agar; (C) starch; (D) collagen (dialyzed); (E) gelatin (dialyzed).

The generality of the EZ phenomenon was tested also with various types of particles. Microspheres with positive charges (amidine functional groups, amino functional groups), microspheres with negative charges (carboxylate functional groups), as well as other particulate

materials (silica microspheres, PDMS, diatomaceous earth, active charcoal powder) were tested with agarose gel for the presence of EZ. EZ was observed with each one of those particulate materials (Fig. 3.2).

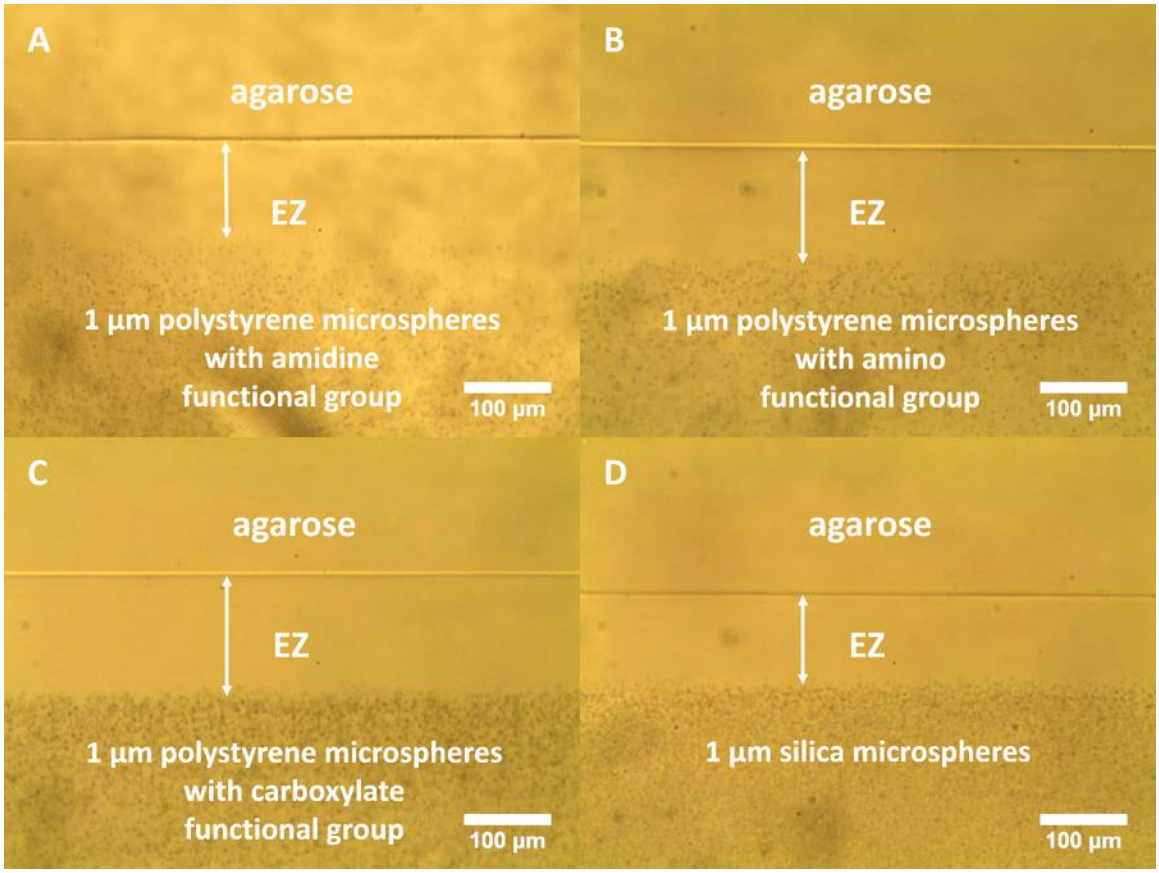

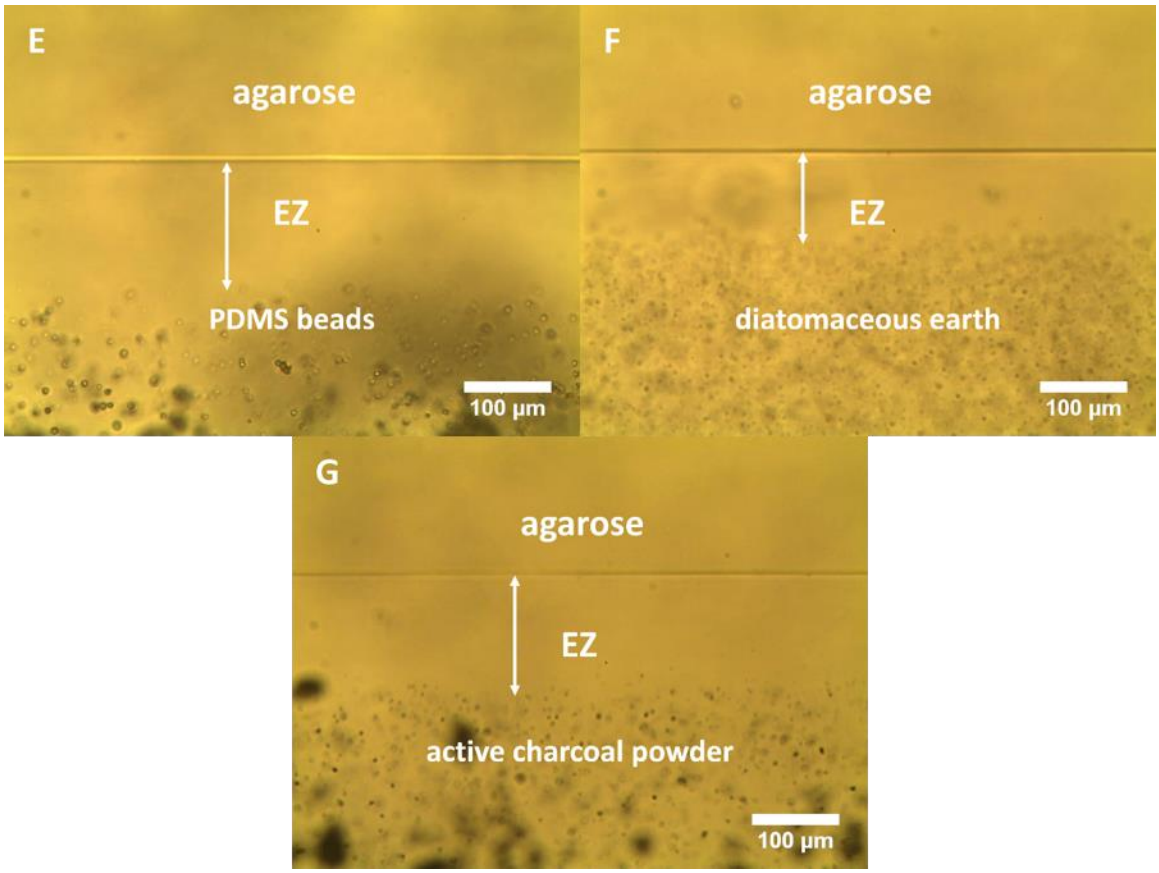

Fig. 3.2. Exclusion zone formed next to agarose gel with various types of solid-particle suspension.(A) 1-µm polystyrene microspheres with amidine functional group (positive); (B) 1-µm polystyrene microspheres with amino functional group (positive); (C) 1-µm polystyrene microspheres with carboxylate functional group (negative); (D) 1-µm silica microspheres; (E) PDMS beads; (F) diatomaceous earth; (G) active charcoal powder.

Hence, EZ is neither an exclusive feature of certain hydrogels nor of certain types of microspheres. It is general.

General existence of self-driven flow

With the confirmed presence of EZ in all cases, I proceeded to build tunnels within the respective hydrogels to study the self-driven flow. The tunnels were fabricated by using a mold.

The liquefied hydrogel was injected into a case, which contained a removable mold (Fig. 3.3A). After the gel had solidified (Fig. 3.3B), the mold was removed, leaving the tunnel behind (Fig. 3.3C). I built tunnels with asymmetric geometry: either a stepwise tunnel composed of a narrower section in series with a wider section; or a tapered tunnel. The asymmetry was designed to help determine the basis underlying the flow direction.

To observe the flow, the tunnel was first filled with an aqueous microsphere suspension to eliminate air-water interface, which may cause unwanted capillary effects. Then, the entire gel-tunnel was fully immersed in the microsphere-suspension bath and the exposed surface of the gel was covered with a coverslip, ready for flow observations (Fig. 3.3D). The flow was determined by tracking the movement of the microspheres, which was recorded by a video camera mounted on a microscope, and later analyzed by particle-image velocimetry (PIV) (Fig. 3.3E).

As a negative control, I built the tunnel inside the hydrophobic material PDMS (polydimethylsiloxane), in which neither an EZ nor any self-driven flow was expected.

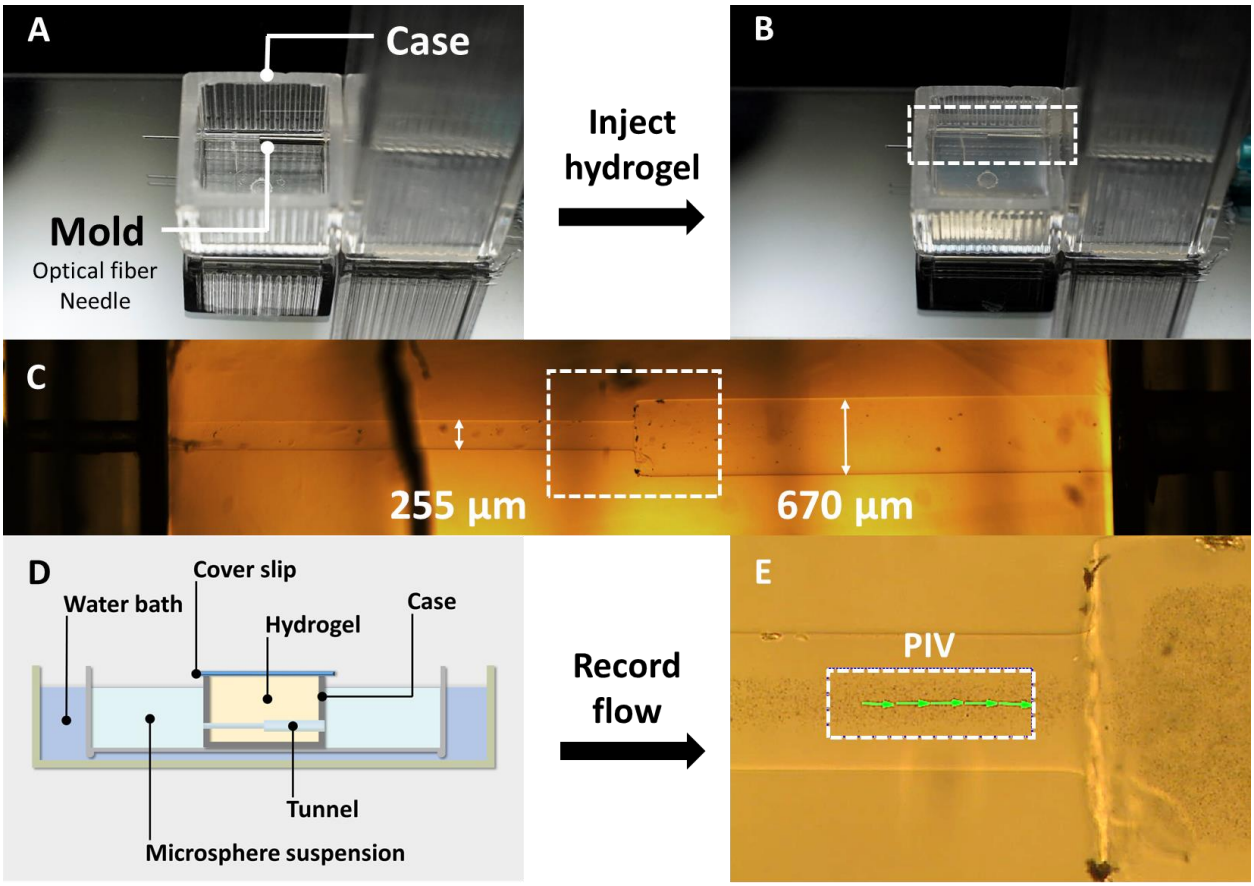

Fig. 3.3. Tunnel fabrication and data acquisition. (A) Case and mold. The case was made from a polystyrene cuvette, and the mold was made of a linear combination of optical fiber and stainless-steel needle. Other molds were used as well (See Chapter 3.5 Materials and methods, Fig. 3.17, Fig. 3.18, Fig. 3.19). (B) Hydrogel material (agarose) was injected into the mold and allowed to cure. (C) A representative tunnel (agarose), seen under 5x objective lens. Flow in the junction region (white rectangle) was recorded by a video camera as raw data. (D) A side view of the experimental setup for observing the flow. The tunnel was filled with, and then immersed in, a microsphere suspension. The tunnel remained in the case, and the top surface of the hydrogel was covered with a cover slip. The level of microsphere suspension was set above both ends of the tunnel. A water bath, heated by a heating stage, provided infrared radiation energy when needed. (E) The flow was visualized by the movement of microspheres (black dots). The white

rectangle shows region of interest (ROI). Flow velocity at the ROI was quantified using particle-image velocimetry (PIV). The green arrows are sample results. Arrow orientation denotes flow direction; arrow length denotes the local flow velocity.

Self-driven flow was confirmed with all the hydrogels tested (Movie 1-5). The flow velocity differed by tunnel material and geometry, but consistently met the criterion for self-driven flow, i.e., higher than 0.5 μm/s, which is the root-mean-square speed of 1-μm Brownian particles at 20 °C (*49*).

No self-driven flow was observed in tunnels created within PDMS — the microspheres exhibited active Brownian motion, but no directional flow (Movie 6).

Direction of the self-driven flow

A common feature shared among the various self-driven flows was the direction — always toward region with lower surface to volume ratio.

In compound tunnels with wider and narrower sections, the flow direction at the junction was consistently from the narrower to the wider part; and, at both ends of the tunnel, the microspheres exited into the outside bath. In tapered tunnels, the microspheres moved from the narrower end to the wider end (Fig. 3.4).

The direction of self-driven flow was also tested with various particles (as described in the caption of Fig. 3.2). Although some differences in dynamics were observed (for example, silica microspheres settled down faster than other microspheres due to their higher density), the direction of the flow was consistent among all microspheres: towards more open space.

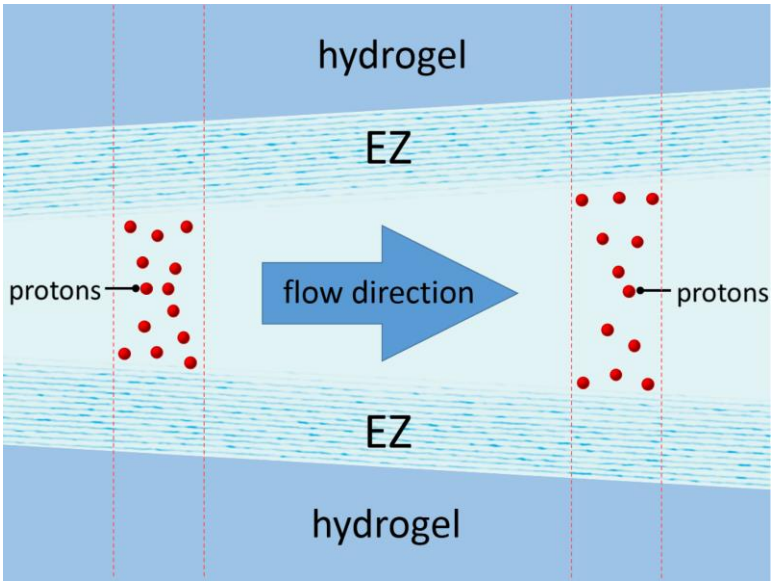

Fig. 3.4. Explanation of the flow direction. EZ forms next to the tunnel wall. During EZ formation, protons (red dots), are released into bulk water in the tunnel core. Assume the protons are released from the boundary of EZ at the same rate along the tunnel. Narrower sections of the tunnel should have higher proton concentration than wider sections, forming a gradient pointing from narrower to wider.

These observations fit the proton concentration gradient hypothesis: Since the protons emerge from a surface interaction, narrower tunnels, with higher surface-to-volume ratios should yield relatively higher proton concentrations. Thus, when a narrower tunnel lies in series with a wider tunnel, the proton concentration gradient should point from the narrower to the wider section, as consistently observed.

Establishing an experimental model

To explore additional features of self-driven flow, an experimental model needs to be established.

I used a compound tunnel made in an agarose gel (Fig. 3.3C). Agarose was chosen for several advantageous features: mechanical strength; optical clarity; and, extremely low swelling rate (which largely excludes tunnel-volume change as a relevant factor). The compound tunnel configuration (with diameters of 255 μm and 670 μm) helped elucidate the flow direction.

Flow dynamics

In this above-stated configuration, the flow could last for approximately 30-40 minutes until all the microspheres were excluded from the region of interest (ROI). After approximately two hours, almost all the microspheres were excluded from the entire tunnel, leaving the tunnel filled with EZ alone.

Sometimes, the EZ extended beyond the tunnel, forming microsphere-free hemispheres at the openings (Movie 7, Fig. 3.5A). The EZ filling the tunnel could stay stable for at least a day (observations longer than a day were not made). Driven by convectional force, microspheres moved freely in the suspension outside the tunnel, but were unable to enter the tunnel. When the tunnel was flushed with new microsphere suspension, the EZ formed once again next to the tunnel wall.

In tunnel made with other materials, the flow terminates similarly. Fig. 3.5B shows the end state of self-driven flow in a collagen tunnel. The tunnel geometry was the same as the standard agarose tunnel.

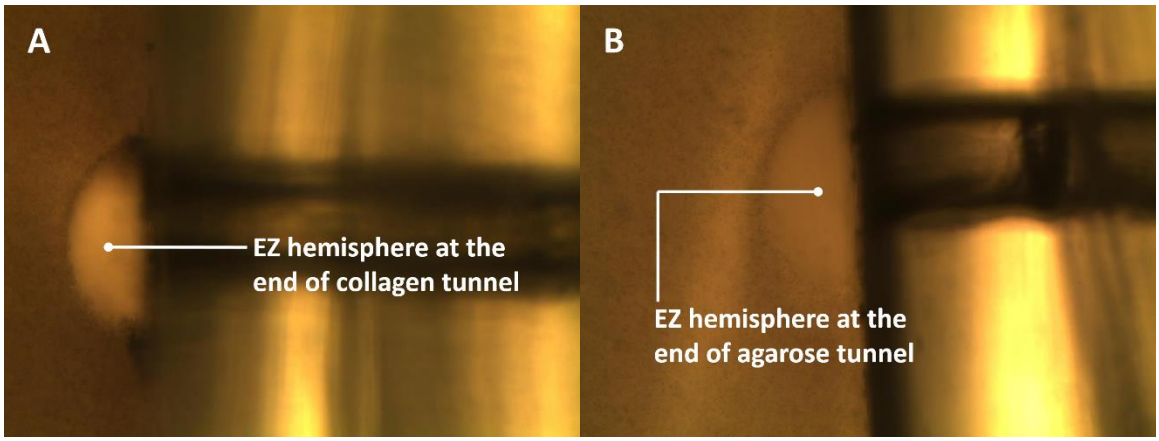

Fig. 3.5. End state of EZ induced self-driven flow. The EZ excluded almost all the microspheres and filled the entire tunnel. Sometimes, the EZ expanded out of the tunnel and formed a hemispherical EZ plug. (A) EZ hemisphere at the end of collagen tunnel. (B) EZ hemisphere at the end of an agarose tunnel.

Confirming the charge separation

It has been already demonstrated that EZ can by observed next to agarose gel. If the surface-water interaction hypothesis stands, then, the existence of the products of such interaction, protons, should be confirmed. The existence of the protons at the agarose-water interface was tested by using a pH-sensitive dye.

Agarose, dialyzed before gelation, was heated and then poured into a micro-centrifuge cuvette to form a gel. The agarose gel was then further dialyzed against DI water for a week. The water was changed twice daily. pH dye diluted with DI water (1:10 v/v) was injected into the micro-centrifuge cuvette. The top surface of the agarose gel was in touch with the pH dye. The result is shown in Fig. 3.6. The pH dye visualized a low pH region at the gel/water interface.

The low pH indicates the existence of protons. Thus, the proton generated at the agarose-water interface is confirmed. Since the agarose was previously dialyzed, thus, the possibility that the protons are generated from the leakage of the agarose could be excluded.

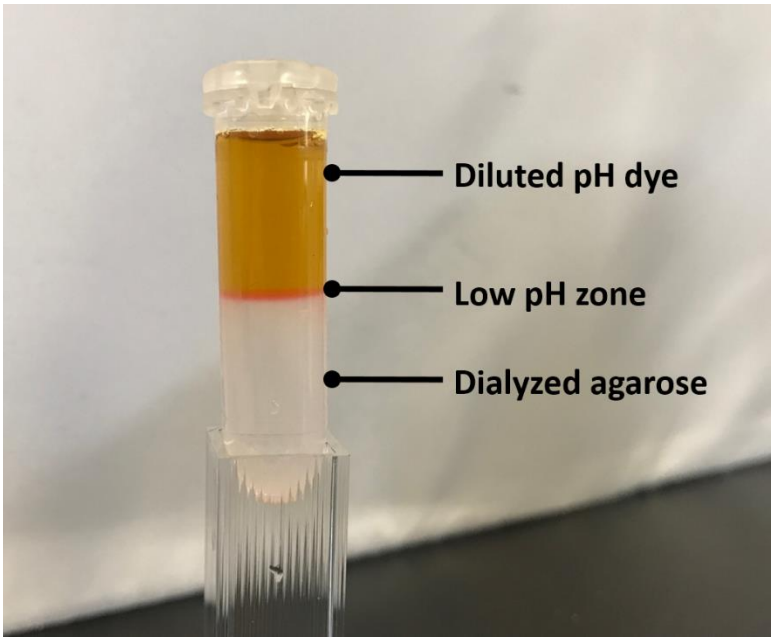

Fig. 3.6. Proton-rich zone formed at the agarose gel/water interface, visualized by pH dye. Red color indicates a low pH. Before this experiment, this piece of gel was dialyzed against DI water for a week in order to remove any foreign ions/molecules from the gel.

Effect of IR on self-driven flow

IR source

To test the effect of IR, I first determined which IR source to use.

In pilot experiments carried out to test the effect of IR on the self-driven flow in Nafion tubes, a ceramic IR lamp was used as an IR source (ZooMed, 150W). This IR source can emit IR wavelengths ranging from 1 μm to 14 μm, with a peak at 2.92 μm. The IR source was placed next

to the microscope, pointed downward to the Petri dish at a 45° angle. The distance between the center of the IR source to the center of the Petri dish was 20 cm.

With this IR source, it was found that the microspheres moved towards the IR radiation source. Such movement had been reported previously (*71*, *72*).

In other pilot experiments, the hands of the experimenter (the author of this thesis) were used as an IR source. The hands were wrapped around the Petri dish that contained the Nafion tube and aqueous suspension of polystyrene microspheres (Fig. 3.7).

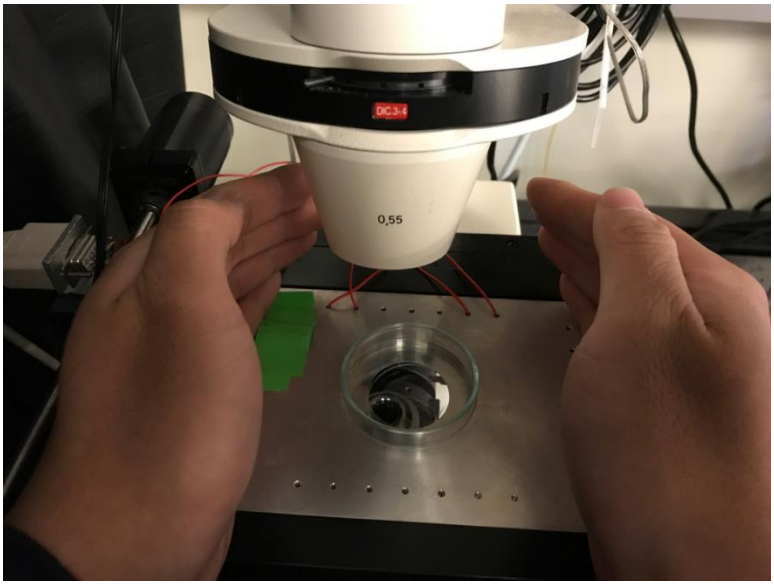

Fig. 3.7. Using hands as an IR source. A demonstration of an experimental configuration.

The EZ was recorded at the beginning and at six minutes after the beginning of the experiment. The result is shown in Fig. 3.8. The IR from the hand effectively expanded the size of the EZ.

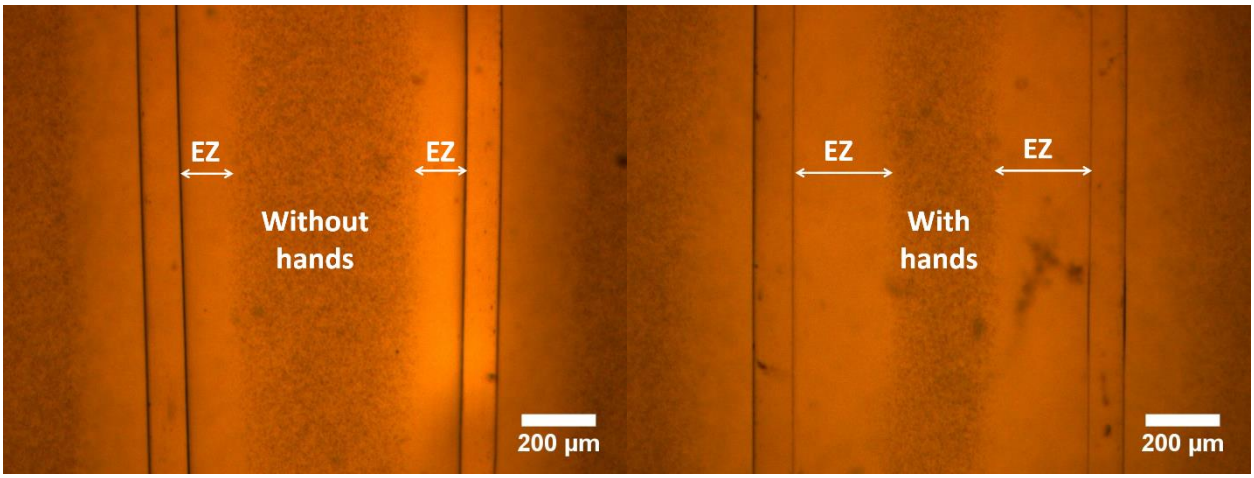

Fig. 3.8. Effect of IR emitted from hands on the size of EZ.Both photos were taken six minutes after the Nafion was immersed in microsphere suspension. Note the difference in EZ size inside the Nafion tube. Unfortunately, the IR from the hands attracted the microspheres, which moved towards the direction of the palm. This caused a disturbance of the EZ outside the Nafion tube.

Using hands as IR source in preliminary experiments inspired an idea: using a surrounding water bath as an IR source. If it is impossible to stop the microspheres from moving toward the direction of the IR source, then, a uniform IR could at least stop the microsphere movement. towards any specific location.

I built a microscope-stage heater (Fig. 3.9), which could warm a water bath. The water bath could then provide uniform IR input into the microsphere suspension (contained in a smaller Petri dish). The infrared output from the water bath could be varied by adjusting the stage temperature.

With this IR source, the microspheres no longer migrated towards any particular direction.

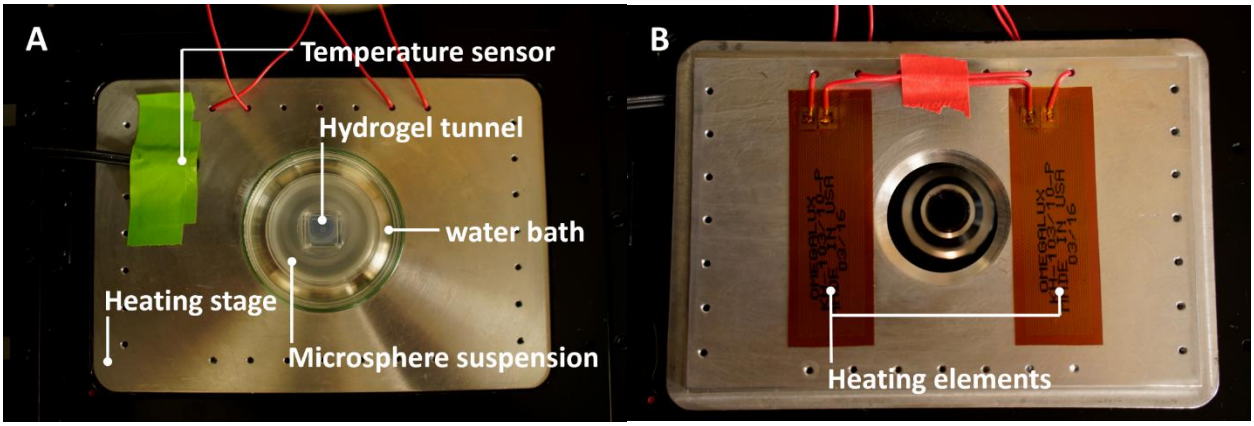

Fig. 3.9. Water bath as a uniform IR source.(A) The water bath (glass Petri dish) was warmed by an aluminum heating stage. The microsphere suspension, contained in a polystyrene Petri dish, was heated by the water bath. (B) Back side of the heating stage.

Effect of IR on self-driven flow in agarose tunnel

Effect of IR on self-driven flow was tested. Increased infrared energy significantly increased the flow velocity (Fig. 3.10).

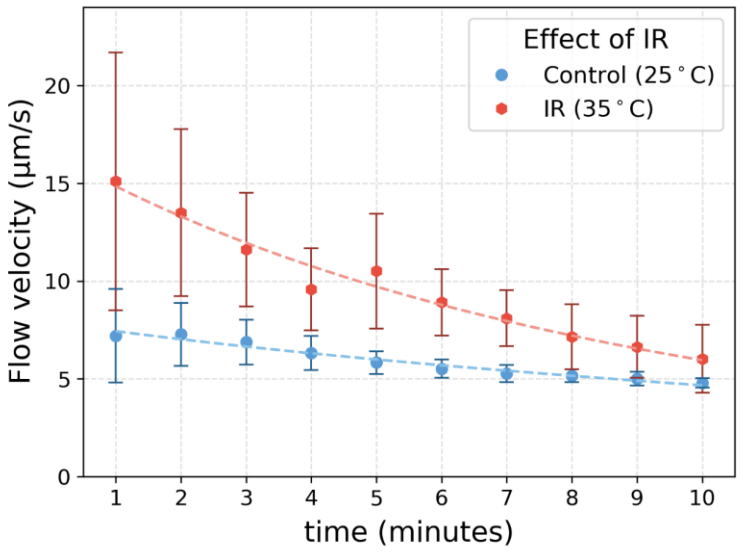

Fig. 3.10. Higher infrared radiation results in faster self-driven flow. Temperature in legend indicates water bath temperature. N = 5, error bars = standard deviation.

Infrared energy may increase the flow in two ways: by enhancing the water-surface interaction, thereby generating protons at a higher rate; and, by creating a higher temperature, thereby enhancing proton diffusion.

The practical significance of IR utilization lies in its ubiquity. It's always present, which implies that the capacity for flow is omnipresent. For biological entities, IR sources can be both exogenous and endogenous. Roughly 50% of solar energy received by earth is in the form of IR (*73*); and, metabolic activities of living organisms generate thermal radiation (heat), which is essentially IR (*74*). All these sources are available to power flow.

Effect of tunnel diameter on self-driven flow

Assuming the proton-release rate per unit area of the annular EZ is spatially invariant, then, since reduced tunnel diameter means increased surface-to-volume ratio, a narrower tunnel should lead to a higher proton concentration in the core (see Fig. 3.4). Assuming the bath's proton concentration remains unchanged, a thinner tunnel results in a steeper proton concentration gradient, which in turn should lead to faster flow in the narrower tunnels. Thus, the proton concentration gradient hypothesis predicts that the velocity of the flow should be faster in narrower tunnels.

I tested this hypothesis by decreasing the diameter of the narrower section of the tunnel (by using a thinner optical fiber as a mold), and the prediction was confirmed: narrower tunnels produce faster flow (Fig. 3.11).

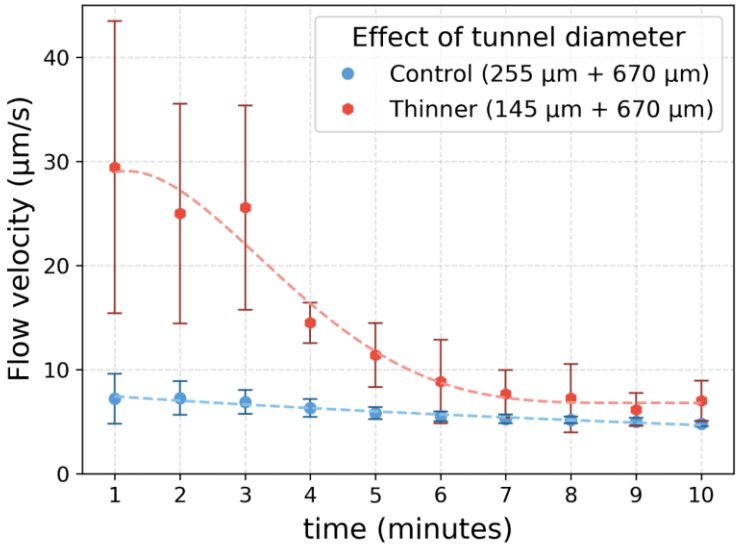

Fig. 3.11. Smaller tunnel diameter results faster self-driven flow.N = 5, error bars = standard deviation.

This result is to the opposite of pressure-driven intratubular flow, where, by the Hagen-Poiseuille equation, narrower tunnels produce slower flow velocity (23).

3.2 Material-exchange-induced flow

With the general existence of the self-driven flow confirmed, and an experimental model established, I moved to explore a related phenomenon: whether tubular flow could be created also through material exchange. Material exchange occurs when solvent/solutes enter/exit the tube through the tubular boundary, which occurs, for example, in capillaries of the circulatory system (*75*).

Solvent-exchange-induced flow

I studied one of the most common material exchange scenarios: water, the universal solvent, continuously exiting the tunnel through the tunnel boundary.

An agarose gel, with compound tunnel, was chosen as a model. The experimental setup was almost identical to that of the self-driven flow study, except that the top surface of the gel was exposed to the air. With that exposure, the water continuously evaporated from the surface of the hydrogel. Evaporation increased hydrogel's osmotic pressure, which drew water from the tunnel into the gel.

With this model, I could again obtain flow (Movie 8). The flow appeared to contain two phases. Phase I was similar the standard self-driven flow, as described above. After approximately 40 minutes the pattern changed: the density of microspheres in the tunnel decreased substantially; the EZ began diminishing in size and became less well defined; and, the flow began to slow down and finally reverse. Reversal denoted the onset of phase II, where flows at the ends and at the junction all reversed direction. The reverse flow increased microsphere density, and the EZ disappeared. (Movie 8). Phase II flow continued so long as the microsphere suspension level stayed above the tunnel openings.

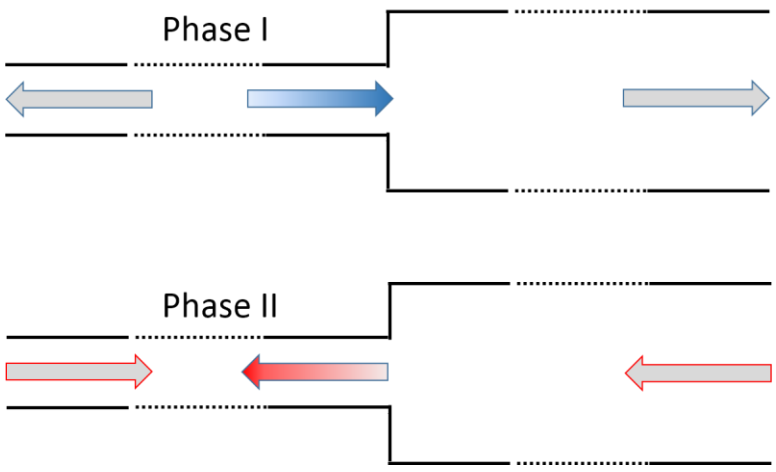

Fig. 3.12. The direction of flow induced by material exchange (loss of water due to evaporation). Top: phase I, self-driven flow. Bottom: phase II, flow started to reverse.

This two-phase flow may result from competition between the two proffered flow mechanisms — the self-driven flow; and, the material-exchange-induced flow, the material in this case being water.

To understand this material-exchange-induced flow, consider a compound tunnel inside a gel that has been subjected to partial dehydration. The dehydrated gel draws water from the tunnel through the boundary. With the same initial osmotic pressure throughout the tunnel, the narrow region loses water faster per unit volume due to that section's higher surface/volume ratio. In other words, the "water concentration" in the narrower section tends to decrease more rapidly than in the wider one. Thus, a "water concentration" potential gradient (or water-potential gradient), forms, pointing from the wider region to the narrower region. This opposes the self-driven flow.

For phase I, the self-driven flow should dominate since the osmotic pressure of the hydrogel is still low. For phase II, as more water evaporates from the gel surface, the tunnel's osmotic pressure increases. Once it dominates, the flow reverses.

While the phase-I self-driven flow was found to end approximately 40 minutes after the initiation of the experiment, phase II flow was observed to continue as long as the level of microsphere suspension was above both ends of the tunnel.

Microspheres that were brought into the tunnel by phase II flow eventually sedimented and accumulated at the location where flow stopped, i.e., at the middle point along the length of the narrower tunnel. Microspheres also sedimented and accumulated in the wide region at the narrow/wide tunnel junction. The accumulation started from the beginning of phase II flow, and the continued throughout the experiment (Fig. 3.13).

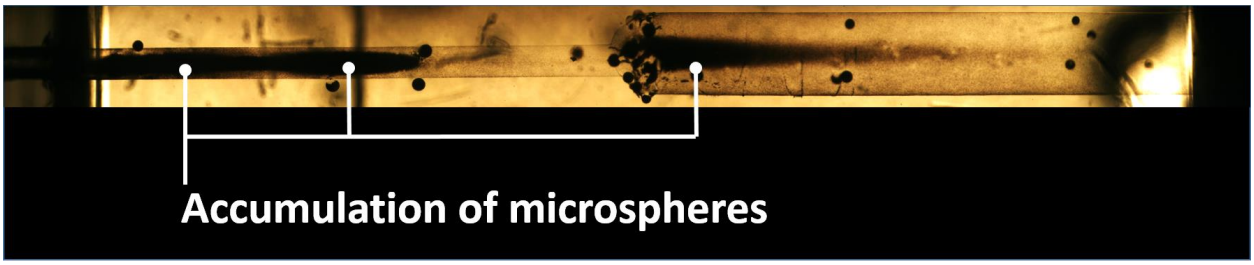

Fig. 3.13. End state of solvent-exchange water induced flow. The microspheres concentrated and accumulated in the agarose tunnel after 48 hours of continuous flow.

Solute-exchange-induced flow

I tested another simple scenario, whether the entrance of solutes into the tunnel through the boundary could induce flow.

A compound agarose tunnel was used as a model. The geometry of the tunnel was identical to that used in self-driven flow study. The agarose gel was made with phosphate-buffered saline (PBS) (Gibco, 10010-031) solution instead of DI water. The microsphere suspension was made with polystyrene microspheres and DI water. The experimental configuration was the same as described in Fig. 3.3D. The top surface of the gel was covered with a glass slide to stop water to evaporate from the gel.

With this configuration, a salt gradient was created between the gel and the microsphere suspension. Salt contained in the gel will diffuse into the microsphere suspension. This mimics the scenario that salt enters a piece of vessel.

The flow obtained with this experimental configuration was faster compared to the self-driven flow. The results are shown in Fig. 3.14.

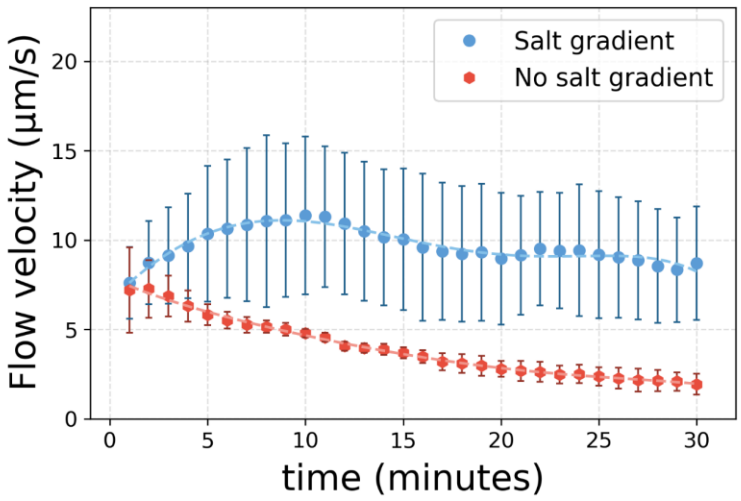

Fig. 3.14. Solute-exchange-induced flow.PBS agarose gel and DI water microsphere suspension were used in salt gradient group (N=4), while DI water agarose and DI water microsphere suspension were used in no-salt-gradient group (N=5). Error bars = standard deviation.

This result can be interpreted as a sum of two types of surface activity:

(i) Hydrogel-water interaction. Protons are released into the tunnel, forming a gradient pointing from the narrow region to the wide region, as described in main text.

(ii) Solutes enter the tunnel. The hydrogel was made with PBS, a solution whose major component is NaCl. When this hydrogel tunnel was immersed in a DI-water-microsphere suspension, salt diffused from the hydrogel into the tunnel through tunnel boundary. The narrower region has a higher surface-to-volume ratio compared to the wider region. Thus, a salt concentration gradient formed, pointing from the narrow region to the wide region. The diffusion of the salts along the concentration gradient drives the flow.

Thus, solute-exchange through the tunnel boundary can induce a flow.

Effect of IR and tunnel diameter on material-exchange-induced flow

Like self-driven flow, higher IR input and narrower tunnel size should enhance material-exchange-induced flow. Higher IR input increases gel temperature, which enhances evaporation and increases the gel's osmotic pressure; that results in faster flow. The narrower tunnel has a higher surface to volume ratio, generating a steeper water concentration gradient, then faster flow.

I tested these hypotheses on the solvent-exchange-induced flow model. The two expectations were confirmed (Fig. 3.15). Higher IR input and narrower tunnel increased flow, during both stages.

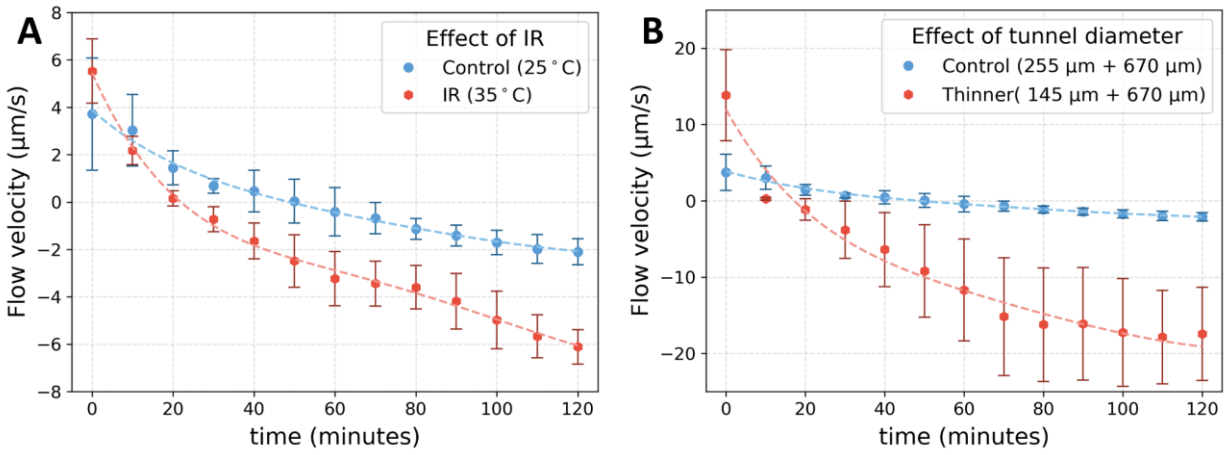

Fig. 3.15. Effect of IR (A) and tunnel diameter (B) on flow induced by material exchange (loss of water due to evaporation). Negative velocity denotes flow in the reverse direction (from thicker to thinner tunnel) In both (A) and (B): N = 5; error bars = standard deviation. (A) Elevated infrared energy resulted in faster flow. Temperature in legend indicates water bath temperature. (B) Smaller tunnel diameter resulted faster flow.

It is not hard to envision that IR and tunnel diameter will have a similar effect on solute-exchange-induced flow. Regarding the effect of IR: the heat resulting from IR and a higher surface-to-volume ratio caused by the narrower tunnel will enhance the rate of material exchange. Regarding the effect of tunnel diameter: assuming the material exchange is uniform along the tube.

No matter the material being exchanged is solvent or solutes, the result is a concentration gradient along the axial direction the tunnel, set by surface to volume ratio along the axial direction the tunnel.

The negative control

PDMS tunnel was used as a negative control. No EZ, self-driven flow or material-exchange-induced flow was expected in PDMS tunnel because PDMS is hydrophobic, which is known for producing no EZ.

This expectation was confirmed.

IR of different intensity levels was applied to a tunnel made with PDMS, and the result is shown in Fig. 3.16. The particles exhibited Brownian motion, which does not qualify as self-driven flow---the average velocity was less than 0.5 μm/s. As the IR input rises, the average speed of the particles increased. This may be due to enhanced convection as well as enhanced Brownian motion from temperature increase.

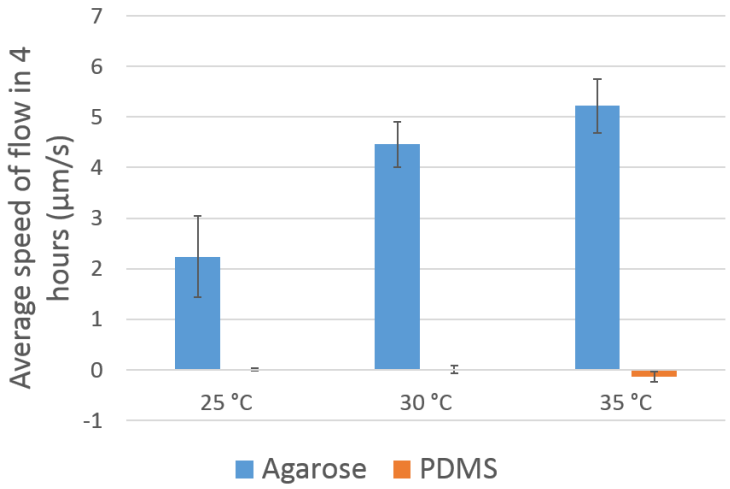

Fig. 3.16. PDMS tunnel gives no flow. The average of flow in agarose tunnel in 4 hours as a control. N = 5, error bars = standard deviation.

The negative control helped me to exclude convection as an explanation for self-driven flow and material-exchange-induced flow. In PDMS tunnel, no EZ was observed; material exchange does not exist since PDMS is not permeable. The extremely slow directional microsphere movement should be due to convection. Although temperature has positive effect on convection, the convection induced flow is 1-2 orders of magnitude slower compared to self-driven flow and material-exchange-induced flow.

3.3 Discussion of chapter 3

In this section, we will provide a general explanation regarding how flow can form without a pressure gradient; why "IR" was used instead of "temperature"; and why EZ results from a surface-water interaction.

How fluid flows without a pressure gradient

In a segment of tube, if a concentration gradient of molecules is generated, then flow can occur without a pressure gradient.

Assuming the molecules are entering or exiting the tunnel via the boundary at a consistent rate per unit surface area, the local concentration change rate will be determined by the tunnel's surface-to-volume ratio. When that ratio varies along the tube's axis, a concentration gradient should develop along the axis.

Once a concentration gradient forms, there are multiple options to generate a flow without a pressure gradient. Examples are abundant: chemical gradients will induce diffusion; water potential gradients will induce osmosis; and, when chemical gradients and charged particles exist together, diffusion-phoresis happens.

Take the self-driven flow as an example. In a hydrogel tunnel, EZ at the hydrogel-water interface releases protons into the core of the tunnel, forming a proton concentration gradient. This gradient manifests through: (1) diffusion of the protons following the proton concentration gradient -- this is an ionic flow. (2) diffusion-phoresies: the particles contained in water will move respectively according to the proton concentration gradient -- this is the particle flow. The sum of these two effects is the flow that we had observed.

Take the material exchange (solvent) induced flow described in section 3.2 as another example. The water continuously leaves the tunnel through the boundary. Due to the varied surface-to-volume ratio, a water potential forms in the tunnel. The water flows along the water potential. This is technically osmotic flow.

This thesis did not focus much on how the concentration gradients can manifest into flow. Instead, it explains how concentration gradients can form in a tube. Surface activities, including water-surface interaction and material exchange, introduce concentration gradients into a tube.

As mentioned in the Introduction, blood vessels transport a water-based suspension — the blood. Also, blood vessels are the major sites for material exchange, especially the capillaries. These activities will generate concentration gradients in the blood vessels. Thus, blood vessels should confer kinetic energy to the blood, without a pressure gradient. A detailed explanation on how SIF mechanism can be utilized in blood circulation is described in Chapter 3.

IR and temperature

Confusion sometimes arises over the use of IR (infrared) energy vs. temperature.

Temperature described the thermodynamic state of a system, and IR described how the state is changed. Which one comes first? This is a chicken-egg question. Infrared energy causes

temperature increase. Higher temperature results in more infrared energy emission. The two are roughly equivalent when it comes to the discussion of a dynamic process.

Therefore, it's not clear which one is more "primary".

Either one could be chosen for discussion. But choosing IR as the primary variable comes with several advantages. It allows us to deal with the fact that different IR wavelengths can bring different amounts of heating. It also allows us to deal more naturally with wavelengths that don't cause appreciable heating, but do expand the EZ. Because of those advantages, I tend to stick with using the term "infrared energy," which is uniquely defined in terms of amplitude and wavelength.

EZ as a water-surface interaction

Diffusion-phoresis has been considered as an alternative explanation for EZ (*76-79*). The microspheres moving away from the surface is explained to "arise from chemotaxis of the microspheres in long-range diffusion gradients of OH^- (or H^+) and salt (*79*)". Chemotaxis is the movement of particles along concentration gradients of a chemical substance; and, concentration gradients were considered to arise from either of several possible sources: ions contained in gel dissolving in water; the gel material itself dissolving in water; or, from functional groups of the microspheres for example, carboxylate groups, which can release H^+ (*79*). This alternative hypothesis denies any interaction between water and surfaces. Water is considered as just an inert background fluid.

This alternative explanation may be partially correct. Microspheres will move in response to chemical gradients. Chemotaxis could be one of the causes of the axial flow, if a chemical concentration gradient exists.

However, a question is: where might these chemical concentration gradients come from?

According to this alternative hypothesis, EZ should not exist if the gradients, originating from the gel or from the microspheres, are eliminated. In the experiments, the potential chemical diffusion from the gel was deliberately neutralized by repeatedly dialyzing the gel against DI water (Fig. 3.1). This should have removed a great majority of diffusible ions and molecules from the gel. When the dialyzed gel was immersed in a polystyrene microsphere suspension — a type of microsphere that does not release ions into water — the EZ did not vanish; in fact, it expanded. The pH dye experiment (Fig. 3.6) further confirmed that the proton concentration gradient was generated from the gel and water interface, and not from the microspheres, since no microspheres were used. The alternative hypothesis failed to explain the experimental observation.

By contrast, the surface-water interaction hypothesis under consideration here acknowledges charge-separation, accounting directly for the chemical concentration gradients (protons) observed in the experiments. Thus, gradients originating from surface-water interaction should not be denied.

3.4 Conclusion to Chapter 3

Tube flows are common natural phenomena. Examples include blood and lymphatic flows in animals, and xylem and phloem flows in plants. These flows serve two main functions: fluid transport and material exchange. The principal driving force for flow is widely considered to be a pressure gradient, driving the fluid either by propulsion (cardiac contraction), or by suction (capillary effect, drawing water to the tops of plants) (*9, 16, 80*).

Here, we have demonstrated, for a section of tunnel/tube that contains a water-based solution, which exchanges across the tunnel/tube boundary, a flow will generate without a pressure gradient.

In other words, naturally occurring tubes can confer kinetic energy to the fluid within.

Self-driven flow exists in tunnels lodged within diverse gels, driven by an axial proton concentration gradient — the latter originating from a water-interface interaction. Material exchange through the boundary of the tunnel can cause a material concentration gradient along the tube, also resulting in a flow. In both cases, the surface activities of the tunnel/tube boundary introduce a gradient into the tunnel/tube, which generates a flow. Hence, we suggest the generic name, "Surface-Induced Flow" (SIF).

Two features of SIF are distinct from those of pressure-driven flow: (i) *IR energy augments the SIF*. Higher IR input enhances the water-interface interaction, which creates a larger proton concentration gradient, thereby boosting the self-driven flow. In the material exchange mechanism, higher IR input increases the temperature, resulting in enhanced material exchange across the boundary, larger axial material concentration gradients, similarly boosting the flow. (ii) *SIF is more effective in narrower tunnels/tubes* — opposite that of pressure-induced flow. This follows because the higher surface-to-volume ratio in narrower tubes facilitates surface activities, regardless surface interaction or material exchange.

3.5 Materials and methods

Case and mold

The tunnel was built by using a mold. Hydrogel material was injected into a case fitted with a mold. After the hydrogel was cured, the molds were removed, leaving a tunnel within the gel.

(A) Case, mold and retainer used for agar, agarose and collagen tunnels

The case holds the hydrogel. The case was made from a polystyrene spectrophotometer cuvette. The top part of the cuvette was cut off, leaving only the bottom section, with a dimension of 1 cm × 1 cm × 0.6 cm (length × width × height). A hole was drilled on each of two opposite sides of the

case to allow the insertion of the mold. The sizes of the holes were the same as the diameters of the mold sections, and the height of the holes to the floor of the case was determined by the working distance of the microscope.

The mold determined the geometry of the tunnel. The mold was assembled by inserting a piece of optical fiber into a needle. With this configuration, the tunnel was composed of a narrow and a wide region. The length of each region was equal, and the total length of the tunnel was 1 cm. Two tunnel geometries, control geometry and narrow geometry, were built respectively to study the effect of tunnel diameter. For different geometries, different optical fibers were used for the narrow region; and the needle for the wide region remained the same.

- Needle: diameter = 670 μm (BD, 305193), tip blunted by a rotary grinder.

- Optical fiber for control geometry: diameter = 255 μm (Corning, LNF 62.5/125).

- Optical fiber for narrow geometry: diameter =145 μm (Nufern, CMF-P).

A retainer facilitated the removal of the mold. It was made from a polystyrene spectrophotometer cuvette and a glass slide. A hole was drilled on each of the two opposite sides of the spectrophotometer cuvette. The size of the holes was the same as the diameter needle, and the location of the holes matched that of the case. The cuvette was then glued onto a glass slide. When the needle was being removed, the two holes on the retainer prevented the needle from wiggling.

To assemble the case, mold and retainer, the optical fiber was first inserted into the case, and then the needle, which was fixed by the retainer, was inserted into the case. Thereafter, the optical fiber was inserted into the needle, all the way to the other side (Fig. 3.17). The junction of the optical fiber and the needle was set at the middle point of the prospective tunnel.

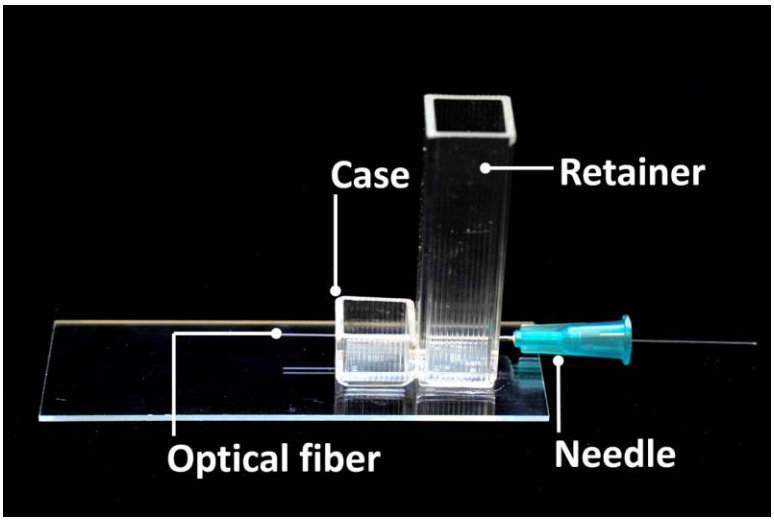

Fig. 3.17. Case, mold and retainer used for agar, agarose and collagen tunnel.

For agar, agarose and collagen tunnels, no extra treatment was needed for the case and the mold prior to gel injection. For PDMS tunnels, Trichloro (1H, 1H, 2H, 2H-perfluoro-octyl) silane (Sigma-Aldrich, 448931-10G) was coated onto the case and mold in order to prevent the mold from sticking to PDMS. The coating was deposited by evaporation: one drop of silane was deposited onto a watch glass. The case, mold and watch glass were placed in a desiccator. The desiccator was connected to the laboratory's vacuum system whose pressure was 41.1 kPa. The vacuum was on for 30 minutes. During this time, silane evaporated and coated on the case and mold.

To remove the mold: first, the needle was rotated slowly to separate from the hydrogel/PDMS. Then the optical fiber was slowly pulled away from the retainer side, and the needle was pulled away afterwards. Removing the optical fiber first, before the needle, prevented hydrogel/PDMS debris being left in the tunnel.

The hydrogel/PDMS tunnel remained in the case during all experiments.

(B) Case and mold used for gelatin tunnel

A case was made from a 1 ml syringe (BD, 309623). The needle from this syringe/needle set was not used. The tip of the syringe was cut off, and two holes that allowed a tight fitting of the molds were drilled on the syringe wall, through the diameter of the cylindrical syringe. The plunger remained in the syringe, and the space formed by the plunger and the syringe wall was used to contain the hydrogel.

A thin needle, a piece of optical fiber, and a thick needle each composed of 1/3 of tunnel length was used as mold (Fig. 3.18).

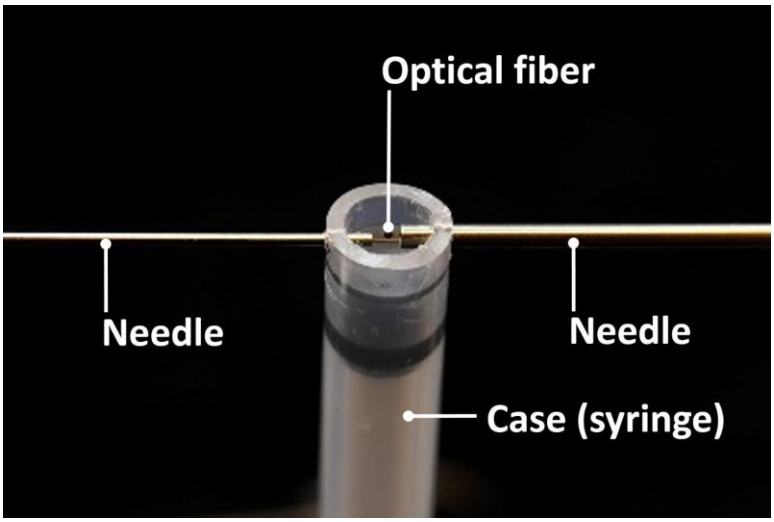

Fig. 3.18. Case and mold used for gelatin tunnel.

Mold:

- Thin needle: diameter = 670 μm (BD, 305193), tip blunted by a rotary grinder.

- Optical fiber for narrow geometry: diameter =145 μm (Nufern, CMF-P).

- Thick needle: diameter = 1070 μm (CML Supply,901-19-100).

The gelatin gel swelled greatly after dialysis. Thus, the tunnel-containing gel was removed from the case for dialysis. To remove the gel, the plunger was pushed, and the gel was softly scraped away with a spatula.

After dialysis, the tunnel diameter was larger than that of the mold due to swelling.

(C) Case and mold used for starch tunnel

In order to see the microspheres clearly through the opaque starch gel, a wider tunnel was built by using a thicker mold. Also, the distance between the gel surface and the tunnel was reduced by using less gel.

The case was made from a polystyrene spectrophotometer cuvette. The top part of the cuvette was cut off, leaving only the bottom section, with a dimension of 1 cm × 1 cm × 0.6 cm (length × width × height). A hole was drilled on each of two opposite sides of the case to allow the insertion of the mold. The size of the holes allowed a tight fitting of the mold, and height of holes to the floor of the case was determined by the working distance of the microscope.

A 20 µl pipette tip (RAININ, RT-L10FLR) was used as a mold. The setup is shown in Fig. 3.19.

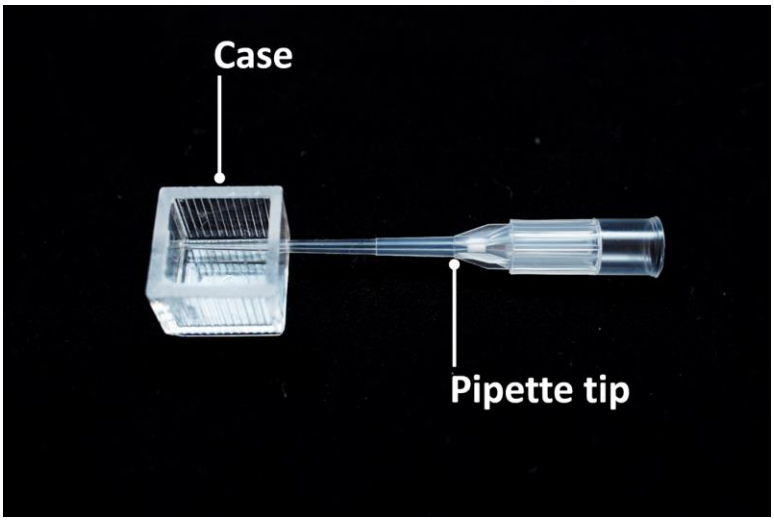

Fig. 3.19. Case and mold used for starch gel.

The starch tunnel remained in the case during all experiments.

Materials

Deionized water

The DI water used in all experiments was obtained from a deionized-water system (Barnstead, Nanopure analytical system, D11901). The resistivity of the DI water was 18.2 MΩ·cm at 25 °C.

Agarose

Agarose (Sigma, A6560) was mixed with DI water at a ratio of 1.5% w/w (0.6g agarose/40g water) in a 50 ml conical centrifuge tube (Corning, 352098). The tube was heated in a boiling water bath for 20 minutes. The mixture was then aliquoted to 2 ml micro-centrifuge tubes (Eppendorf, 022363344) and stored at 4 °C.

When needed, the aliquoted agarose was reheated in a boiling water bath for 2 minutes to melt. The liquefied agarose was immediately placed in a desiccator, cooled at atmospheric pressure for 1 minute, and then degassed with the laboratory's vacuum system (41.4 kPa) for 1 minute. After

degassing, the liquefied agarose gel was injected into the case until full, and solidified at 4 °C for 8 minutes.

Agar

Agar (Sigma-Aldrich, A9799) was mixed with DI water at a ratio of 1.5% w/w (0.6g agar/40g water) in a 50 ml conical centrifuge tube (Corning, 352098). The tube was then heated in a boiling water bath for 20 minutes. The mixture was then aliquoted into 2 ml micro-centrifuge tubes (Eppendorf, 022363344) and stored at 4 °C.

When needed, the aliquoted agar was reheated in a boiling water bath for 2 minutes to melt. The liquefied agar was immediately placed in a desiccator, cooled at atmospheric pressure for 1 minute, and then degassed with the laboratory's vacuum system (41.4 kPa) for 1 minute. After degassing, the liquefied agar gel was injected into the case until full, and solidified at 4 °C for 8 minutes.

Starch

Hydrolyzed potato starch (Sigma-Aldrich, S5651) was mixed with DI water at a ratio of 40% w/w (1.2 g starch/3 g DI water). The mixture was added to 7 ml boiling DI water contained in a 50 ml conical centrifuge tube (Corning, 352098) to form a thick starch gel suspension at a ratio of 12% w/w (1.2 g starch/10 g DI water) (*81*). The mixture was heated in a boiling water bath and stirred with a glass rod. After 20 minutes of heating, the gel was degassed briefly under a negative pressure of 41.1 kPa, and then injected into the case. The starch gel was solidified at 4 °C overnight.

Gelatin

Gelatin (Carolina, 86-4660) was mixed with DI water at a ratio of 15% w/w (6 g gelatin /40 g water) in a 50 ml conical centrifuge tube (Corning, 352098), and heated in a boiling-water bath for

10 minutes. The mixture was then aliquoted to 2 ml micro-centrifuge tubes (Eppendorf, 022363344) and stored at 4 °C.

When needed, the aliquoted gelatin was reheated in a boiling water bath for 5 minutes to melt. The melted gelatin gel was injected into the case until full. The gel was then cooled at room temperature for 15 minutes to solidify.

Collagen

Collagen gel with a concentration of 5 mg/ml was made by diluting and cross-linking the stock collagen solution (type I collagen from rat tail, 8-10 mg/ml, BD, 354249). The stock collagen solution came suspended in 0.02N acetic acid. The gel cross-linking began once the pH was adjusted to neutral (*70*).

A neutralizing agent was prepared to adjust the gel pH as well as to dilute the collagen concentration to the desired level. The neutralizing agent consisted of 10x PBS pH 7.4, (Gibco, 70011-044), distilled water (Gibco, 15230-162) and 1 N NaOH (Fisher Chemical, SS266-1). The amounts of components were calculated based on the final concentration of collagen gel (5mg/ml) as well as the concentration of the stock collagen solution (varied in different batches). For each batch, pilot experiments were conducted to determine the optimum recipe for the neutralizing agent. The amounts of NaOH and distilled water were adjusted until the pH of the collagen-neutralizing agent mixture matched the pH of 1x PBS, which was 7.4. The pH was measured by litmus paper. After the finalizing the recipe, a bulk volume of the neutralizing agent was prepared, the amounts of each component confirmed by weighing with a scale. Preparing a bulk volume at one time reduced errors; also weighing has less error than volume measurement. The neutralizing agent was stored at 4 °C until use.

When needed, a desired amount of stock collagen was injected into a 2 ml micro-centrifuge tube (Eppendorf, 022363344), and the neutralizing agent was added to the stock collagen thereafter. The amounts of stock collagen and neutralizing agent were confirmed by weighing. The mixture was homogenized by alternatively vortexing (VWR, Vortex-genie 2) and dipping the collagen contained centrifuge tube into ice water. The ice water kept the temperature of the mixture low. Both vortexing and cooling extended for 10 seconds each, and this pair of processes was repeated six times (two minutes in total).

After being mixed, the collagen was degassed at a negative pressure of 41.1 kPa for 5 minutes and then spun in a centrifuge (Fisher, 05-090-100) at 4 °C for 5 minutes to remove the bubbles generated during mixing and vacuuming. Thereafter, 200 μl collagen was injected into the mold immediately and cured at room temperature (21 °C) for an hour.

PDMS (Polydimethylsiloxane)

PDMS was made from a silicone elastomer kit (Dow Corning, Sylgard® 184). The base and the curing agent of the kit were well mixed at a ratio of 10:1, and then, the PDMS mixture was injected into the case. PDMS was cured by heating at 60 °C for 5 hours. After mold removal, the PDMS tunnel was washed with detergent and rinsed with DI water.

PDMS tunnels were reused since no difference in microsphere behavior was observed in new or old PDMS tunnels.

Hydrogel dialysis

Hydrogels were sometimes dialyzed against DI water to reduce ion concentration and allow full hydration. In exploring the presence of EZ, all the hydrogels were tested with and without

dialysis. In all the quantitative studies exploring the two flow regimes, the agarose gel was not dialyzed.

The dialysis procedure depended on the gel type. For agar, agarose, and starch, the raw material was dialyzed in a dialysis tube (Thermo, 88242) prior to gelation (heating). For gelatin and collagen, the gel was dialyzed after gelation.

The duration of the dialysis was set by the value of water conductivity. Ideally, if the conductivity of water used in dialyzing cannot further increase after changing water regularly, then the dialysis can be considered complete. However, components of air may dissolve in DI water, thereby increasing water's conductivity. To exclude this change, an extra container was used as a reference to determine the end point, as follows.

Two mason jars, with a volume of 1 L each, were used for dialyzing: one jar contained the hydrogel and DI water, while the other contained only DI water. Conductivity in both jars was tracked with a conductivity meter (Oakton, CON 100). The water was changed in both jars every 4 hours. The dialysis was considered complete when the conductivity of dialyzing water matched that of the reference water remain unchanged after two consecutive water changing cycles

Microsphere suspensions

Unless stated otherwise, in all experiments described in main text, the microsphere suspensions were made by mixing 1-μm non-functionalized polystyrene microspheres (Polysciences, 07310-15) with DI water at a ratio of 45 μl (1 drop)/15 ml. The microsphere-to-water volume ratio was 1 to 300.

However, for visualizing the EZ next to hydrogels under varied conditions, the following microsphere suspensions were also used:

1. 1-μm polystyrene microspheres with amidine functional groups (Invitrogen, A37322). The ratio of microsphere to DI water was 45 μl (1 drop)/30 ml.

2. 1-μm polystyrene microspheres with amino functional groups (Polysciences, 17010). The ratio of microsphere to DI water was 20 μl/15 ml.

3. 1-μm polystyrene microspheres with carboxylate functional groups (Polysciences, 08226). The ratio of microsphere to DI water was 45 μl (1 drop)/15 ml.

4. 1-μm silica microspheres, (Polysciences, 24326-15). The ratio of microspheres to DI water was 40 μl/15 ml.

5. PDMS beads. The base and the curing agent of the PDMS kit (Dow Corning, Sylgard® 184) were well mixed at a ratio of 10:1 (v/v) to form PDMS mixture. A 0.1% (v/v) Tween 20 (Sigma-Aldrich, P2287) and DI water solution was prepared. The PDMS mixture was mixed with this Tween 20 solution at a ratio of 10:1 (v/v). The mixture was shaken vigorously with a vortex mixer and placed at 60 °C overnight to allow hardening into solid PDMS beads. The PDMS beads were then allowed to settle and was then washed by replacing the supernatant with DI water. This washing procedure was carried out twice, to remove the surfactant (Tween 20) used during preparation (*82*).

When used, the concentration of the PDMS-bead suspension was adjusted with DI water until the turbidity roughly matched that of polystyrene microsphere suspension.

6. Food-grade diatomaceous earth (Perma-Guard), 0.1% w/v. The diatomaceous earth was well mixed with DI water and allowed to settle for 20 minutes. Larger particles settled down during this time. Only the supernatant was used for the experiment, because the size of diatomaceous earth particles suspended in the supernatant was comparable to that of polystyrene microspheres.

7. Food-grade active charcoal powder (Essential Elements®), 0.04% w/v. The carbon powder was well mixed with DI water and allowed to settle for 20 minutes. Larger particles settled down during this time. Only the supernatant was used for the experiment, because the size of active charcoal powder in supernatant was comparable to that of polystyrene microspheres.

Applying IR

The thermal radiation from a water bath, heated by a heating stage beneath, was used as the IR source (Fig. 3.9A). Using a water bath ensured uniform IR input around the Petri dish. The level of IR output could be adjusted by appropriately adjusting the temperature of the water bath. The temperature of the heating stage could be stabilized to ±0.5° C, while the temperature of the water bath could be stabilized to ±0.1° C during the span of an experiment.

The heating stage was milled from an aluminum plate. Two film heating elements (Omega, KH-103/10-P) were attached to the bottom of the stage (Fig. 3.9B). The power of the heating element, which determined the heating rate, was controlled by a power controller (Payne, 18TBP-1-15). The temperature of the heating element was controlled by a temperature controller (AGPtek, STC-1000). A temperature sensor read the temperature of the stage and provided feedback to the temperature controller.

The temperature controller turned on the heating element when the temperature was below the set point; when the temperature was above the set point, the heating element was turned off and the stage was cooled by ambient air. The power of the heating element was adjusted to a level that matched the cooling rate.

Observing self-driven flow

A glass Petri dish (60 mm diameter x 15 mm height, Corning, 70165-60) containing 6 ml DI water was used as water bath. A polystyrene Petri dish (35 mm diameter x 15 mm height, Falcon, 351008) filled with 6 ml of microsphere suspension was placed in the water bath. For experiments with IR application, both water bath and microsphere suspension were preheated with the heating stage for 30 minutes prior to experiments.

After the tunnel was made, the microsphere suspension was injected into the tunnel with a 20-μl pipette through the larger opening on the case. Then, the tunnel was examined microscopically for any air bubbles inside. If necessary, the tunnel was flushed again until all bubbles were removed.

Next, the tunnel-containing case was placed in the middle of the Petri dish containing the microsphere suspension. A drop of DI water was released onto the top surface of the gel, and then the surface was covered with a piece of glass cover slip. The glass cover slip stopped water from evaporating from the hydrogel, and the drop of DI water helped the glass slide to stick to the gel surface.

Further, the water bath and microsphere suspension were covered by a polystyrene Petri dish lid in order to isolate the system from the environment as much as possible. Any water droplets deposited onto the lid appreciably diminishes image quality. Thus, a small observation window was opened on the lid (Fig. 3.20).

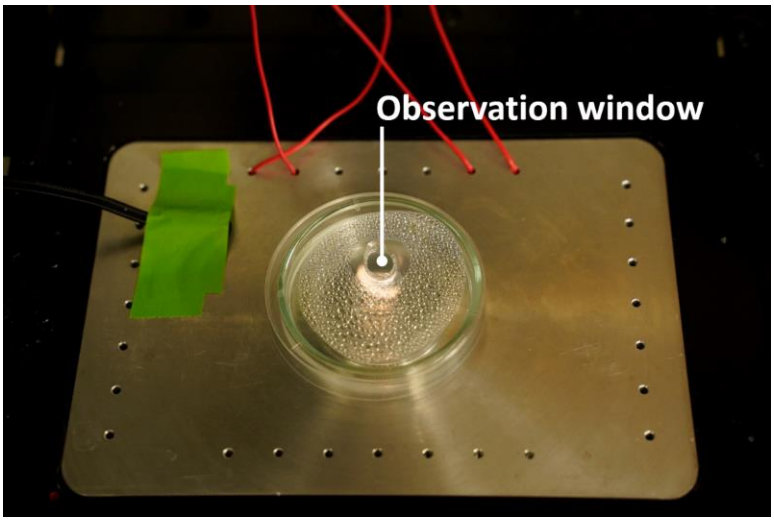

Fig. 3.20. Observation window.During all experiments, the water bath and microsphere suspension was covered with a Petri dish lid containing a small observation window.

A recording of the flow was obtained by using a video camera (Edmund Optics, EO-3112C), mounted on the microscope (Zeiss, Axiovert 100 TV) fitted with a 5x objective (Zeiss, N.A = 0.13) and a 10x objective (Zeiss, N.A. = 0.25). To minimize interference with experimental protocols, the microscope light intensity was kept constant throughout all experiments.

Observing material (solvent)-exchange induced flow

I used the same configuration as for studying self-driven flow, except that the surface of the gel was exposed to the air.

Flow-velocity quantification

The video recording of the flow was pre-processed by ImageJ (*83*). The pre-processing procedure included the following: (i) Splitting the video frames into segments of 20 seconds. Each data point is an average of 20 seconds of flow velocity. (ii) Cropping the regions of interest. (iii) Removing the background. The pre-processed data were then ready for analysis by Particle Image Velocimetry (PIV) (*84-87*) to obtain the flow velocity.

Due to the presence of EZ, the region next to the tunnel wall is devoid of microspheres. Thus, only the middle part of the tunnel was used for data quantification.

Captions for movies

Movie 1. Self-driven flow in agar tunnel.

Movie 2. Self-driven flow in agarose tunnel.

Movie 3. Self-driven flow in gelatin tunnel. The left side of the tunnel was a narrow region, and the right side of the tunnel was a wide region.

Movie 4. Self-driven flow in collagen tunnel.

Movie 5. Self-driven flow in starch tunnel.

Movie 6. No flow in PDMS tunnel.

Movie 7. The end state of self-driven flow in an agarose tunnel.

Movie 8. Material-exchange (water) driven flow in an agarose tunnel.

Chapter 4. Effect of IR on postmortem blood flow

Blood vessels are responsible both for blood transport and for material exchange. Since the SIF mechanism can involve both these features, it is possible that SIF plays a role in driving flow in blood vessels, both under ordinary physiological conditions, and, also when the heart is not beating. Since IR fuels SIF, it should also fuel vascular flow if the hypothesis is tenable. Thus, I studied the effects of IR on both intact and post-mortem circulatory systems.

In this chapter, I will answer the two remaining questions from Section 1.4 Aims. They are:

4) What would be a good *in vivo* model to explore the existence of self-driven flow in circulatory system?

5) Will that effective light for drive self-driven flow drive the blood flow? Even after the heart has stopped beating?

4.1 Chick embryo as a model

Chick embryo vitelline vascular network overview

I employed the chick embryo vascular model for this study (Fig. 4.1). The embryo was incubated for 72 to 75 hours in a commercial egg incubator prior to the experiment, developing to the HH stage 18-20 (*88*). At this stage, the vascular network has a diameter of about 3 cm and floats on the top of the yolk. This is a relatively undeveloped vascular model: neither the smooth muscle nor the sympathetic nerves are fully functional yet (*89-92*); the pulmonary circulation has not started to develop; and, the heart contains only one atrium and one ventricle, without any valves (*93*). Yet, this model contains the necessary elements of a circulatory system, including heart, arteries, capillaries, veins, and blood.

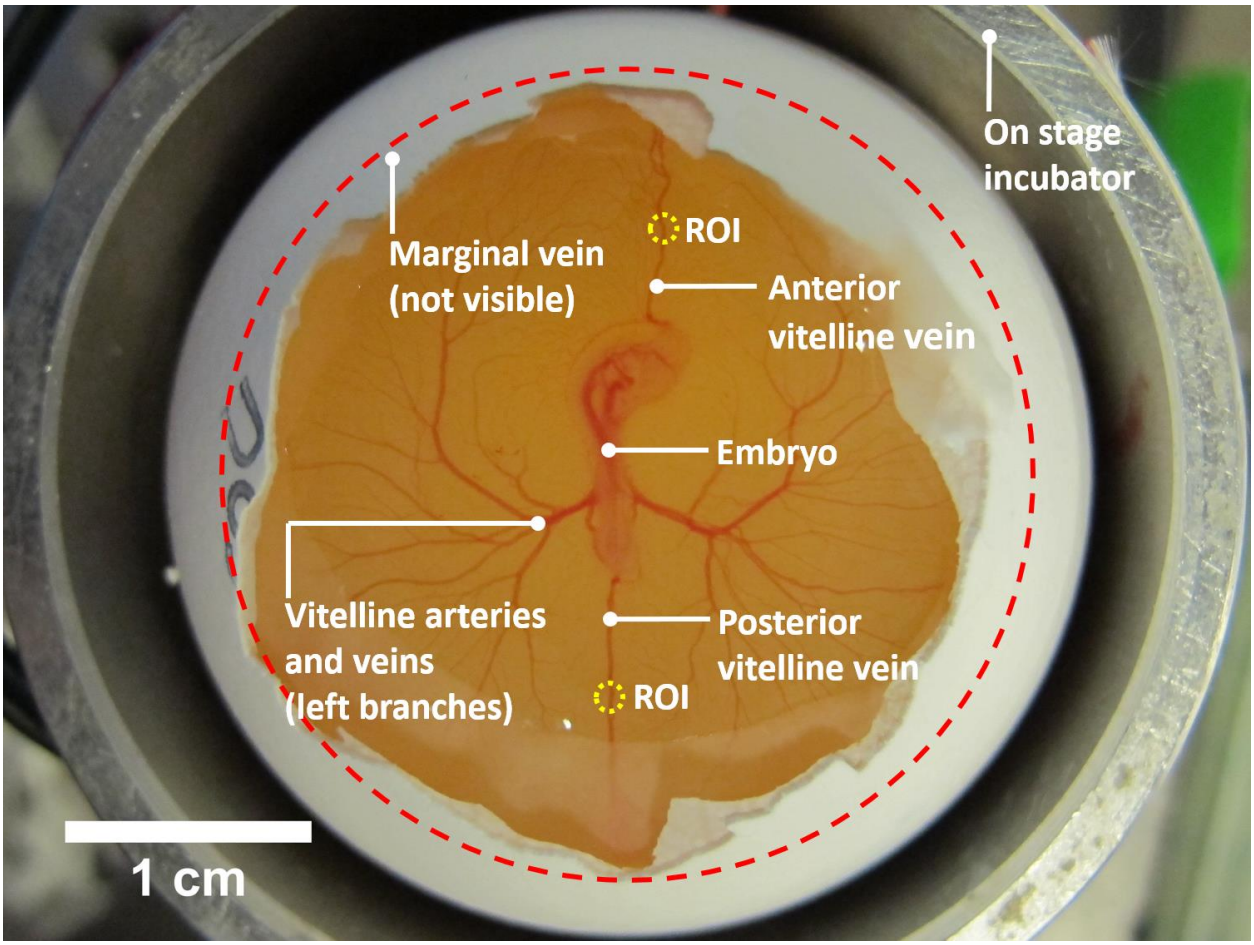

Fig. 4.1. Experimental setup involving three-day old chick embryo, showing vitelline vascular network. The egg was situated in an onstage incubator. The shell's blunt end and the eggshell membrane were removed. The embryo lies on the top-middle of the egg yolk; vitelline arteries and veins grow out of the embryo, and connect to the marginal vein, whose approximate location is marked with dashed red circle. The circle denotes the boundary of the network. Anterior and posterior vitelline veins connect the marginal vein with the embryo. The midpoints of either the anterior or posterior vitelline vein, marked with yellow circles, were selected as regions of interest (ROI), where quantitative blood flow measurements were made.

Choose region of interest

I chose the anterior or posterior vitelline veins for quantitative studies (Fig. 4.1). A consistent region of interest (ROI) of those veins can be selected, due to the vein's non-branching nature and relatively uniform diameter along its length. The middle section along one or the other vein was selected as the ROI (Fig. 4.1, yellow circles). Pilot experiments showed that the blood flow velocities were similar in the two veins; hence, vein selection was based primarily on accessibility.

Vitelline arteries and capillaries, on the other hand, were studied only qualitatively. This is because the vitelline arteries lie beneath the vitelline veins (Fig. 4.2), making visibility difficult; also, the branching nature of the vitelline arteries made it hard to select a consistent ROI.

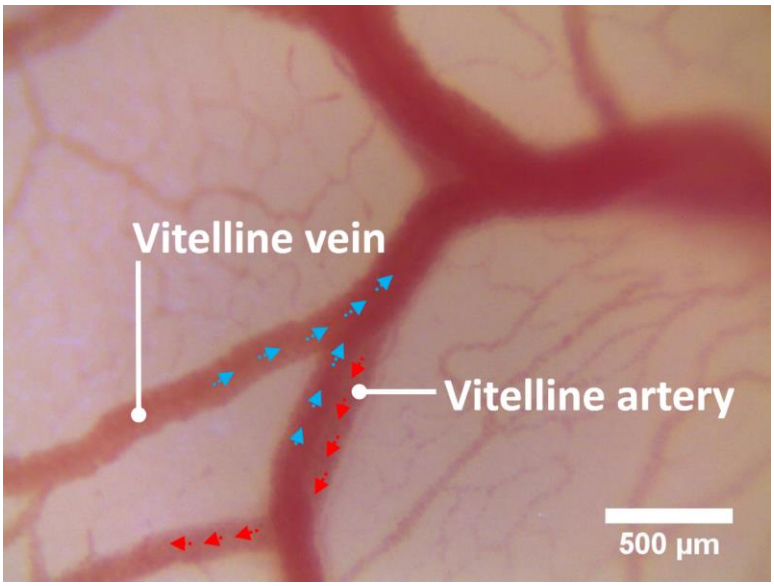

Fig. 4.2. Close-up photo of vitelline artery and vein in live chick embryo. Artery and vein overlap, the artery lying partially beneath the vein. Blue arrows indicate the direction of venous flow, red arrows, arterial flow.

Measure blood flow

Blood flow was recorded using a camera outfitted with an objective lens; and, velocity was quantified by particle image velocity (PIV). In all experiments, the chick embryo was situated in an on-stage incubator, whose temperature was maintained at 37 ± 0.5 °C. A ceramic IR lamp was used as an IR source. The experimental configuration is shown in Fig. 4.3.

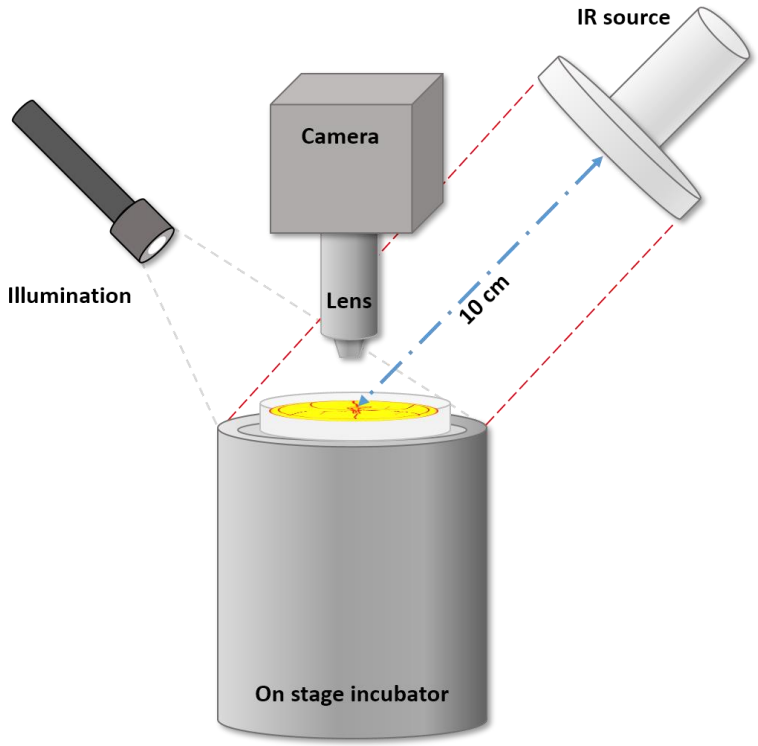

Fig. 4.3. Experimental configuration for applying IR to the chick embryo.

4.2 Postmortem blood flow

Establish postmortem circulation model

To establish the postmortem circulation model, cardiac contraction was arrested by injecting 10-30 µl of 3M KCl solution into the embryonic heart (*19*). The heart stopped within one or two seconds after injection.

Dynamics of postmortem blood flow

I began this study by observing the dynamics of the postmortem blood flow.

Vein

Postmortem venous blood flow was observed at the ROI. With the cessation of cardiac contraction, blood flow slowed substantially, but did not stop. In most cases, flow diminished from ~1,200 μm/s to ~ 15 μm/s within approximately 5 seconds. At approximately two minutes, a minor acceleration typically occurred, stabilizing the flow at ~25 μm/s (Movie 9). The flow direction remained essentially unchanged throughout. In some cases, blood flow at the ROI briefly stopped after euthanization and turned transiently towards the opposite direction; however, the flow restarted and resumed its original direction within half a minute to one minute (Movie 10). Essentially, the postmortem venous blood flow direction was the same as the natural venous flow direction. This feature was observed in all experiments without exception.

The blood accumulated in the vein. This occurred because the blood continuously flowed towards the heart, but the non-beating heart blocked passage. The accumulation began in the region proximal to the heart; once a region became filled with blood cells, the flow stopped. Postmortem blood flow could persist for up to 20 minutes at the ROI. And, in regions farther from the heart, i.e., closer to the marginal vein, the flow could persist for up to 1 hour (Movie 11).

Capillary

Observations were also made on postmortem blood flow in capillaries. The flow stopped after cardiac arrest in most capillaries, but persisted in a small fraction. In those open capillaries, the majority flow direction was from artery to vein, i.e., in the natural direction (Movie 12).

Artery

In addition to observing blood flow in veins, I also observed postmortem blood flow in arteries. Immediately after the cardiac arrest, arterial blood flow close to the heart stopped, and could even change direction. The reversal (flowing towards the heart) could last for several minutes. After approximately 10 minutes, however, the flow gradually resumed its natural direction, away from the heart. The restitution of natural flow in arteries occurred first at the peripheral region of the circulatory network, gradually moving upstream and ultimately reaching the heart region by the end of the experiment (Movie 13).

But ultimately, the blood flow resumed its original direction, away from the non-beating heart. Eventually the arteries emptied (see 4.6 Materials and methods and Movie 13 for detailed dynamics). They became pale, indicating loss of red blood cells (Fig. 4.4). The tendency to empty was consistent in all experiments.

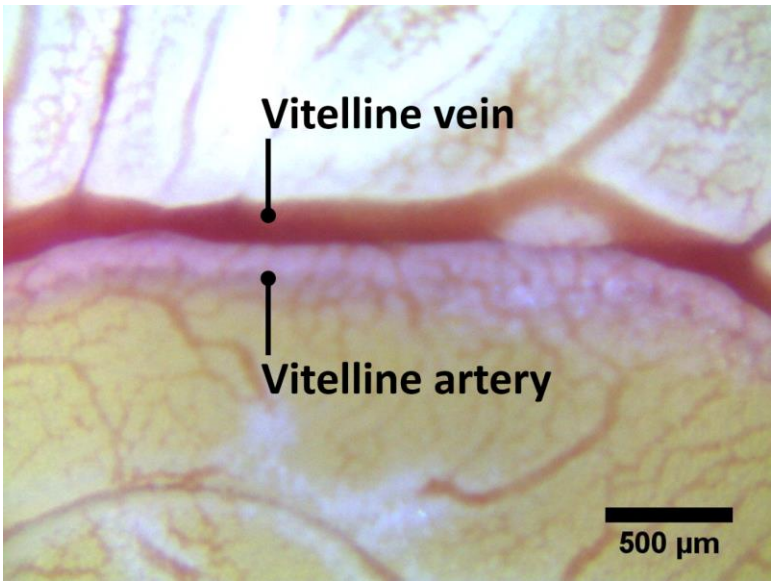

Fig. 4.4. Postmortem blood flow empties arteries and fills veins. Blood distribution 20 minutes after the heart stopped. Blood tends to leave arteries (pale vessels) and accumulate in veins (dark red vessels).

Cell-free layers

After cardiac arrest, I observed cell-free layers, i.e., layers devoid of red blood cells, showing up as annuli, just inside the blood vessel wall. Fig. S3A shows vitelline arteries of an intact embryo. The cell-free layer was not visible. Fig. S3B shows the same blood vessels, about 150 seconds after the heart was stopped, where a cell-free layer showed up just inside the vessel wall.

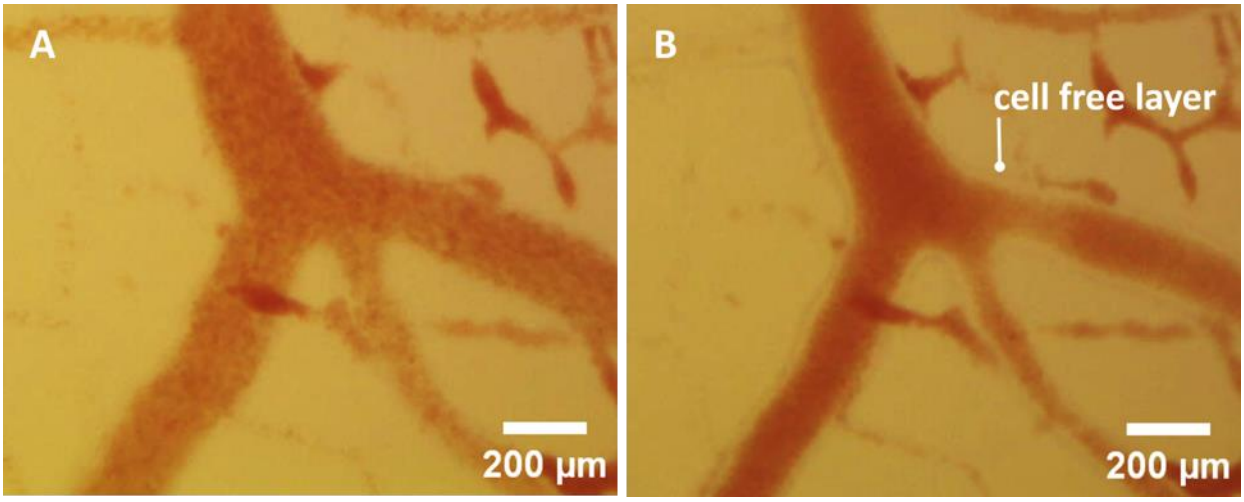

Fig. 4.5. The presence of cell-free layer (exclusion zone) in postmortem blood vessels. (A) Vitelline arteries of live chick embryo. The cell-free layer was not visible. (B) Vitelline arteries of embryo 150 seconds after cardiac arrest. Note the cell-free layer at the vessel wall. These figures are snapshots from Movie S5, in which the dynamics of the cell-free layer and postmortem flow were shown.

In the postmortem venous blood flow, even though the blood vessel wall could not be clearly observed, the fact that the blood stream became narrower indicates that the red blood cells were excluded from the region of the wall (Movie 9).

Potential alternative explanation for postmortem blood flow

It is worth noting that the emptiness of postmortem arteries is hardly a new observation. As mentioned in introduction, even the word 'artery' originated from the observation that the postmortem arteries are empty. Generally, the emptiness of arteries is considered to be caused by gravitational force (*94*) and/or vascular contraction (*18*).

However, when this happened on chick embryo, things are different. Gravitational force could impact postmortem blood distribution (*94*), especially in biological entities with a prominent 3D

structure, such as rat, mouse, or human. However, the chick embryo vascular network formed an almost horizontal plane. The only exception is at the middle of the vascular network, where the embryo pressing on the center of the yolk sac membrane created a dent, like a ball pressing down a rubber membrane. If gravitation were the major driving force, the blood should accumulate in the blood vessels in the dent, regardless of whether they are arteries or veins. However, in the arteries close to the heart, blood flowed against the direction of the gravitational pull, ultimately emptying. Thus, gravitational force does not appear to cause the chick embryo postmortem circulation.

Another hypothesis is that a progressive contraction in some region of the vascular system caused the postmortem blood flow. If the postmortem blood flow were solely caused by any such vascular squeeze, then the blood should flow consistently away from the site of that contraction, i.e., in both directions. The contraction could occur somewhere in the vascular system (although vascular smooth muscles are not yet fully developed in the 3-day old embryo). At the end of each experiment, the blood in both vitelline arteries flowed away from the heart. According to this logic, the heart could have been squeezing continuously. Fist, the non-nourished, valveless heart was arrested by KCl, which relaxed the cardiac muscle (*95*). Second, any contraction of the non-nourished, valveless heart should have expelled the blood out of the vein as well, but this was not observed.

The observations on postmortem blood flow indicate that some mechanism beyond cardiac contraction exists to drive blood flow from artery to vein. The SIF mechanism is capable of generating directional flow in a tube (see supplemental material for detailed explanation). Thus, the SIF mechanism maybe responsible for the postmortem blood flow.

4.3 Effect of IR on blood circulation

The utilization of IR as a fuel is a signature feature of SIF. If SIF is playing a role in circulatory system, IR should likewise fuel blood flow, with or without a beating heart.

Effect of IR on live circulation

I began this study by testing whether IR would increase flow in the intact, physiological situation.

After the embryo was prepared, blood flow was measured at the ROI for three minutes, as a control. Following that, IR was applied, also for three minutes.

The result is shown in Fig. 4.6: blood flow velocity increased by ~30% with IR application. The increase began almost immediately, and diminished after the IR was removed. The positive effect of IR on blood circulation is therefore confirmed, and this result is in line with other studies (*74*, *96*).

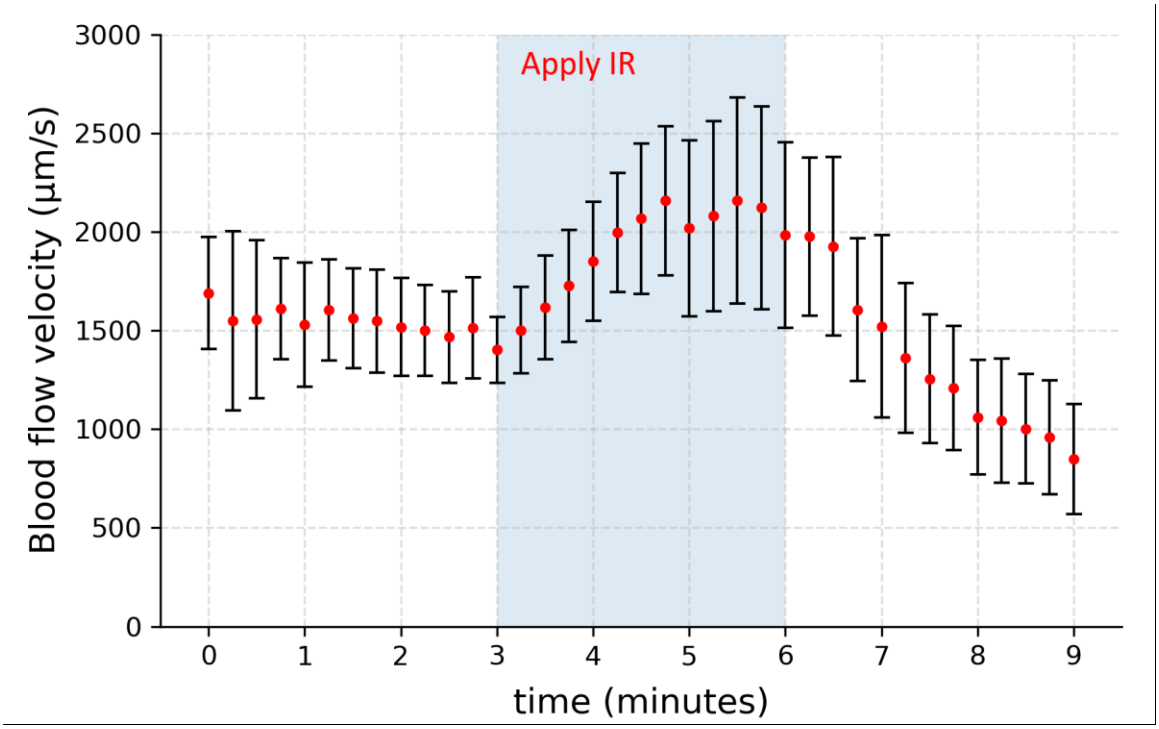

Fig. 4.6. Effect of IR on live chick embryo circulation. Blood flow increased appreciably when IR was turned on, and decreased after the IR was removed. N=4. Error bars show standard deviation.

However, the heart rate rose as well. The change of heart rate was tracked on one embryo. In four IR application cycles, the heart rate rose from 100.5 ± 14.3 beats/minute (SD) to 139.8 ± 10.3 beats/minute (SD), and then diminished to below baseline values after IR was removed. Given the increase of heart rate, I cannot say for sure whether the increase of flow came from that rate increase or from the SIF. Thus, I turned to the postmortem circulation model, to eliminate the heart as a factor.

Effect of IR on postmortem blood flow

IR-induced flow enhancement is a signature feature of the SIF mechanism, and I tested the effect of IR using the postmortem circulation model. The protocol was similar to the IR study with the intact embryo: After the heart was stopped, blood flow was measured at the ROI for three

minutes, as a control. Following that, IR was applied, also for three minutes, and then withdrawn. Postmortem blood velocity significantly increased during IR exposure, reaching a peak more than three times the control value after approximately three minutes (Fig. 4.7). Following removal of the IR source, the velocity returned near to its original value.

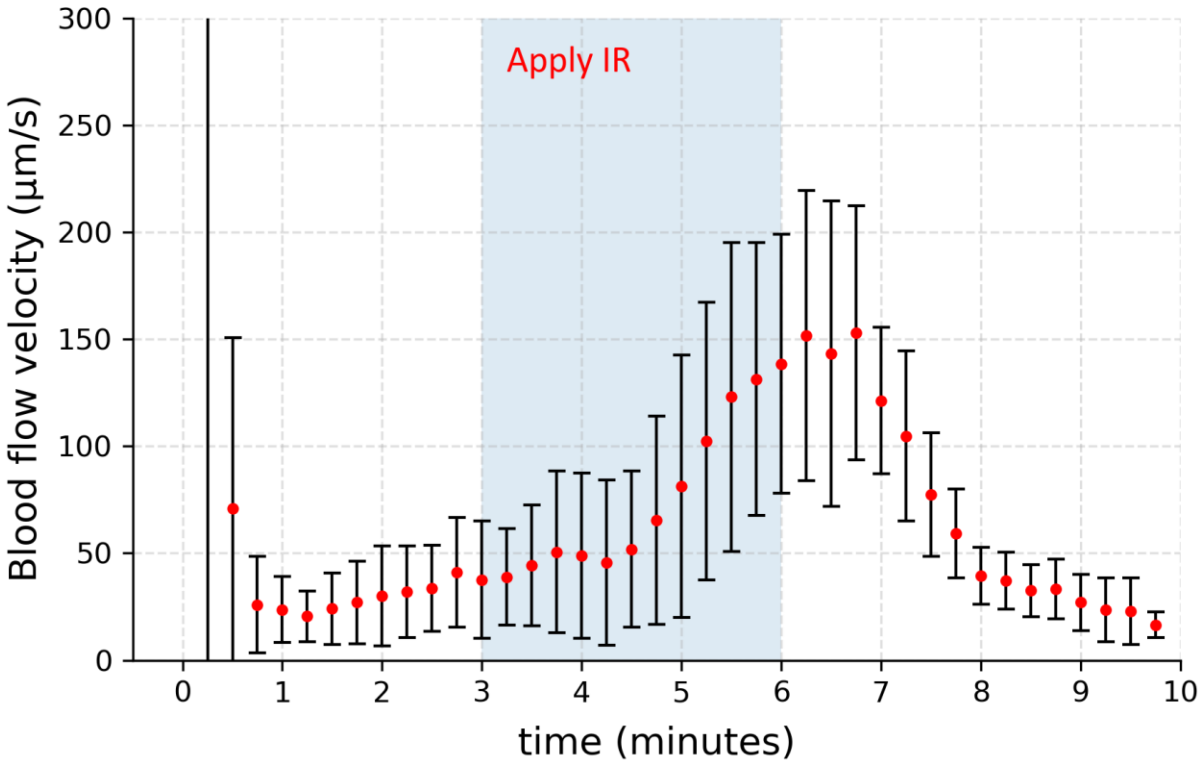

Fig. 4.7. Effect of IR on postmortem circulation. N = 6. Error bars show standard deviation. Postmortem flow increased appreciably after IR was turned on.

A potential alternative explanation for the effect of IR is convection. When IR is applied, an increase of temperature is inevitable. In fact, the embryo's surface temperature, rose 5.05 +/- 0.10 °C (SD; N=5) following 3 minutes of exposure (Fig. 4.8). It is tempting to suggest that the IR enhancement of the flow might occur through convection. Natural convection is driven by buoyancy: If the heat source lies at the bottom of the container, the liquid at the warmer bottom should rise because of its lower density, while liquid at the cooler surface level ought to sink

because of its higher density, thus forming a convection circuit. Following this hypothesis, IR application may introduce steeper temperature and density gradients, thereby enhancing the convectional flow. Any such enhanced flow could theoretically occur in two configurations: in single blood vessels; or, between arteries and veins.

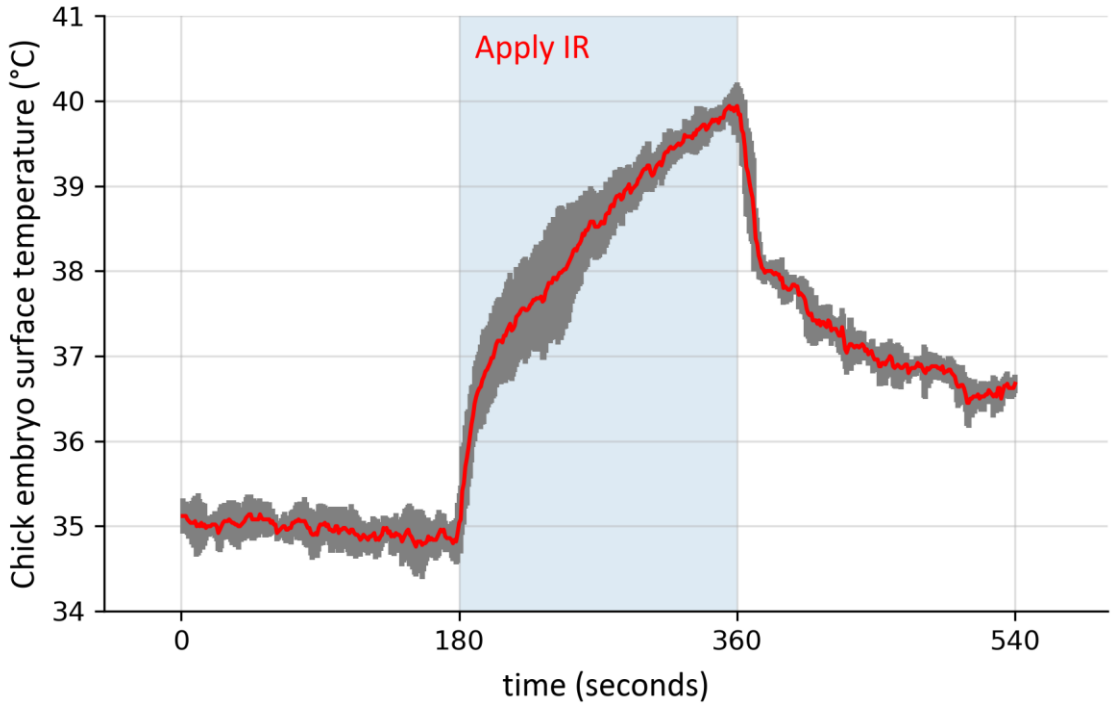

Fig. 4.8. Chick embryo surface temperature change resulting from IR radiation. N = 5. Error bars (grey) show standard deviations.

In the case of the single blood vessel, the flow pattern inside the vessel should be an up-down loop, with two streams of oppositely directed flow in the same vessel segment. This was never seen; I consistently observed flow in only one direction at a time. For the second case, if convection caused the directional flow, then when the temperature gradient reversed, the flow direction should likewise change. When the external IR comes from the egg incubator, positioned below, instead of the IR lamp above, the temperature gradient is reversed; nevertheless, the flow pattern stayed

the same, always from artery to vein. Thus, thermally induced convection appears unable to explain the effect of IR on postmortem blood flow.

Since IR-driven flow is a signature feature of the SIF mechanism, the observed positive effect of IR on postmortem blood flow supports the SIF mechanism as being responsible for the observed flow.

Effect of deficient IR on intact circulation

If IR plays an important role in driving blood circulation, it is logical to think the circulation will be comprised when IR is deficient.

Manteuffel-Szoege and colleagues (*22*) studied the effect of hypothermia (low IR) on the vitelline circulation of the four-day-old live chick embryo at different temperatures. When the temperature was reduced to 20-25°C (less IR), the heart kept beating. However, the blood was not able to pass through the capillaries; it collected in peripheral regions of the arterial circulation, resulting in capillary overfilling.

I repeated their experiment. A three-day-old chick embryo was carefully transferred into a beaker which was held at room temperature, varying between 19 to 23°C.

At lower temperature, capillary blood flow mostly stopped with blood cells filling the capillaries (Fig. 4.9).

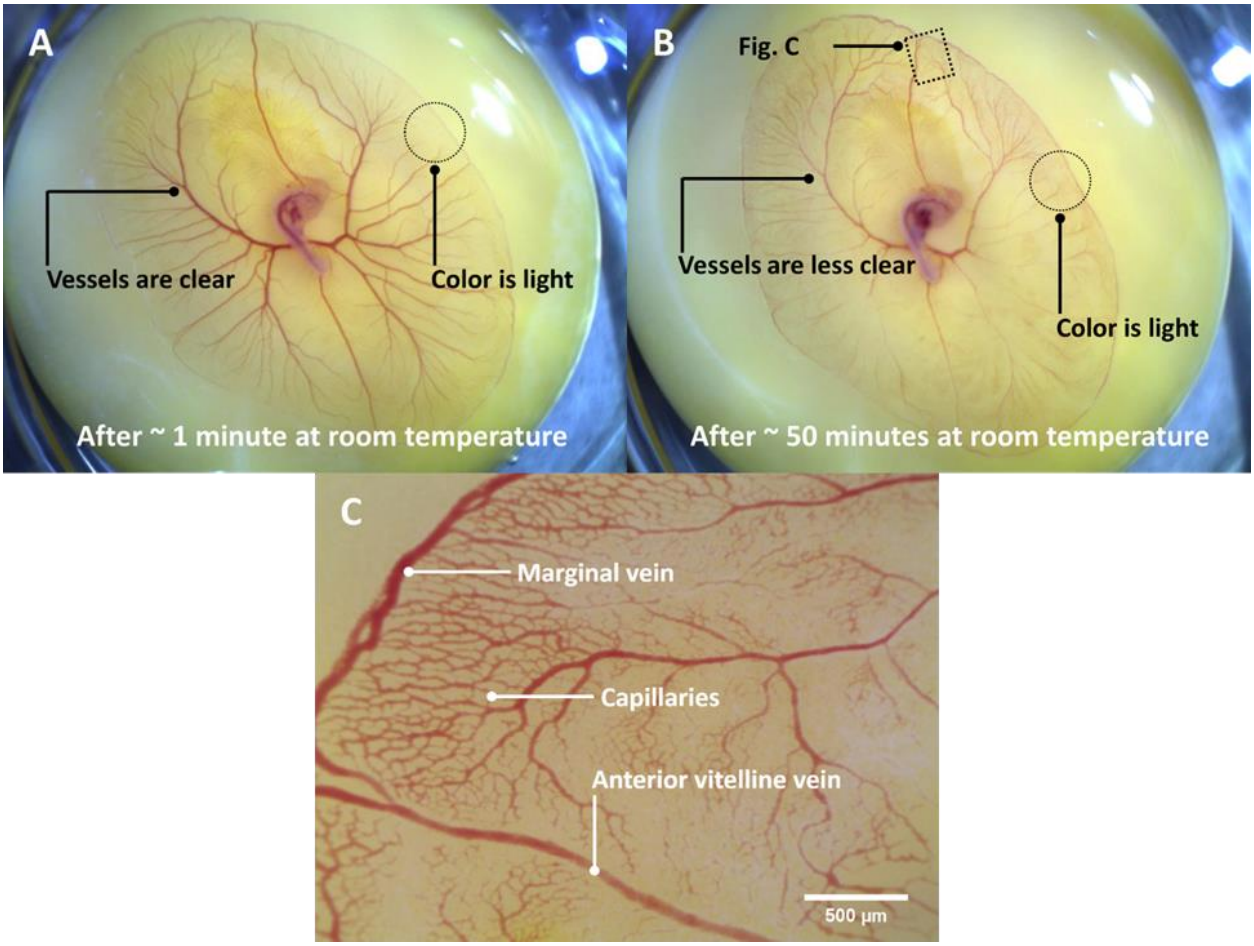

Fig. 4.9. Effect of IR deficiency on live chick embryo circulation. (A) The embryo was placed at room temperature for 1 minute. The major vessels, arteries and veins, were clear. The capillaries, which located around the ends of the major blood vessels (the boundary region of the vascular network) was light in color. (B) The embryo was placed at room temperature for 50 minutes. The major vessels were less clear, and the region at the end of major blood vessels became darker in color. (C) Capillaries at higher magnification. Red blood cells accumulated in capillaries.

Fig. 4.9A shows the vitelline vascular network, 1 minute after the embryo was placed at room temperature. The heart was beating at a normal rate (~ 160 beats per minute). The major blood vessels, arteries and veins, were red and clear. The red and distinct blood vessels indicated that the vessels were well filled with blood. Capillaries, which located at the ends of arteries and veins (e.g.

boundary of the vascular network) had light color. The light color indicates the red blood cells were not accumulated in capillaries.

Fig. 4.9B shows the vitelline vascular network, 50 minutes after the embryo had been placed at room temperature. The heart was still beating, but at a very slow rate (~10 beats per minute). The major blood vessels became pale and less clear, indicating a loss of blood cells. At the end of arteries and veins, where capillaries located, the color became darker. The dark color indicated that red blood cells were accumulated in capillaries. With a higher magnification, I could observe that the blood cells accumulated in capillaries (Fig. 4.9C). Only a small number of capillaries provided a passageway for blood circulation.

When the embryo was returned to the incubator, the closed capillaries gradually opened, and the blood flow resumed. Thus, deficient IR associated with the lowered temperature apparently did reversibly diminish blood circulation. Possibly, the SIF mechanism was compromised by deficient IR.

4.4 Discussion of Chapter 4

In this section, I provide an explanation on how the SIF mechanism can be used to explain the postmortem blood flow, as well as intact blood flow.

SIF in the postmortem circulatory system

As analyzed in Chapter 3, chemical concentration gradients in a blood vessel may arise from surface activities: water-surface interaction, as well as material exchange.

After the heart stops beating and the embryo begins dying, the rate of material exchange should slow down. Thus, material exchange should not be considered as the main mechanism for driving blood flow in the postmortem situation.

The presence of a cell-free layer next to the vessel wall (Fig. 4.5) implies the existence of an EZ, and therefore a water-hydrogel interaction. Thus, the same self-driven flow found in gels may exist as well in the blood vessels.

Self-driven flow follows the direction of the proton concentration gradient, a direction that should be determined by the surface to volume (S/V) ratios along the tube. In a tapered tube, self-driven flow drives flow towards region with more capacity — from high S/V to low S/V (Fig. 3.4).

Blood vessels branch and decrease in diameter from the artery to the capillary. Thus, S/V in individual vessels increases. From capillary to vein, the opposite occurs: S/V decreases.

If this S/V paradigm applies, then in the venous vessels, the self-driven flow mechanism should drive the postmortem blood from capillaries to veins. This corresponds to the natural course of blood flow direction. This explains why the direction of postmortem blood-flow was consistent in veins, with only transient reversals if any.

In the arterial system, the self-driven flow mechanism predicts a flow from capillaries to arteries. This is against the natural course of the blood flow direction. This reversal (from artery to the heart) of the predicted blood flow direction in the wider arteries. With the presence of the cell-free layer — a signature of self-driven flow — postmortem blood flow reversed in those wider arteries that lie far from capillaries, and this reversal lasted a lot longer than that of postmortem venous blood flow. The reversal of the blood flow direction actually suggested the existence of self-driven flow.

In arterioles, which connect directly to capillaries, things are different. The capillaries connect arterioles and venules. Both arterioles and venules have a lower S/V than capillaries. Since self-

driven flow should point from high S/V to low S/V, the question becomes: between the arterial system and venous system, which S/V is lower?

In general, individual veins have a larger cross-section than the corresponding arterioles (*97*). The venules have a lower S/V than the arterioles. Thus, in capillaries, the direction of the self-driven flow should point to the veins.

Even though the direction of the self-driven flow in larger arteries did not follow the natural course at the beginning, in arterioles, the direction did follow the natural course — due to the larger S/V of the veins. In capillaries, self-driven flow continuously transports blood into the vein, gradually, the blood in larger arteries that is distal from capillaries will reinstitute the natural blood flow direction. This explains why the reinstitution of the arterial blood flow direction originated from the capillaries, gradually reaching the larger arteries.

SIF in the live, physiological circulatory system

As argued above, the self-driven flow mechanism should exist not only in the postmortem situation but also in the live circulatory system.

On the other hand, the material-exchange is not negligible in the live circulatory system. That exchange can fall into two categories: materials entering the blood vessels, and materials exiting the blood vessels.

Where materials enter the blood vessels, the situation is in some ways comparable to self-driven flow mechanism — materials entering the vessel through the vessel wall vs. protons released into the vessel from EZ at the vessel wall. The phenomena are similar, since chemicals are released into the vessel through the boundary. For this scenario, material entering the tunnel, a flow should generate pointing from high S/V to low S/V (narrow to wide).

The opposite scenario, materials exiting the blood vessel, should generate a flow pointing from low S/V to high S/V (wide to narrow). This was described in Section 2.5, where water leaves the tunnel through the boundary.

Capillaries are the sites for material exchange. A question arises: In a length of capillary, where exactly do materials enter/exit? In the middle? At either end? The answer should have relevance for the expected direction of flow.

Then answer can be found in standard physiology textbooks. The materials leave the capillaries at the arterial end; and, they enter the capillaries at the venous end. Fig. 4.10 shows this process. This is not an artifact of what the illustrator has drawn. Capillary hydrostatic pressure pushes fluid out of the blood vessel wall at the arterial end, and blood colloidal osmotic pressure absorbs fluid into the blood vessel at the venous end.

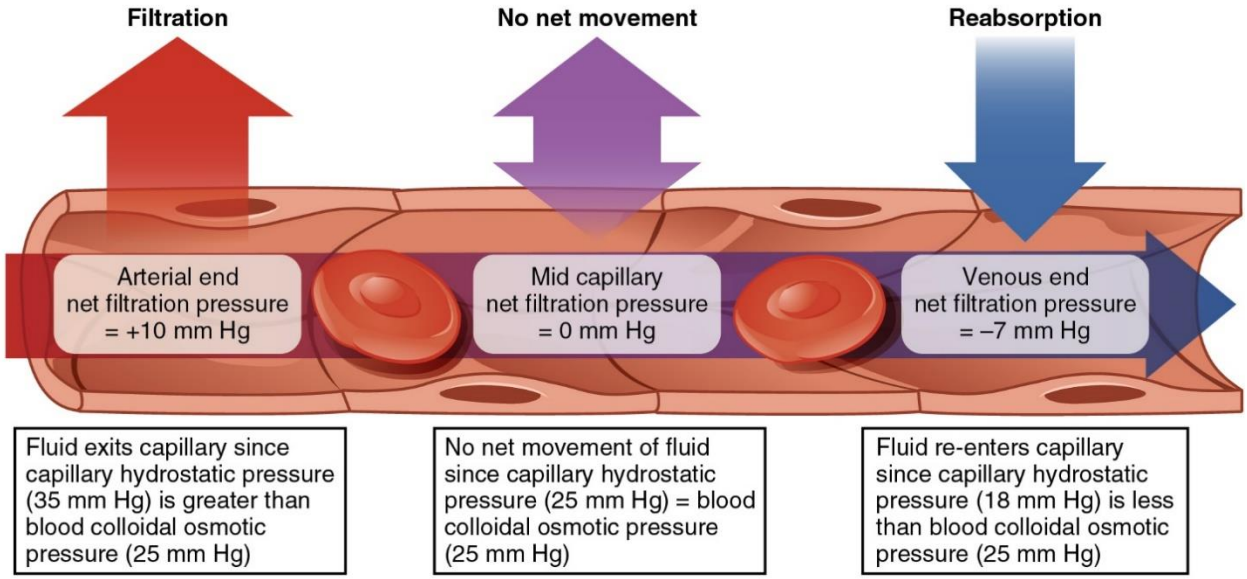

Fig. 4.10. Materials leave the capillaries at the arterial end, and enter the capillaries at the venous end (*98*).

Thus, the material exchange-induced flow should confer kinetic energy at the arterial end, pointing from artery to vein due to materials leaving the capillaries through the wall; and, at the venous end, since materials are entering the capillaries through the wall, material exchange induced flow should exist as well, pointing from arteries to vein. Thus, the blood may gain the kinetic energy to transport itself in capillaries through material exchange, and the direction should be consistently from artery to vein.

It is worth noting that the pressure gradient helps the process of material exchange — hydrostatic pressure drives fluid out of the blood vessel. Thus, the pressure gradients should still be important for driving the blood flow, but how pressure gradient drives a flow need to be reconsidered. In larger blood vessels, the pressure gradient can efficiently drive a flow by pushing directly. In narrower blood vessels, the pressure gradient may drive the blood more efficiently through SIF.

Another point worth noting: flowing fluid will exert a force on the vessel wall, generate a pressure. Since capillaries can generate SIF pointing from arteries to veins, SIF should generate a pressure at the venous side, and this venous pressure should be proportional to the kinetic energy of SIF generated by the capillaries.

4.5 Conclusion to Chapter 4

In 1628, William Harvey published his discovery of the blood circulation, proposing that the heart pumps the blood around the body (*9*). Harvey's contribution is considered a monumental advance in understanding the circulation. For most, Harvey's ideas stand. As the clock turns today, however, the limitations of that simple model have seemed sufficient to prompt the emergence of multiple publications questioning aspects of that long-held model, including a 2014 book citing

numerous pieces of experimental and clinical evidence demonstrating the inconsistency of the conventional pressure-gradient driven model (*28*).

The results obtained here lead us to suggest one addition to the standard model: the vessels themselves may drive blood flow, the power coming from IR energy. That energy may come both from the external environment and/or from metabolic reactions, which generate heat and IR.

Identifying this supplementary driver of blood flow may have important implications not only for understanding cardiovascular dynamics but also for developing novel therapeutic approaches.

4.6 Materials and methods

On-stage incubator

An on-stage incubator was used to maintain the temperature of the egg during the experiment. The incubator was made by wrapping a flexible strip heating element (TEMPCO, SHS80389) around an aluminum tube (inner diameter: 4.5 cm; outer diameter: 5.1 cm; height: 6.5 cm). The heating element heated the aluminum tube, while the tube's thermal radiation heated the egg. The power of the heating element, which determined the heating rate, was controlled by a power controller (Payne, 18TBP-1-15). The temperature of the heating element was controlled by a temperature controller (AGPtek, STC-1000). A temperature sensor read the stage temperature and provided feedback to the temperature controller. The temperature of the incubator was maintained at 37±0.5°C throughout the experiment.

Embryo model preparation

Pathogen-free white leghorn chicken eggs (Charles River, specific pathogen-free, research grade, fertile, 55-59 grams) were incubated for 72 to 75 hours (corresponding to Hamburger–Hamilton stage 18-20) in a commercial egg incubator (Brinsea Mini Advance Hatching Egg

Incubator). The temperature of the incubator was set at 37.5 °C and the humidity of the incubator was maintained by continuously evaporating water in a built-in water reservoir. An integrated motor of the incubator rotated the eggs 15 degrees every 45 minutes.

After incubation, the embryo was ready for experiments. The egg was transferred to the on-stage incubator, in an upright position with the blunt end up. Extra padding was added at the bottom of the egg to ensure stability, and to adjust the height of the egg. A portion of the eggshell and the eggshell membrane were carefully removed by using a pair of tweezers (Dumont tweezer, Style 55, Domostar, 72707-01) to expose the embryo.

For post-mortem experiments, the embryonic heart was arrested by directly injecting 10-30 µl 3 M potassium chloride (J.T.Baker, 3040-01) solution into the heart with a syringe outfitted with a 27G x ½ inch needle (BD, 309623) (*7*). Occasionally, the intrusive nature of this procedure caused cardiac hemorrhaging; those specimens with hemorrhage were excluded from the study.

For the qualitative studies of postmortem arterial and microcirculatory flow, the entire contents of the egg were poured into a 50-ml beaker (Fisher, fb-100-50), which was kept warm in the on-stage incubator. This configuration allowed visualization of the boundary portion of the embryo's blood vessel network, which was ordinarily blocked by the eggshell.

Flow data acquisition and quantification

The embryo was illuminated with white light from an LED flashlight (CREE, XLAMP XP-E LED). In quantitative studies, blood flow was recorded using a video camera (Edmund Optics, EO-3112C) outfitted with a 32x objective lens (Leitz Wetzlar, 32x, N.A. = 0.40). The lens was mounted onto the camera by a C-Mount to a DIN objective ring mount (Edmund Optics, #03-627).

The camera was connected to a computer via a USB interface. By decreasing the camera field through camera-software control, the frame rate could reach 80 frames per second.

With red blood cells as tracers, the flow video could be analyzed by Particle Image Velocimetry (PIV) to obtain red blood cell velocity (*84-86, 99*). Due to changes of blood-stream width, the flow velocities were routinely measured at the middle part of the vessels (Fig. S2), where red blood cells were always available for tracking.

In the qualitative studies of postmortem arterial flow and postmortem microcirculation, videos were recorded with the same camera but using a 6x or a 10x objective lens (Ernst Leitz Weltzar, 6x, N.A. = 0.18; Bausch & Lomb Opt. CO., 10x, N.A. = 0.25). The relatively larger field of view permitted easy tracking of circulatory dynamics in different vessels simultaneously.

External IR application

To apply infrared radiation to the chick embryo, a 150-watt ceramic heat emitter (Zoo Med, CE150) was used. This lamp emitted IR at wavelengths ranging from 1 μm to 14 μm, with a peak at 2.9 μm.

In all experiments the IR source was turned on for 30 minutes prior to experimentation to stabilize the output, and then brought to the experimental setup. The IR lamp was fixed to a claw holder, with adjustable height and angle. This source was directed down to the surface of the exposed chick embryo at an angle of 45° with respect to horizontal surface. The distance between the center of the IR source and the center of the embryo surface was 10 cm. The height and angle of the IR lamp were adjusted beforehand; and the experimental location of the claw holder was marked on the table with tape. Thus, the stabilized IR lamp could be quickly applied and removed as needed.

In the postmortem circulation experiments, the first three minutes of the blood-flow recording immediately after cardiac arrest was considered as the control, while in the live circulation experiments, the first three minutes of the blood-flow recording after the embryo had been properly prepared was used as control. In both experiments, the second three minutes of recording tracked the blood flow during IR exposure, while the final three minutes recorded the blood flow after IR exposure. These time points were marked in the video by blocking the illumination light briefly.

Temperature measurement

The temperature increase arising from IR treatment was measured with a thermometer (Omega, HH306A) outfitted with a type-K thermocouple. The thermocouple was inserted immediately underneath the surface of the egg yolk. Due to the principle of humane use of animals, the temperature measurements were performed on non-experimental samples, either on less-developed or non-developed eggs.

Caption for Movies

Movie 9: Postmortem venous blood flow at ROI.

Movie 10: Postmortem venous blood flow at ROI, with brief reversal.

Movie 11: Postmortem venous blood flow at the boundary of the vascular network.

Movie 12: Postmortem blood flow in capillaries.

Movie 13: Postmortem arterial blood flow dynamics. This footage was taken on an embryo with the vascular network deformed, so as to expose the vitelline artery.

Bibliography

1. R. F. Rushmer, *Cardiovascular dynamics*. (Saunders, Philadelphia [Pa.], 1976), pp. 1-5.
2. G. Friedland, Discovery of the function of the heart and circulation of blood. *Cardiovascular journal of Africa* **20**, 160-160 (2009).
3. W. C. Aird, Discovery of the cardiovascular system: from Galen to William Harvey. *Journal of Thrombosis and Haemostasis* **9**, 118-129 (2011).
4. K. Patwardhan, The history of the discovery of blood circulation: unrecognized contributions of Ayurveda masters. *Advances in Physiology Education* **36**, 77-82 (2012).
5. *Huang Di nei jing su wen: An Annotated Translation of Huang Di's Inner Classic – Basic Questions*. (University of California Press, Berkeley Los Angeles), vol. 1, pp. 584.
6. P. Ebers, *Papyrus Ebers. Die Maasse und das Kapitel über die Augenkrankheiten*. (1890).
7. M. Akmal, M. Zulkifle, A. H. Ansari, Ibn Nafis – a forgotten genius in the discovery of pulmonary blood circulation. *Heart Views : The Official Journal of the Gulf Heart Association* **11**, 26-30 (2010).
8. J. M. S. Pearce, Malpighi and the Discovery of Capillaries. *European Neurology* **58**, 253-255 (2007).
9. W. Harvey, *On the Motion of the Heart and Blood in Animals*. (Prometheus Books, 1993).
10. P. Ebers, B. Ebbell, *The Papyrus Ebers, the greatest Egyptian medical document. Translated by B. Ebbell*. (Copenhagen; Oxford University Press: London, Levin & Munksgaard, 1937).
11. R. E. Klabunde, *Cardiovascular physiology concepts*. (Wolters Kluwer Health/Lippincott Williams & Wilkins, Philadelphia, 2012).
12. H. M. Knower, Effects of early removal of the heart and arrest of the circulation on the development of frog embryos. *The Anatomical Record* **1**, 161-165 (1907).
13. N. E. Kemp, Morphogenesis and metabolism of amphibian larvae after excision of heart. I. Morphogenesis of heartless tadpoles of rana pipiens. *The Anatomical Record* **117**, 405-425 (1953).
14. N. E. Kemp, B. L. Quinn, Morphogenesis and metabolism of amphibian larvae after excision of heart II. Morphogenesis of heartless larvae of amblystoma punctatum. *The Anatomical Record* **118**, 773-787 (1954).
15. R. Skalak, P. I. Branemark, Deformation of Red Blood Cells in Capillaries. *Science* **164**, 717 (1969).
16. R. Rushmer, in *Cardiovascular dynamics*. (Saunders, Philadelphia, 1970), pp. 9-12.
17. V. Kalchenko *et al.*, In vivo dynamic light scattering imaging of blood coagulation. *J Biomed Opt* **12**, 052002 (2007).

18. I. V. Meglinski, V. V. Kal'chenko, Y. L. Kuznetsov, B. I. Kuznik, V. V. Tuchin, Towards the nature of biological zero in the dynamic light scattering diagnostic modalities. *Doklady Physics* **58**, 323-326 (2013).

19. E. S. Stiukhina, D. E. Postnov, *Modeling study of terminal transients of blood flow*. Saratov Fall Meeting 2015 (SPIE, 2016), vol. 9917.

20. L. Manteuffel-Szoege, J. Michalowski, J. Grundman, W. Pacocha, On the possibility of blood circulation continuing after stopping the heart. *J Cardiovasc Surg (Torino)* **7**, 201-208 (1966).

21. L. Manteuffel-Szoege, Energy Sources of Blood Circulation and the Mechanical Action of the Heart. *Thorax* **15**, 47-53 (1960).

22. L. Manteuffel-Szoege, On Stopping and Restarting of Circulation in Deep Hypothermia. *J Cardiovasc Surg (Torino)* **5**, 76-80 (1964).

23. J. L. W. Thudichum, On the cause of the emptiness of the arteries after death. *Association Medical Journal* **3**, 122-127 (1855).

24. S. Vogel, *Life in moving fluids : the physical biology of fluids*. (Princeton University Press, Princeton, N.J., 1996), pp. 323-329.

25. A. S. Forouhar *et al.*, The Embryonic Vertebrate Heart Tube Is a Dynamic Suction Pump. *Science* **312**, 751 (2006).

26. C. D. De Langen, The vis a tergo, capillary pressure and capillary function. *Acta Med Scand* **140**, 437-445 (1951).

27. Y. Henderson, S. C. Harvey, Acapnia and shock VIII .The Veno-Pressor Mechanism. *American Journal of Physiology-Legacy Content* **46**, 533-553 (1918).

28. B. Furst, *The Heart and Circulation: An Integrative Model*. (Springer-Verlag, London, 2014).

29. W. Alexander, Branko Furst's Radical Alternative: Is the Heart Moved by the Blood, Rather Than Vice Versa? *P & T : a peer-reviewed journal for formulary management* **42**, 33-39 (2017).

30. B. Furst, The Heart: Pressure-Propulsion Pump or Organ of Impedance? *Journal of Cardiothoracic and Vascular Anesthesia* **29**, 1688-1701 (2015).

31. J. Snow, On the circulation in the capillary blood-vessels, and on some of its connections with pathology and therapeutics. *London Med. Gazette* **31**, 810-816 (1843).

32. Y. Henderson, A. W. Oughterson, L. A. Greenberg, C. P. Searle, The Third Major Mechanical Factor in the Circulation of the Blood. *Science* **79**, 508-510 (1934).

33. T. Cowan, *Human Heart, Cosmic Heart: A Doctor's Quest to Understand, Treat, and Prevent Cardiovascular Disease*. (Chelsea Green Publishing, 2016).

34. R. H. Petrucci, *General chemistry : principles and modern applications*. (Pearson/Prentice Hall, Upper Saddle River, N.J., 2007).

35. M. S. Cracolice, E. I. Peters, *Basics of introductory chemistry : an active learning approach*. (Brooks/Cole Cengage Learning, Belmont, CA, 2011).

36. A. Szent-Györgyi, *Bioenergetics*. (Academic Press, New York, ed. 1st, 1957).

37. G. Ling, *In search of the physical basis of life*. (Plenum Press, New York, ed. 1st, 1984).

38. J. Zheng, G. H. Pollack, Long-range forces extending from polymer-gel surfaces. *Physical Review E* **68**, 031408 (2003).

39. J. Zheng, W. Chin, E. Khijniak, E. Khijniak, G. H. Pollack, Surfaces and interfacial water: Evidence that hydrophilic surfaces have long-range impact. *Advances in Colloid and Interface Science* **127**, 19-27 (2006).

40. B. Chai, A. G. Mahtani, G. H. Pollack, Unexpected presence of solute-free zones at metal-water interfaces. *Contemporary materials* **3**, 1-12 (2012).

41. R. Das, G. H. Pollack, Charge-Based Forces at the Nafion–Water Interface. *Langmuir* **29**, 2651-2658 (2013).

42. X. A. Figueroa, G. H. Pollack, Exclusion-Zone Formation From Discontinuous Nafion Surfaces. *International journal of design & nature and ecodynamics : a transdisciplinary journal relating to nature, science and the humanities* **6**, 286-296 (2011).

43. B. Chai, H. Yoo, G. H. Pollack, Effect of radiant energy on near-surface water. *J Phys Chem B* **113**, 13953-13958 (2009).

44. J. Zheng, G. H. Pollack, in *Water and the Cell*, G. H. Pollack, I. L. Cameron, D. N. Wheatley, Eds. (Springer Netherlands, Dordrecht, 2006), pp. 165-174.

45. G. Pollack, *The Fourth Phase of Water*. (Ebner & Sons, Seattle, WA, 2013), pp. 64-66.

46. G. Pollack, *The Fourth Phase of Water*. (Ebner & Sons, Seattle, WA, 2013), pp. 85-86.

47. G. Pollack, *The Fourth Phase of Water*. (Ebner & Sons, Seattle, WA, 2013), pp. 87.

48. G. Pollack, *The Fourth Phase of Water*. (Ebner & Sons, Seattle, WA, 2013), pp. 45-69.

49. A. Yu, P. Carlson, G. H. Pollack, Unexpected axial flow through hydrophilic tubes: Implications for energetics of water. *The European Physical Journal Special Topics* **223**, 947-958 (2014).

50. M. Rohani, G. H. Pollack, Flow through Horizontal Tubes Submerged in Water in the Absence of a Pressure Gradient: Mechanistic Considerations. *Langmuir* **29**, 6556-6561 (2013).

51. G. Pollack, *The Fourth Phase of Water*. (Ebner & Sons, Seattle, WA, 2013), pp. 112-115.

52. J. Flammer *et al.*, The eye and the heart. *European heart journal* **34**, 1270-1278 (2013).

53. K. Hasselbach, H. Jacobäus, Ueber die Behandlung von Angina pectoris mit starken Kohlenbogenlichtbäden. *Berl. Klin. Wochenschr* **44**, 1247-1252 (1907).

54. D. T. Harris, The effect of light on the circulation. *Proceedings of the Royal Society of London. Series B* **99**, 28 (1925).

55. V. Drouard, D. R. Wilson, H. I. Maibach, R. H. Guy, Quantitative Assessment of UV-Induced Changes in Microcirculatory Flow by Laser Doppler Velocimetry. *Journal of Investigative Dermatology* **83**, 188-192 (1984).

56. C. Oplander *et al.*, Whole body UVA irradiation lowers systemic blood pressure by release of nitric oxide from intracutaneous photolabile nitric oxide derivates. *Circ Res* **105**, 1031-1040 (2009).

57. H. Bertalanffy, T. Kawase, S. Toya, In vivo effect of visible light on feline cortical microcirculation. *Acta Neurochirurgica* **121**, 174-180 (1993).

58. K. Kobayashi *et al.*, Increase in peripheral blood flow due to extraocular direct irradiation of visible light in rats. *American Journal of Physiology-Heart and Circulatory Physiology* **279**, H1141-H1146 (2000).

59. G. Sikka *et al.*, Melanopsin mediates light-dependent relaxation in blood vessels. *Proceedings of the National Academy of Sciences* **111**, 17977 (2014).

60. Y. Maegawa, T. Itoh, T. Hosokawa, K. Yaegashi, M. Nishi, Effects of near-infrared low-level laser irradiation on microcirculation. *Lasers Surg Med* **27**, 427-437 (2000).

61. A. Schindl, G. Heinze, M. Schindl, H. Pernerstorfer-Schon, L. Schindl, Systemic effects of low-intensity laser irradiation on skin microcirculation in patients with diabetic microangiopathy. *Microvasc Res* **64**, 240-246 (2002).

62. S. Y. Yu *et al.*, Biological effect of far-infrared therapy on increasing skin microcirculation in rats. *Photodermatol Photoimmunol Photomed* **22**, 78-86 (2006).

63. Y. Asagai, T. Sujaritpong, L. Tranvan, T. Ohshiro, Assessment of changes in carotid blood flow following LLLT of the neck. *Laser therapy* **16**, 127-132 (2007).

64. 万. 小森, 低出力レーザーおよび直線偏光近赤外線直接照射の皮膚微小循環に対する効果. *日本レーザー歯学会誌* **19**, 26-29 (2008).

65. M. C. H. Mak, G. L. Y. Cheing, Immediate Effects of Monochromatic Infrared Energy on Microcirculation in Healthy Subjects. *Photomedicine and Laser Surgery* **30**, 193-199 (2012).

66. P. Fratzl, in *Collagen: Structure and Mechanics*, P. Fratzl, Ed. (Springer US, Boston, MA, 2008), pp. 1-13.

67. C.-B. Laurell, Quantitative estimation of proteins by electrophoresis in agarose gel containing antibodies. *Analytical Biochemistry* **15**, 45-52 (1966).

68. C. R. Shaw, R. Prasad, Starch gel electrophoresis of enzymes—A compilation of recipes. *Biochemical Genetics* **4**, 297-320 (1970).

69. E. M. Ahmed, Hydrogel: Preparation, characterization, and applications: A review. *Journal of Advanced Research* **6**, 105-121 (2015).

70. J. P. Morgan *et al.*, Formation of microvascular networks in vitro. *Nature Protocols* **8**, 1820 (2013).

71. K. Ovchinnikova, G. H. Pollack, Cylindrical phase separation in colloidal suspensions. *Phys Rev E Stat Nonlin Soft Matter Phys* **79**, 036117 (2009).

72. K. W. Kimura, G. H. Pollack, Particle Displacement in Aqueous Suspension Arising from Incident Radiant Energy. *Langmuir* **31**, 10370-10376 (2015).

73. ASTM, in *Standard Tables for Reference Solar Spectral Irradiances: Direct Normal and Hemispherical on 37° Tilted Surface*. (ASTM International, West Conshohocken, PA, 2012).

74. F. Vatansever, M. R. Hamblin, Far infrared radiation (FIR): its biological effects and medical applications. *Photonics & lasers in medicine* **4**, 255-266 (2012).

75. R. E. Klabunde, *Cardiovascular Physiology Concepts*. (Lippincott Williams & Wilkins, Baltimore, MD, ed. Second, 2012), pp. 187-191.

76. D. Florea, S. Musa, J. M. R. Huyghe, H. M. Wyss, Long-range repulsion of colloids driven by ion exchange and diffusiophoresis. *Proceedings of the National Academy of Sciences* **111**, 6554 (2014).

77. J. M. Schurr, B. S. Fujimoto, L. Huynh, D. T. Chiu, A Theory of Macromolecular Chemotaxis. *The Journal of Physical Chemistry B* **117**, 7626-7652 (2013).

78. G. H. Pollack, Comment on "A Theory of Macromolecular Chemotaxis" and "Phenomena Associated with Gel–Water Interfaces. Analyses and Alternatives to the Long-Range Ordered Water Hypothesis". *The Journal of Physical Chemistry B* **117**, 7843-7846 (2013).

79. J. M. Schurr, Phenomena Associated with Gel–Water Interfaces. Analyses and Alternatives to the Long-Range Ordered Water Hypothesis. *The Journal of Physical Chemistry B* **117**, 7653-7674 (2013).

80. R. K. Sinha, *Modern Plant Physiology*. (Narosa, ed. 1st, 2003).

81. P. B. Aebersold, G. A. Winans, D. J. Teel, G. B. Milner, F. M. Utter, Manual for starch gel electrophoresis: A method for the detection of genetic variation. *NOAA Technical Report NMFS* **61**, (1987).

82. A. J. Mach, J. H. Kim, A. Arshi, S. C. Hur, D. Di Carlo, Automated cellular sample preparation using a Centrifuge-on-a-Chip. *Lab on a Chip* **11**, 2827-2834 (2011).

83. C. A. Schneider, W. S. Rasband, K. W. Eliceiri, NIH Image to ImageJ: 25 years of image analysis. *Nature methods* **9**, 671-675 (2012).

84. W. Thielicke, E. J. Stamhuis, PIVlab – Towards User-friendly, Affordable and Accurate Digital Particle Image Velocimetry in MATLAB. *Journal of Open Research Software* **2**, e30 (2014).

85. C. D. Meinhart, S. T. Wereley, J. G. Santiago, A PIV Algorithm for Estimating Time-Averaged Velocity Fields. *Journal of Fluids Engineering* **122**, 285-289 (2000).

86. P. Vennemann *et al.*, In vivo micro particle image velocimetry measurements of blood-plasma in the embryonic avian heart. *Journal of Biomechanics* **39**, 1191-1200 (2006).

87. Q. Tseng *et al.*, Spatial organization of the extracellular matrix regulates cell–cell junction positioning. *Proceedings of the National Academy of Sciences* **109**, 1506 (2012).

88. V. Hamburger, H. L. Hamilton, A series of normal stages in the development of the chick embryo. *J Morphol* **88**, 49-92 (1951).

89. M. E. Murphy, E. C. Carlson, An ultrastructural study of developing extracellular matrix in vitelline blood vessels of the early chick embryo. *Am J Anat* **151**, 345-375 (1978).

90. M. L. Kirby, J. W. McKenzie, T. A. Weidman, Developing innervation of the chick heart: A histofluorescence and light microscopic study of sympathetic innervation. **196**, 333-340 (1980).

91. M. Kirby, *Innervation of the developing heart*. (Oxford University Press, New York, 2007), pp. 179-197.

92. J. Y. Lee, S. J. Lee, Hemodynamics of the omphalo-mesenteric arteries in stage 18 chicken embryos and "flow-structure" relations for the microcirculation. *Microvasc Res* **80**, 402-411 (2010).

93. B. J. Martinsen, Reference guide to the stages of chick heart embryology. **233**, 1217-1237 (2005).

94. R. E. Ferner, Post-mortem clinical pharmacology. *British journal of clinical pharmacology* **66**, 430-443 (2008).

95. B. Surawicz, S. Gettes Leonard, C. Shive James, O. Brooks Harry, Two Mechanisms of Cardiac Arrest Produced by Potassium. *Circulation Research* **12**, 415-421 (1963).

96. R. Shemilt, H. Bagabir, C. Lang, F. Khan, Potential mechanisms for the effects of far-infrared on the cardiovascular system – a review. *Vasa*, 1-10 (2018).

97. M. P. Wiedeman, Dimensions of blood vessels from distributing artery to collecting vein. *Circ Res* **12**, 375-378 (1963).

98. O. College, *Anatomy & physiology.*, Retrieved from: https://opentextbc.ca/anatomyandphysiology/chapter/20-3-capillary-exchange/ (OpenStax CNX. , Houston, TX, 2013).

99. J. Y. Lee, H. S. Ji, S. J. Lee, Micro-PIV measurements of blood flow in extraembryonic blood vessels of chicken embryos. *Physiol Meas* **28**, 1149-1162 (2007).

Vita

Education

University of Washington, Seattle, USA 2011 - 2019

Ph.D. in Bioengineering

Beijing University of Aeronautics and Astronautics, Beijing, China 2008 - 2011

Master of Science in Physics

Beijing University of Aeronautics and Astronautics, Beijing, China 2004 - 2008

Bachelor of Science in Physics

Publications

Surface-Induced Flow: a Natural Microscopic Engine Using Infrared Energy as Fuel, in progress

Infrared Radiation as an Auxiliary Energy Source for Blood Circulation, in progress

Miscellaneous

Lab Manager, Pollack Lab, BioE. Dept., UW 2014 – 2019

Campus Representative, GE Healthcare 2015 –2016

Teaching Assistant for BioMEMS, UW 2015

People’s Choice Awards of Inaugural Three Minute Thesis competition, UW 2017

Doctoral Student Speaker at 2019 Bioengineering Graduation Ceremony 2019